



CIVIL ENGINEERING STUDIES

Illinois Center for Transportation Series No. 21-018

UILU-ENG-2021-2018

ISSN: 0197-9191

Bench-scale Electrochemical Treatment of Co-contaminated Clayey Soil

Prepared By

Austin Pelletier

Amanda Hohner

Idil Deniz Akin

Indranil Chowdhury

Richard Watts

Xianming Shi

Washington State University

Brendan Dutmer

Highland Community College

James Mueller

Provectus Environmental Products, Inc.

Research Report No. FHWA-ICT-21-013

The third of four reports of the findings of

ICT PROJECT R27-183-HS

**Evaluation of On-Site and In Situ Treatment Alternatives
for Contaminated Soils**

<https://doi.org/10.36501/0197-9191/21-018>

Illinois Center for Transportation

June 2021



TECHNICAL REPORT DOCUMENTATION PAGE

1. Report No. FHWA-ICT-21-013		2. Government Accession No. N/A		3. Recipient's Catalog No. N/A	
4. Title and Subtitle Bench-scale Electrochemical Treatment of Co-contaminated Clayey Soil				5. Report Date June 2021	
				6. Performing Organization Code N/A	
7. Authors Austin Pelletier, Amanda Hohner (https://orcid.org/0000-0001-7704-4464), Idil Deniz Akin (https://orcid.org/0000-0002-1946-4951), Indranil Chowdhury, Richard Watts, Xianming Shi (https://orcid.org/0000-0003-3576-8952), James Mueller				8. Performing Organization Report No. ICT-21-018 UILU-2021-2018	
9. Performing Organization Name and Address Illinois Center for Transportation Department of Civil and Environmental Engineering University of Illinois at Urbana-Champaign 205 North Mathews Avenue, MC-250 Urbana, IL 61801				10. Work Unit No. N/A	
				11. Contract or Grant No. R27-183-HS	
12. Sponsoring Agency Name and Address Illinois Department of Transportation (SPR) Bureau of Research 126 East Ash Street Springfield, IL 62704				13. Type of Report and Period Covered Task 3 report 2/1/18–6/30/21	
				14. Sponsoring Agency Code	
15. Supplementary Notes Conducted in cooperation with the U.S. Department of Transportation, Federal Highway Administration. https://doi.org/10.36501/0197-9191/21-018					
16. Abstract Industrial soil contamination is frequently unearthed by transportation agencies during construction within the right-of-way. As a result, transportation agencies may experience construction delays. Soils co-contaminated with high-molecular-weight polycyclic aromatic hydrocarbons (HMW-PAHs) and metals are commonly encountered in Illinois and exhibit recalcitrance towards conventional treatment technologies. This issue is exacerbated in the fine-grained soils common to Illinois, where low-permeability and immense sorption capacity increase treatment complexity, cost, and duration. Contaminated sites are spatially and temporally restrictive and require rapid in situ treatments, whereas conventional soil remediation requires 1 to 3 years on average. Consequently, transportation agencies typically pursue excavation and off-site disposal for expediency. However, this solution is expensive, so a comparatively expeditious and affordable treatment alternative is needed to combat the increasing cost of hazardous waste disposal. The objective of this work was to develop an accelerated in situ treatment approach adaptable for use at any construction site to cost-effectively remove HMW-PAHs and metals from clayey soil. It was hypothesized that an in situ electrochemical treatment which augments electrokinetics with H ₂ O ₂ could remediate both HMW-PAHs and metals in less than a month. Bench-scale reactors resembling field-scale in situ electrokinetic systems were designed and fabricated to assess the electrochemical treatment of clayey soils contaminated with HMW-PAHs and metals. Pyrene, chromium, and manganese were used as model contaminants, spiked into kaolinite as a model clay. Electrokinetics were imposed by a low-intensity electrical field distributed by graphite rods. Electrolytic H ₂ O ₂ systems were leveraged to distribute electrical current and facilitate contaminant removal. Average contaminant removals of 100%, 42.3%, and 4.5% were achieved for pyrene, manganese, and chromium, respectively. Successful development of this bench-scale treatment approach will serve to guide transportation agencies in field-scale implementation. The results from this work signify that electrochemical systems that leverage eco-friendly oxidant addition can replace excavation and disposal as a means of addressing clayey soils co-contaminated with HMW-PAHs and metals.					
17. Key Words Soil Contamination, Metals, PAHs, Electrochemical Treatment			18. Distribution Statement No restrictions. This document is available through the National Technical Information Service, Springfield, VA 22161.		
19. Security Classif. (of this report) Unclassified		20. Security Classif. (of this page) Unclassified		21. No. of Pages 65 + appendices	22. Price N/A

ACKNOWLEDGMENT, DISCLAIMER, MANUFACTURERS' NAMES

This publication is based on the results of **ICT-R27-183-HS: Evaluation of On-Site and In Situ Treatment Alternatives for Contaminated Soils**. ICT-R27-183-HS was conducted in cooperation with the Illinois Center for Transportation; the Illinois Department of Transportation; and the U.S. Department of Transportation, Federal Highway Administration.

Members of the Technical Review Panel (TRP) were the following:

- Doug Dirks—TRP Co-chair, Illinois Department of Transportation
- Jim Curtis—TRP Co-chair, Illinois Department of Transportation
- Doug Liniger—Illinois Department of Transportation
- Greg Dunn—Illinois Environmental Protection Agency
- Viraj Perera—Illinois Department of Transportation
- Tyler Petersen—Illinois Department of Transportation
- Kyle Rominger—Illinois Environmental Protection Agency
- Bart Sherer—Illinois Department of Transportation
- JD Stevenson—Federal Highway Administration
- Heather Shoup—Illinois Department of Transportation
- Megan Swanson- Illinois Department of Transportation
- Dan Wakefield—Illinois Department of Transportation
- Andrew Anderson—Illinois State Geological Survey

The contents of this report reflect the view of the authors, who are responsible for the facts and the accuracy of the data presented herein. The contents do not necessarily reflect the official views or policies of the Illinois Center for Transportation, the Illinois Department of Transportation, or the Federal Highway Administration. This report does not constitute a standard, specification, or regulation.

Trademark or manufacturers' names appear in this report only because they are considered essential to the object of this document and do not constitute an endorsement of product by the Federal Highway Administration, the Illinois Department of Transportation, or the Illinois Center for Transportation.

The work presented in this report was previously published in 2019 by Washington State University in Austin Pelletier's master's thesis (Pelletier, 2019). Tables, figures, and text presented within this report were taken from the student's thesis (Pelletier, 2019), unless otherwise indicated.

EXECUTIVE SUMMARY

Industrial soil contamination is frequently unearthed by transportation agencies during construction within the right-of-way (ROW), threatening both public health and the environment. As a result, transportation agencies may experience construction delays. Soils co-contaminated with high-molecular-weight polycyclic aromatic hydrocarbons (HMW-PAHs) and metals are commonly encountered in Illinois and exhibit recalcitrance toward conventional treatment technologies. This issue is exacerbated in the fine-grained soils common to Illinois, where low-permeability and immense sorption capacity increase treatment complexity, cost, and duration. Contaminated sites are spatially and temporally restrictive and require rapid in situ treatments, whereas conventional soil remediation requires 1–3 years on average. Consequently, transportation agencies typically pursue excavation and off-site disposal for expediency. However, this solution is expensive, so a comparatively expeditious and affordable treatment alternative is needed to combat the ever-increasing cost of hazardous waste disposal. The objective of this work was to develop an accelerated in situ treatment approach adaptable for use at any construction site to cost-effectively remove HMW-PAHs and metals from clayey soil. It was hypothesized that an in situ electrochemical treatment that augments electrokinetics with H_2O_2 could remediate both HMW-PAHs and metals in less than a month.

Bench-scale reactors resemblant of field-scale in situ electrokinetic systems were designed and fabricated to assess the electrochemical treatment of clayey soils contaminated with HMW-PAHs and metals. Pyrene, chromium, and manganese were used as model contaminants, spiked into kaolinite as a model clay. Electrokinetics were imposed by a low-intensity electrical field distributed by graphite rods. Electrolytic H_2O_2 systems were leveraged to distribute electrical current and facilitate contaminant removal. Average contaminant removals of 100%, 42.3%, and 4.5% were achieved for pyrene, manganese, and chromium, respectively.

Successful development of this bench-scale treatment approach will serve to guide transportation agencies in field-scale implementation. The results from this work signify that electrochemical systems that leverage eco-friendly oxidant addition can replace excavation and disposal as a means of addressing clayey soils co-contaminated with HMW-PAHs and metals.

TABLE OF CONTENTS

CHAPTER 1: INTRODUCTION	1
BACKGROUND AND MOTIVATION	1
CASE STUDY: CONTAMINATED SOILS IN ILLINOIS	1
Soil Contaminant Inventory	1
Soil Characteristics	2
RESEARCH HYPOTHESIS.....	4
CHAPTER 2: LITERATURE REVIEW.....	5
HIGH-MOLECULAR-WEIGHT POLYCYCLIC AROMATIC HYDROCARBONS.....	5
CHROMIUM.....	6
CONTAMINANT INTERACTIONS	6
PHYSICOCHEMICAL TREATMENT MECHANISMS	6
Enhanced Hydrogen Peroxide Systems	6
Electrokinetics	11
CHAPTER 3: METHODOLOGY	21
MATERIALS.....	21
Soil Characteristics	21
Chemical Reagents	22
Bench-scale Electrochemical Reactor.....	22
EXPERIMENTAL DESIGN	24
Soil Spiking	24
Electrochemical Regime	25
Laboratory Soil Sampling for Analyses	27
ANALYTICAL METHODS	29
Auxiliary Methods	29
Reactor Performance Checks.....	29
Polycyclic Aromatic Hydrocarbons and Degradation Product Analysis	29
Metals Analysis.....	30
Unconfined Compressive Strength.....	31

CHAPTER 4: RESULTS AND DISCUSSION	32
OVERVIEW	32
EXPERIMENT 1: PYRENE TREATMENT WITH H₂O₂ AND CITRATE BUFFER.....	32
EXPERIMENT 2: PYRENE TREATMENT WITH A NONIONIC SURFACTANT, H₂O₂, AND CITRATE BUFFER.....	36
EXPERIMENT 3: PYRENE TREATMENT WITH A NONIONIC SURFACTANT.....	41
EXPERIMENT 4: PYRENE TREATMENT WITH A SURCHARGE, H₂O₂, CITRATE BUFFER, AND CATHODE-WELL PH AMENDMENTS.....	43
EXPERIMENT 5: MANGANESE TREATMENT WITH A SURCHARGE, H₂O₂, SCPS, CITRATE BUFFER, AND CATHODE-WELL PH AMENDMENTS	45
EXPERIMENT 6: PYRENE AND CHROMIUM TREATMENT WITH A SURCHARGE, H₂O₂, CITRATE BUFFER, AND EXPLORATORY ELECTRODE-WELL PH AMENDMENTS	49
COMPARISON OF EXPERIMENTS.....	53
CHAPTER 5: SUMMARY OF FINDINGS, FUTURE WORK, AND CONSIDERATIONS	55
SUMMARY AND CONCLUSIONS	55
FUTURE WORK AND CONSIDERATIONS	56
Recommended Next Steps.....	56
REFERENCES	58
APPENDICES	66
APPENDIX A: CHAPTER 1 SUPPLEMENTARY INFORMATION	66
APPENDIX B: CHAPTER 3 SUPPLEMENTARY INFORMATION.....	73
APPENDIX C: CHAPTER 4 SUPPLEMENTARY INFORMATION.....	74

LIST OF FIGURES

Figure 1. Equation. Equation 1 showing the decomposition of hydrogen peroxide to water and oxygen gas.....	7
Figure 2. Equation. Equation 2 showing dilution of hydrogen peroxide.....	7
Figure 3. Schematic. Field-scale in situ electrochemical treatment with a diagram of electrokinetic transport mechanisms between clay particles.	12
Figure 4. Schematic. The GCSG model interpretation of the electrical double layer theory with respect to a particle surface in a clay-electrolyte system.....	13
Figure 5. Equation. Nernst-Planck equation.	14
Figure 6. Equation. Equation 43.	17
Figure 7. Equation. Equation 48.	18
Figure 8. Equation. Equation 49.	18
Figure 9. Equation. Equation 50.	19
Figure 10. Schematic. Cross-sectional schematic of the bench-scale electrochemical reactor. (A): Direct current power supply; (B): Digital multimeter; (C): Power relay; (D): Peristaltic pump; (E): Anode-well solution reservoir; (F): Reactor outflow reservoir; (G): Cathode; (H): Anode; (I) Auxiliary electrode; (J): Copper grounding rod clamp; (K) Normally closed float switch; (L): Tygon tubing sight glass; (M): Glass fiber filter; (N) Nested CPVC Pipes referred to as electrode wells; (O): HDPE soil cell; and, (P) Contaminated soil.....	23
Figure 11. Schematic. Parts and detailed schematic of the modular electrode-well components. (A): Removable cap with access ports; (B): Electrode-well reservoir; (C): Well bottom connected to the outer pipe only; (D): Glass fiber filter; (E): Outer CPVC pipe; (F): Inner CPVC pipe; (G): Normally closed float switch; (H): Electrode; (I) Electrode-well inflow/outflow.....	23
Figure 12. Schematic. Top-down schematic of the bench-scale electrochemical reactor.....	24
Figure 13. Plan. Pretreatment batch sampling plan for soil characterization. Sample points: red triangle = pH/secondary contaminant; blue square = moisture content; and green circle = contaminant concentration.	27
Figure 14. Schematic. Post-treatment reactor sampling plan with relative coordinate system defined to scale. Top image = Top-down view. Bottom image = Cross-sectional view.....	28
Figure 15. Graph. Final pyrene concentration distribution by depth below soil surface (experiment 1). The numbers shown for each sample point indicate the treated concentration normalized by the initial concentration (C/C_0).....	33
Figure 16. Graph. Final pyrene concentration distribution by normalized depth below the soil surface (depth/total depth) (experiment 1). The lower horizontal lines (inside of box) represent the final	

median values and the upper horizontal lines represent the initial averages for each box and whisker column.	34
Figure 17. Graph. Final pyrene concentration distribution by orthogonal distance from electrodes (experiment 1). The lower horizontal lines (inside of box) represent the final median values and the upper horizontal lines represent the initial averages for each box and whisker column.	34
Figure 18. Graph. Final moisture content (MC) distribution by depth below soil surface (experiment 1). The numbers shown for each sample point indicate the final MC normalized by the initial MC (MC/MC_0).	35
Figure 19. Graph. Final pH distribution by depth below soil surface (experiment 1). The numbers shown for each sample point indicate the change in pH from the initial conditions (Δ pH).	36
Figure 20. Graph. Final pyrene concentration distribution by depth below soil surface (experiment 2). The numbers shown for each sample point indicate the treated concentration normalized by the initial concentration (C/C_0).....	37
Figure 21. Graph. Final pyrene concentration distribution by orthogonal distance from electrodes (experiment 2). The lower horizontal lines (inside of box) represent the final median values and the upper horizontal lines represent the initial averages for each box and whisker column.	38
Figure 22. Graph. Final pyrene concentration distribution by normalized distance (distance/total distance) from anode to cathode (experiment 2). The lower horizontal lines (inside of box) represent the final median values and the upper horizontal lines represent the initial averages for each box and whisker column.	38
Figure 23. Graph. Final moisture content distribution by depth below soil surface (experiment 2). The numbers shown for each sample point indicate the final MC normalized by the initial MC (MC/MC_0).	39
Figure 24. Graph. Final pH distribution by depth below soil surface (experiment 2). The numbers shown for each sample point indicate the change in pH from the initial conditions (Δ pH).	40
Figure 25. Graph. Final pyrene concentration distribution by depth below soil surface (experiment 3). The numbers shown for each sample point indicate the treated concentration normalized by the initial concentration (C/C_0).....	42
Figure 26. Graph. Final pyrene concentration distribution by normalized depth below the soil surface (depth/total depth) (experiment 3). The lower horizontal lines (inside of box) represent the final median values and the upper horizontal lines represent the initial averages for each box and whisker column.	42
Figure 27. Graph. Final moisture content distribution by depth below soil surface (experiment 3). The numbers shown for each sample point indicate the final MC normalized by the initial MC (MC/MC_0).	43

Figure 28. Graph. Final pyrene concentration distribution by depth below soil surface (experiment 4). The numbers shown for each sample point indicate the treated concentration normalized by the initial concentration (C/C_0).....	44
Figure 29. Graph. Pyrene concentration as a function of moisture content and each spatial dimension (experiment 4). The shaded regions represent the 95% confidence intervals of the linear regressions.	45
Figure 30. Graph. Final manganese concentration distribution by depth below soil surface (experiment 5). The color-bar scale excludes outlier 17.5, +5, 2.5 (X,Y,Z: cm). The numbers shown for each sample point indicate the treated concentration normalized by the initial concentration (C/C_0).	46
Figure 31. Graph. Final manganese concentration distribution by normalized distance (distance/total distance) from anode to cathode. Outlier 17.5, +5, 2.5 (X,Y,Z: cm) was excluded (experiment 5). The lower horizontal lines (inside of box) represent the final median values and the upper horizontal lines represent the initial averages for each box and whisker column.....	47
Figure 32. Graph. Final pH distribution by depth below soil surface (experiment 5). The numbers shown for each sample point indicate the change in pH from the initial conditions (Δ pH).	48
Figure 33. Graph. Final moisture content distribution by depth below soil surface (experiment 5). The numbers shown for each sample point indicate the final MC normalized by the initial MC (MC/MC_0).	49
Figure 34. Graph. Final chromium concentration distribution by depth below soil surface (experiment 6). The numbers shown for each sample point indicate the treated concentration normalized by the initial concentration (C/C_0).....	50
Figure 35. Graph. Final chromium concentration distribution by normalized distance (distance/total distance) from anode to cathode (experiment 6). The lower horizontal lines (inside of box) represent the final median values and the upper horizontal lines represent the initial averages for each box and whisker column.	51
Figure 36. Graph. Final pH distribution by depth below soil surface (experiment 6). The numbers shown for each sample point indicate the change in pH from the initial conditions (Δ pH).	52
Figure 37. Graph. Final moisture content distribution by depth below soil surface (experiment 6). The numbers shown for each sample point indicate the final MC normalized by the initial MC (MC/MC_0). .	53
Figure 38. Photo. Post-treatment soil surface with swelling induced changes in soil structure (experiment 1).....	77
Figure 39. Photos. Post-treatment electrodes. Left = anode. Right = Cathode (experiment 1).....	77
Figure 40. Photo. Post-treatment electrodes. Top = Anode. Bottom = Cathode (experiment 2).	81
Figure 41. Photos. Surfactant induced saponification during post-treatment sample centrifugation (experiment 3).....	84
Figure 42. Photo. Ponding on day 14 due to surfactant induced soil pore clogging (experiment 3). ...	84
Figure 43. Photo. Post-treatment electrodes. Left = anode. Right = Cathode (experiment 3).	85

Figure 44. Photo. Post-treatment soil surface riddled with sponge-like voids (experiment 4).....	89
Figure 45. Photo. Post-treatment electrodes. Left photo: Cathode. Right photo: Left = cathode, Right = anode (experiment 4).	89
Figure 46. Photos. Post-treatment cathode shown in both photos (experiment 5).	93
Figure 47. Photo. Post-treatment cathode well caked with manganese concretions (experiment 5). .	93
Figure 48. Graph. Chromium concentration as a function of moisture content and each spatial dimension (experiment 6). The shaded regions represent the 95% confidence intervals of the linear regressions.	102

LIST OF TABLES

Table 1. Top 10 Most Frequently Encountered Contaminants in Exceedance of the MACs.....	2
Table 2. Typical Drummer Soil Series	3
Table 3. Equations 3–8 (Watts & Teel, 2005).....	8
Table 4. Equations 9–12.....	8
Table 5. Additional Mechanisms of Catalyzed Hydrogen Peroxide Propagations	10
Table 6. Example Recipe of Simulated Concrete Pore Solution.....	11
Table 7. Equations 26–27	15
Table 8. Equations 28–29.....	16
Table 9. Equations 30–33	16
Table 10. Equations 34–42	16
Table 11. Equation. Equations 44–45	17
Table 12. Equations 46 and 47	18
Table 13. Index Properties and Mineralogy of Kaolinite Clay.....	21
Table 14. Summary of Initial Soil Properties.....	24
Table 15. Summary of Electrochemical Regime by Experiment	25
Table 16. ICPMS Program Conditions	30
Table 17. Summary of Unconfined Compressive Strength Testing Results (Experiment 5).....	48
Table 18. Summary of Post-Treatment Results by Experiment	54
Table 19. Summary of Initial Field Soil Properties for Future Experiments.....	57
Table 20. Summary of Actual and Lowest MAC Exceedances from the Preliminary Dataset.....	66
Table 21. Approximate Soil Properties for Sites with MAC Exceedances from the Preliminary Dataset	70
Table 22. MACs for the 10 Most Frequently Encountered Contaminants Resulting in Exceedance.....	72
Table 23. Equations B1–B6.....	73
Table 24. Post-treatment Soil Parameters (experiment 1).....	74
Table 25. Summary of Statistics for Post-treatment Samples (experiment 1).....	75
Table 26. Summary of Operational Parameters Monitored during Treatment (Experiment 1).....	76
Table 27. Post-treatment Soil Parameters (Experiment 2).....	78

Table 28. Summary of Statistics for Post-treatment Samples (Experiment 2)	79
Table 29. Summary of Operational Parameters Monitored during Treatment (Experiment 2).....	80
Table 30. Post-treatment Soil Parameters (Experiment 3).....	81
Table 31. Summary of Statistics for Post-treatment Samples (Experiment 3)	82
Table 32. Summary of Operational Parameters Monitored during Treatment (Experiment 3).....	83
Table 33. Post-treatment Soil Parameters (Experiment 4).....	86
Table 34. Summary of Statistics for Post-treatment Samples (Experiment 4)	87
Table 35. Summary of Operational Parameters Monitored during Treatment (Experiment 4).....	88
Table 36. Post-treatment Soil Parameters (Experiment 5).....	90
Table 37. Summary of Statistics for Post-treatment Samples (Experiment 5)	91
Table 38. Summary of Operational Parameters Monitored during Treatment (Experiment 5).....	92
Table 39. Post-treatment Soil Parameters (Experiment 6).....	94
Table 40. Summary of Statistics for Post-treatment Samples (Experiment 6)	96
Table 41. Summary of Operational Parameters Monitored during Treatment (Experiment 6).....	98

LIST OF ACRONYMS AND ABBREVIATIONS

ASTM:	American Society for Testing and Materials (Now ASTM International)
BaP:	Benzo(a)pyrene
CHP:	Catalyzed hydrogen peroxide propagations
CMC:	Critical micelle concentration
COC:	Contaminant of concern
DNAPL:	Dense nonaqueous phase liquid
EPA:	Environmental Protection Agency
FRTR:	Federal Remediation Technologies Roundtable
GCMS:	Gas chromatography mass spectrometry
HLB:	Hydrophile-lipophile balance
HOC:	Hydrophobic organic contaminant
HMW:	High molecular weight
IAC:	Illinois Administrative Code
ICPMS:	Inductively coupled mass spectrometry
IDOT:	Illinois Department of Transportation
ILCS:	Illinois Compiled Statutes
ISCO:	In situ chemical oxidation
LMW:	Low molecular weight
MAC:	Maximum allowable concentration
MC:	Moisture content
MSA:	Metropolitan statistical area
NAN:	Not a number
NAPL:	Nonaqueous phase liquid
PAH:	Polycyclic aromatic hydrocarbon
ROS:	Reactive oxygen species
ROW:	Right-of-way
SCPS:	Simulated concrete pore solution
SD:	Standard deviation
SHP:	Stabilized hydrogen peroxide
SVOC:	Semivolatile organic compound/contaminant

CHAPTER 1: INTRODUCTION

BACKGROUND AND MOTIVATION

Industrial activities and vehicular transportation often pollute roadside soils with toxic mixtures of petroleum derivatives, combustion byproducts, and metal contaminants (Diamond & Hodge, 2007). Of these contaminants, semivolatile organic compounds and metallic inorganics are commonly copresent. Among the most commonly encountered contaminants are high-molecular-weight polycyclic aromatic hydrocarbons (HMW-PAHs) and metals such as chromium, arsenic, lead, and manganese. The individual properties of these contaminants and co-contaminant interactions yield immense recalcitrance toward conventional soil-treatment technologies. Additionally, the recalcitrance of soil contamination toward conventional treatment technologies increases with decreasing soil particle size and permeability, thereby increasing associated complexity, costs, and treatment times. These challenges are especially problematic in Illinois where fine-grained low-permeability soils (i.e., silty clays) are predominant and soil regulations are among the most stringent (35 IAC §1100 §5F, 2012; Cahill, 2017; ELI, 2013). Additionally, projects are often spatially and temporally restrictive and require in situ treatments viable within short periods (ICT, 2017), whereas most conventional soil remediation processes are slow, with average timelines of 1–3 years (FRTR, 2007c). Consequently, transportation agencies often pursue costly excavation and off-site disposal rather than treatment to prevent extensive delays in construction. Excavation and off-site disposal were the most commonly employed methods for cleaning up hazardous waste sites prior to 1984 and remain the most cost-competitive options in many urban settings (FRTR, 2007b). However, contemporary issues have led transportation agencies to seek comparatively expeditious and affordable treatment technologies in lieu of excavation and disposal for use at all construction sites (ICT, 2017).

For these reasons, the objective of this work was to develop an accelerated in situ treatment approach adaptable for use at a typical Illinois construction site to remove HMW-PAHs and metals from clayey soil in a time frame comparable to excavation and disposal.

CASE STUDY: CONTAMINATED SOILS IN ILLINOIS

A preliminary subset of an Illinois Department of Transportation (IDOT) dataset of Illinois projects was used to determine the typically encountered roadside soil contaminants in Illinois. The dataset contained comprehensive analytical results from the environmental site assessments of 11 projects from 2004 to 2017. The dataset was analyzed to determine both the most commonly encountered contaminants that resulted in exceedance of the Maximum Allowable Concentrations (MACs) of Chemical Constituents in Uncontaminated Soil Used as Fill Material at Regulated Fill Operations (35 IAC §1100 §5F, 2012) as well as the most commonly encountered soil types in Illinois.

Soil Contaminant Inventory

An inventory of commonly encountered soil contaminants in exceedance of the MACs was developed from a review of Illinois projects. The dataset was analyzed using a combination of structured query language (SQL) scripting, Python scripting, data wrangling, and geographical information system (GIS)

processing, by means of the open-source programs DB Browser for SQLite, Anaconda (Spyder), OpenRefine, and QGIS, respectively. Two major contaminant categories were determined to typically exceed MAC regulations at IDOT construction sites: (1) semivolatile organic compounds (SVOCs) primarily as HMW-PAHs and (2) metals, majorly toxic and of industrial nature, and also some nontoxic common earth metals such as manganese. Table 1 provides the top 10 most frequently encountered contaminants in exceedance of the MACs. Because the geographic location of contamination influences only risk of exposure, not toxicity or hazard, it was chosen to evaluate MAC exceedances in two ways. The first is “Actual MAC Exceedance,” which refers to true violations of the geographically dependent MAC corresponding to the site’s location. The second is “Lowest MAC Exceedance,” which refers to cases in which the contaminant concentrations would have exceeded State regulations had the site been subject to geographically dependent regulations located elsewhere in Illinois. Of these contaminants, 50% were metals and 50% were HMW-PAHs. Further, metals and HMW-PAHs were copresent at 78% of sites where MAC exceedances occurred. Such a high copresence of metals and HMW-PAHs corroborates findings of the United States Environmental Protection Agency (EPA) that over 67% of contaminated sites contain both heavy metals and organic contaminants (USEPA, 2004). Refer to the tables in Appendix A for detailed data related to MAC exceedances for the selected sites.

Table 1. Top 10 Most Frequently Encountered Contaminants in Exceedance of the MACs

Contaminant	Sites with Actual MAC Exceedances		Sites with Lowest MAC Exceedances		Classification
	#	%	#	%	
Arsenic	6	54.5	6	54.5	Inorganic: Metalloid
Chromium	6	54.5	6	54.5	Inorganic: Metal
Manganese	6	54.5	6	54.5	Inorganic: Metal
Lead	5	45.5	5	45.5	Inorganic: Metal
Aluminum	4	36.4	4	36.4	Inorganic: Metal
Benzo(a)pyrene	4	36.4	9	81.8	SVOC: HMW-PAH
Dibenzo(a,h)anthracene	4	36.4	7	63.6	SVOC: HMW-PAH
Benzo(a)anthracene	4	36.4	7	63.6	SVOC: HMW-PAH
Benzo(b)fluoranthene	4	36.4	6	54.5	SVOC: HMW-PAH
Indeno(1,2,3-cd)pyrene	4	36.4	4	36.4	SVOC: HMW-PAH

*Out of 11 total sites. Because the geographic location of contamination influences only risk of exposure, not toxicity or hazard, it was chosen to evaluate MAC exceedances in two ways. The first is “Actual MAC Exceedance,” which refers to true violations of the geographically dependent MAC corresponding to the site’s location. The second is “Lowest MAC Exceedance,” which refers to cases in which the contaminant concentrations would have exceeded State regulations had the site been subject to geographically dependent regulations located elsewhere in Illinois.

Soil Characteristics

The success of soil-treatment technologies is highly a function of the physical and chemical properties of the soil matrix. As such, classification of the porous media is essential to prescribing any treatment, especially in cases where generalized approaches are desired. The most commonly encountered soil types at Illinois sites were determined. One common type of soil in Illinois is known as the Drummer soil series, which are defined as “very deep, poorly drained soils formed in loess or other silty material and in the underlying loamy stratified outwash on nearly level or depressional parts of outwash plains, stream terraces, and till plains” (USDA, 2015, p. 1). The Drummer soils are widely distributed in Illinois, located in over one-third of Illinois, and are most concentrated within the

central to northeastern regions of the state (USDA, 2019). These regions of highly concentrated Drummer soils coincide with the greatest project density in Illinois.

Drummer soils typically consist of eight stratified layers and belong to the taxonomic class Fine-silty, mixed, superactive, mesic Typic Endoaquolls (Table 2). The typical Drummer soil series spans the uppermost 5 ft of the surface and is composed primarily of silty clay loam. Clay, silt, and sand are soil particles with diameters less than 0.002 mm, between 0.002 mm and 0.05 mm, and between 0.05 mm and 2.0 mm, respectively (Adewunmi, 2019). The composition of silty clay loams may vary, but usually consist of 40%–72% silt, 27%–40% clay, and 0%–20% sand (USDA, 2010). On average, Drummer soils consist of 20%–35% clay, with less than 15% sand content, and are primarily composed of fine-grained silts (USDA, 2015, p. 1). The Drummer soils have relatively high levels of natural organic matter in the A horizon and a high presence of oxidized iron and manganese below. Natural organic matter has a high affinity for strongly bound contaminant sorption, and mineral oxides present a risk of prematurely catalyzing and quenching reactive oxidant species in the case of in situ chemical oxidation (ISCO) treatments. Furthermore, data from the National Resource Conservation Service (NRCS) Web Soil Survey, corresponding to coordinates of the MAC exceedances, display that most Illinois projects will overlie fine-grained, low-permeability clayey soil. See Appendix A for additional information related to soils in Illinois.

Table 2. Typical Drummer Soil Series

Horizon	Depth (cm)	Classification	pH	Notes
Ap	0–2.8	Silty Clay Loam	Moderately Acidic	A
A	2.8–5.5	Silty Clay Loam	Slightly Acidic	A
BA	5.5–7.5	Silty Clay Loam	Slightly Acidic	A, C
Bg	7.5–9.8	Silty Clay Loam	Neutral	A, C
Btg1	9.8–12.6	Silty Clay Loam	Neutral	A, C
Btg2	12.6–16.1	Silty Clay Loam	Neutral	B, C
2Btg3	16.1–18.5	Loam	Neutral	B, C
2Cg	18.5–23.6	Stratified Loam/Sandy Loam	Slightly Alkaline	C

(USDA, 2015, p. 1); Notes: A—High levels of natural organic matter in the form of fine, medium-sized roots; B—Medium levels of natural organic matter in the form of fine, medium-sized roots; C—High levels of oxidized iron and manganese masses in the soil matrix.

Previous research found that the statewide average minimum manganese content was 0.2% in the A horizon and 0.19% in the B horizon, with maximums of 3.13% and 7.75%, respectively (Cahill, 2017). These minimum percentages correspond to concentrations of 2000 mg/kg and 1900 mg/kg, which are well above the MAC thresholds for manganese (630–636 mg/kg). These concentrations mean that the average soil in Illinois will exceed the MACs simply because of naturally occurring mineral contents. Similarly, results adapted from the Dreher and Follmer Series indicate mean manganese concentrations of 1.43% across all soil horizons (14,300 mg/kg), which is roughly 23-fold higher than the regulatory threshold (Cahill, 2017). This information highlights the need for a treatment technology capable of reducing metals concentrations to meet regulations, even in the case of elements like manganese, which are naturally occurring and integral components of Illinois soils.

RESEARCH HYPOTHESIS

The goal of this research was to develop and test a treatment technology that was field scalable and rapid (i.e., one month) for removing HMW-PAHs and/or metals from clayey soil. Combinations of conventional in situ treatment technologies were leveraged to overcome their respective limitations and develop a promising approach. In situ chemical oxidation (ISCO) has been demonstrated to rapidly address organic contaminants yet faces difficulties in clayey soil and cannot remove inorganics (Huling & Pivetz, 2006). Electrokinetic separation has been demonstrated as an effective means of extracting both organic and inorganic contaminants from clayey soil, yet this process is both cost- and time-prohibitive without chemical enhancement (Reddy & Cameselle, 2009). The combination of electrokinetics with surfactant soil flushing can significantly reduce treatment duration; however, minimal contaminant destruction occurs, the surfactants persist, and costly ex situ treatment of the process fluid is required (Saichek & Reddy, 2005). For these reasons, the ability to couple electrokinetics with ISCO systems that exhibit surfactant-like properties may overcome such limitations for the cost- and time-effective remediation of co-contaminated clayey soils.

The combination of electrokinetics with chemical systems is called electrochemical treatment. Variations of electrochemical treatment have been demonstrated to remove both organic and inorganic contaminants from clayey soils by destruction and extraction respectively (Reddy & Al-Hamdan, 2013; Reddy et al., 2011). It was hypothesized that an in situ electrochemical treatment that augments conventional electrokinetics with pH control and enhanced hydrogen peroxide systems could rapidly and concurrently remove HMW-PAHs and/or metals from clayey soils.

CHAPTER 2: LITERATURE REVIEW

This chapter reviews the mechanistic properties pertinent to the electrochemical treatment of clayey soil co-contaminated with high-molecular-weight polycyclic aromatic hydrocarbons (HMW-PAHs) and metals. The following sections outline the recalcitrance of HMW-PAHs toward conventional soil-treatment technologies; the properties of chromium, which highlight it as an especially challenging metal contaminant to remove from soil; and interactions between HMW-PAHs and chromium, which increase their recalcitrance toward conventional treatment. The chapter also highlights the physicochemical mechanisms that partake during the electrochemical treatment of soils by electrokinetics augmented with electro-osmotically supplied hydrogen peroxide and conventional enhancements.

HIGH-MOLECULAR-WEIGHT POLYCYCLIC AROMATIC HYDROCARBONS

HMW-PAHs are environmentally ubiquitous, persistent, and among the most recalcitrant contaminants toward conventional in situ treatment technologies because of their stability and hydrophobicity (Kuppusamy et al., 2017; Menzie et al., 1992). HMW-PAHs are carcinogenic, poorly water-soluble aromatic compounds consisting of four or more fused rings. HMW-PAHs are hydrophobic organic contaminants (HOCs) with a high affinity for sorption to soil contents including mineral fractions and soil organic matter (SOM) (Duan et al., 2015; Patnaik, 2007). HOCs often diffuse within SOM, mineral aggregates, and across the fixed solid-liquid interface along soil particles (Alexander, 2000; Hatzinger & Alexander, 1995; Luthy et al., 1997). As such, HMW-PAHs must be desorbed from soil matrices prior to accessibility; however, their desorption is negligible under standard environmental conditions (Semple et al., 2003). These issues are amplified in clayey soils because of their naturally high SOM contents and extremely high particle surface areas, which yield ample sites for sorptive binding. The strength of contaminant sorption increases with longer contact time, greater SOM content, and smaller soil particle size, making aged HMW-PAH contamination in clayey soils especially arduous to treat (Duan et al., 2015).

HMW-PAHs are often present as nonaqueous phase liquids (NAPLs), which must be solubilized prior to most treatments (Brown et al., 1999). NAPLs are prone to entrapment within soil matrices, further limiting their accessibility and causing higher degrees of heterogenous distribution in the subsurface (Wick, 2009). NAPLs may exist in soil as residual pore fluid via retainment by capillary attraction between soil particles. This characteristic in addition to sorption results in isolated residual globules as opposed to singular continuous phase NAPLs (FRTR, 2007a). Isolated NAPL globules are difficult to detect and address, often resulting in inadequate remedial designs by which contaminants are left untreated. Further, HMW-PAHs are typically present as dense nonaqueous phase liquids (DNAPLs), which slowly disperse downwards throughout saturated soils. Isolated DNAPL globules may also be found on top of water in temporary or perched aquifers within the vadose zone, sorbed to soils throughout the capillary fringe (FRTR, 2007a). These features contribute to the highly heterogenous distribution of HMW-PAH contamination in soil systems and high recalcitrance to conventional treatment.

CHROMIUM

Chromium is prevalent, toxic, and challenging to remove from soils because of its sorptive tendencies and complex multiphase nature (James, 1996). The speciation of chromium in soil is highly dependent upon soil geochemical and physical properties, which influence its existence in either the trivalent form $[\text{Cr(III)}; \text{Cr}^{3+}]$ or one of the hexavalent forms $[\text{Cr(VI)}; (\text{CrO}_4)^{-2} \text{ \& } (\text{Cr}_2\text{O}_7)^{-2}]$. The sorption, solubility, and toxicity of chromium are dependent upon the speciation, as are co-contaminant interactions (Jardine et al., 2013). Hexavalent chromium species are highly toxic and mobile in clayey soils because Cr(VI) only bonds to cations in clayey soil systems. Conversely, trivalent chromium species are relatively nontoxic and stable in the environment. Cr(III) readily bonds to negatively charged clayey soils and precipitates to hydroxyl compounds at neutral pH; however, soil acidification or complexation with organic ligands may increase the mobility of Cr(III) . Several treatment technologies aim to reduce Cr(VI) to Cr(III) , yet this transformation is only temporary and fails to satisfy stringent soil regulations, which specify removal of total chromium content (35 IAC §1100 §§F, 2012). Further, Cr(III) displays some toxicity which it cannot be permanently degraded beyond. For these reasons, the complete removal of total chromium is necessary to achieve lasting reductions in site toxicity, yet the in situ extraction of soil-bound contaminants is immensely challenging.

CONTAMINANT INTERACTIONS

According to the USEPA (2004), over 67% of contaminated sites contain both heavy metals and organic contaminants. Soils co-contaminated by HMW-PAHs and Cr(III) are increasingly difficult to address. Trivalent chromium yields the ability to increase the hydrophobicity of HMW-PAHs, resulting in an increase in sorption capacity by over 100% (Liang et al., 2016). This interaction furthers the need for enhanced desorption and solubilization of HMW-PAHs to increase contaminant availability and dissolve NAPLs. However, treatments that successfully desorb HMW-PAHs may worsen site conditions through increasing the mobility and toxicity of chromium. Similarly, in situ processes that extract chromium may mobilize HMW-PAHs yet do nothing to lower their toxicity. This caveat significantly increases the difficulty of addressing sites where HMW-PAHs and chromium are copresent, as conventional treatment trains yield too much risk of dispersing these contaminants from soil toward underlying groundwater. For these reasons, clayey soils co-contaminated by HMW-PAHs and chromium require treatment technologies that concurrently exhibit (1) enhanced desorption and solubilization of both organic and inorganic compounds; (2) complete destruction of organic compounds; (3) reduction in toxicity of inorganic compounds; and (4) extraction of inorganic compounds. Further, the system must treat the soil homogenously to ensure no residual NAPLs are missed. This series of requirements is especially challenging to achieve in clayey soils, which maintain hydraulic conductivities (k_h) between 10^{-6} – 10^{-9} cm/s, whereas most conventional treatments rely upon hydraulic flow through permeable media ($k_h > 10^{-3}$ cm/s) (Reddy & Cameselle, 2009).

PHYSICOCHEMICAL TREATMENT MECHANISMS

Enhanced Hydrogen Peroxide Systems

The environmentally innocuous nature of hydrogen peroxide (H_2O_2) decomposition products allows for its common use for the in situ chemical oxidation (ISCO) of organic contaminants during

groundwater remediation. H_2O_2 is a thermodynamically unstable (ΔH° : $-98.2 \text{ kJ mol}^{-1}$; ΔS : $70.5 \text{ J mol}^{-1} \text{ K}^{-1}$), powerful oxidant (1.8 V), which readily decomposes to water and oxygen gas (Figure 1), absent of stabilization or reaction.



Figure 1. Equation. Equation 1 showing the decomposition of hydrogen peroxide to water and oxygen gas.

This mode of H_2O_2 decomposition is catalyzed by increasing solution temperature, pH, and H_2O_2 concentration. For this reason, the premature decomposition of highly concentrated H_2O_2 solutions is conventionally minimized via (1) acidification; (2) the addition of carboxylate stabilizers (e.g., sodium stannate); and (3) the addition of metal-ion inactivators (e.g., disodium phosphate), which serve to preserve stabilizer dispersion in the presence of otherwise interactive/catalytic metal contaminants (Schumb, 1957). Despite such stabilization being commercially commonplace to prolong the shelf life of H_2O_2 solutions, its application for ISCO is relatively innovative. In 2007, Watts et al. found that sodium -citrate, -malonate, and -phytate could be used to stabilize H_2O_2 in the subsurface, prolonging its residence time by up to 50-fold. Use of these solutions is referred to as stabilized hydrogen peroxide (SHP) systems. Alternatively, catalyzed hydrogen peroxide propagation (CHP) systems, which aggressively rely upon the catalyst-accelerated decomposition of H_2O_2 to yield potent reactive oxygen species (ROS), are a conventional means of addressing organic contamination.

In the context of remediation, CHP systems are typically named by misnomer as the conventional Fenton's reaction (Figure 2), which is the decomposition of dilute hydrogen peroxide (H_2O_2) as catalyzed by ferrous iron (Fe^{2+}) to produce ferric iron (Fe^{3+}), hydroxide anion (OH^-), and hydroxyl radical ($\text{HO}\bullet$) (Garrido-Ramírez et al., 2010; Haber & Weiss, 1934; Watts & Teel, 2005):



Figure 2. Equation. Equation 2 showing dilution of hydrogen peroxide.

The efficacy of this system toward degrading HMW-PAHs is primarily attributed to the $\text{HO}\bullet$, a powerful (2.8 V) nonselective oxidant capable of destroying *most* organic contaminants, excluding only highly halogenated alkanes, at near diffusion-controlled rates ($k_{\text{OH}\bullet} \approx 10^9 \text{ M}^{-1} \text{ s}^{-1}$) (Haag & Yao, 1992; Watts & Teel, 2005). CHP systems, correctly labeled Modified Fenton's reagent or Fenton's-like reactions, are a modern variation of the conventional Fenton's reaction, which differs in two ways. First, CHP systems sometimes substitute Fe^{2+} for various other catalysts, most typically multivalent metals, metal complexes, chelates, minerals, or the naturally occurring soil contents. Second, excess H_2O_2 concentrations relative to the analytical Fenton's Reagent (e.g., > 2%) are used to chain-propagate reactions that produce further potent reactive oxygen species (ROS) such as perhydroxyl radical ($\text{HO}_2\bullet$), superoxide anion radical ($\text{O}_2\bullet$), and hydroperoxide anion (HO_2^-) (Table 3, Eq. 3–8; Watts & Teel, 2005):

Table 3. Equations 3–8 (Watts & Teel, 2005)

Equations			Eq #
$\text{H}_2\text{O}_2 + \text{HO}\bullet \rightarrow \text{HO}_2\bullet + \text{H}_2\text{O}$		$k = 2.7 \times 10^7 \text{ M}^{-1} \text{ s}^{-1}$	$E_a = 14 \text{ kJ mol}^{-1}$ (Eq. 3)
$\text{HO}_2\bullet + \text{Fe}^{2+} \rightarrow \text{HO}_2^- + \text{Fe}^{3+}$		$k = 1.2 \times 10^6 \text{ M}^{-1} \text{ s}^{-1}$	$E_a = 42 \text{ kJ mol}^{-1}$ (Eq. 4)
$\text{H}_2\text{O}_2 + \text{Fe}^{3+} \rightarrow \text{Fe}^{2+} + \text{HO}_2\bullet + \text{H}^+$	pH \approx 3	$k = 2 \times 10^{-3} \text{ M}^{-1} \text{ s}^{-1}$	$E_a = 126 \text{ kJ mol}^{-1}$ (Eq. 5)
$\text{HO}_2\bullet + \text{Fe}^{3+} \rightarrow \text{Fe}^{2+} + \text{O}_2 + \text{H}^+$		$k = 1.2 \times 10^6 \text{ M}^{-1} \text{ s}^{-1}$	$E_a = 33 \text{ kJ mol}^{-1}$ (Eq. 6)
$\text{HO}\bullet + \text{RH} \rightarrow \text{R}\bullet + \text{H}_2\text{O}$	*RH = Organic Contaminant; R• = Alkyl Radical		(Eq. 7)
$\text{H}_2\text{O}_2 + \text{R}\bullet \rightarrow \text{ROH} + \text{HO}\bullet$		$k = 10^6 - 10^8 \text{ M}^{-1} \text{ s}^{-1}$	(Eq. 8)

Key features of the ROS generated via these chain-propagations include the following. First, HO_2^- acts as a strong nucleophile capable of attacking the bonds of organic contaminants with electron-deficient functional groups and undergoes perhydrolysis reactions at near diffusion-controlled rates (Siegrist et al., 2011). Second, $\text{O}_2\bullet^-$ acts as a weak nucleophile and reductant capable of destroying highly persistent compounds recalcitrant toward $\text{HO}\bullet$, such as hexachloroethane and carbon tetrachloride, in water-solid matrices (Furman et al., 2009; Smith et al., 2004; Watts et al., 1999). Third, excess H_2O_2 cycles the valence state of iron to reinitiate the chain-propagations and yield further ROS under an acidic pH regime (Figure 6). Fourth, and most pertinent to the treatment of HMW-PAHs and metals, $\text{O}_2\bullet^-$ exhibits surfactant-like properties responsible for the enhanced desorption of soil-partitioned contaminants and dissolution of NAPLs by CHP systems (Corbin et al., 2007; Smith et al., 2006, 2009). The significant $\text{O}_2\bullet^-$ flux generated by CHP systems can even desorb and mobilize substitutable components of the soil's crystalline matrix and metals strongly bound by electrostatic forces (Monahan et al., 2005; Rock et al., 2001). As such, CHP systems utilizing excess H_2O_2 may be considered an enhanced desorption and dissolution process, applicable toward removing strongly soil-bound contaminants including both metals and HMW-PAHs, including those present in the nonaqueous phase.

Furthermore, iron species are not the only appreciable catalyst when CHP systems are implemented in soils contaminated with metals. First, chromium can initiate CHP reactions resembling iron in conventional and Fenton-like reactions. The various valence states of chromium can catalyze H_2O_2 decomposition in a manner consistent with Equations 2 and 5 to produce additional $\text{HO}\bullet$, which significantly contributes to the destruction of HMW-PAHs (Table 4, Equations 9–12) (Bokare & Choi, 2010, 2011; Haight et al., 1970; Shi & Dalal, 1990; Shi et al., 1993; Shi et al., 1994, 1998; Tsou & Yang, 1996).

Table 4. Equations 9–12

Equation	PH Level	E #
$\text{Cr(III)} + \text{H}_2\text{O}_2 \rightarrow \text{Cr(VI)} + \text{OH}^- + \text{HO}\bullet$	pH \geq 5	(Eq. 9)
$\text{Cr(VI)} + \text{H}_2\text{O}_2 \rightarrow \text{Cr(V)} + \text{OH}^- + \text{HO}\bullet$	pH $<$ 5	(Eq. 10)
$2\text{Cr(VI)} \rightarrow \text{Cr(V)} + \text{Cr(III)}$	pH $<$ 5	(Eq. 11)
$\text{Cr(V)} + \text{H}_2\text{O}_2 \rightarrow \text{Cr(VI)} + \text{OH}^- + \text{HO}\bullet$	pH $<$ 5	(Eq. 12)

Chromium-mediated hydroxyl radical formation has been demonstrated as the longest-lasting CHP reaction (Genaro-Mattos et al., 2009). This feature helps to overcome the limited lifetime of ROS generated by CHP systems in highly catalytic soils such as those common to Illinois (Cahill, 2017; Kwan & Voelker, 2003; Watts et al., 1999). As shown by Equations 9–12 in Table 4, CHP systems in chromium-contaminated soils operate over a wide pH range (3–11) (Bokare & Choi, 2011), providing a wider window of operation than that of Fe-CHP systems. The caveat to Cr-CHP is the requirement that chromium is present as a contaminant. Unlike iron, chromium cannot be added to the soils for catalytic purposes because of its toxicity.

When leveraging chromium as a CHP catalyst, it is important to carefully manage its speciation. The oxidation of Cr(III) to Cr(VI) primarily occurs at $\text{pH} \geq 5$, whereas the reduction of Cr(VI) to Cr(III) by H_2O_2 occurs under acidic conditions. For this reason, operating CHP systems under an acidic pH regime allows for utilization of Equations 2–6 in combination with Equations 9–12 to generate immense ROS flux in the presence of excess H_2O_2 . This regime will also limit the deleterious conversion of Cr(III) to the more toxic hexavalent forms. Further, Cr(III) forms stable hydroxylated species in natural soil systems, which adsorb strongly to clay yet remain detached and soluble below a pH of 4.5 (Françoise & Bourg, 1991). These pH dependencies mean that operating CHP systems at an approximate pH of 3–5 will (1) convert Cr(VI) to less-toxic Cr(III) while destroying HMW-PAHs; (2) solubilize Cr(III) for extraction by concurrent technologies; and (3) leave residual chromium in a stable soil-bound form upon end of treatment, helping to avoid risk of Cr(VI) mobilization toward groundwater.

The manganese-rich Illinois soils (Cahill, 2017) may further enhance the desorption potential of CHP systems. In these soils, H_2O_2 is rapidly consumed by reaction with manganese to produce substantial $\text{O}_2^{\bullet-}$ flux as an intermediate in the formation of molecular oxygen (Watts et al., 2005). This reaction significantly contributes to the desorption of HOCs, while yielding highly exothermic conditions to stimulate the kinetics of concerted CHP reactions. Table 5 displays additional information on the mechanisms of CHP.

Catalytic minerals rapidly consume H_2O_2 , and significant concentrations are necessary to sustain CHP cycles that generate ample $\text{O}_2^{\bullet-}$ flux for the desorption of HOCs prior to their destruction by HO^{\bullet} (Quan et al., 2003; Watts et al., 2008). For this reason, contaminant hydrophobicity and the abundance of NAPLs are driving factors for determining oxidant dosage in CHP systems (Huling & Pivetz, 2006; Ko et al., 2012; Quan et al., 2003; Teel et al., 2009). However, reagent expenditure can be minimized through enhanced distribution systems, which ensure homogenous contaminant-oxidant contact and contribute to contaminant desorption (Reddy & Karri, 2008; Saichek & Reddy, 2005). Several chemical-based enhancements to CHP systems such as surfactants, pH amendments, and chelating agents may also be used to increase treatment efficacy and minimize H_2O_2 expenditure.

Table 5. Additional Mechanisms of Catalyzed Hydrogen Peroxide Propagations

Reactive Oxygen Species			
H ₂ O ₂	Hydrogen Peroxide	E ⁰ (H ₂ O ₂ /H ₂ O): 1.77V <i>Oxidant</i>	E ⁰ (O ₂ /H ₂ O ₂): 0.68V <i>Reductant</i>
HO•	Hydroxyl Radical		E ⁰ (HO•, H ⁺ /H ₂ O): 2.31V
O ₂ • ⁻	Superoxide Radical Anion		E ⁰ (O ₂ • ⁻ , 2H ⁺ /H ₂ O ₂): 0.94V
HO ₂ ⁻	Hydroperoxide Anion		
HO ₂ •	Perhydroxyl Radical		E ⁰ (HO ₂ •, H ⁺ /H ₂ O ₂): 1.06V
¹ O ₂	Singlet Oxygen		
H ₂ O ₂ ↔ HO ₂ ⁻ + H ⁺		pK _a = 11.7	(Eq. 13)
HO ₂ • ↔ O ₂ • ⁻ + H ⁺		pK _a = 4.8	(Eq. 14)
HO ₂ • + O ₂ • ⁻ + H ⁺ → H ₂ O ₂ + O ₂			(Eq. 15)
Cr(III)/Cr(IV)/Cr(V)/Cr(VI): CHP			(Bokare & Choi, 2010, 2011)
[Cr ^{VI} O ₄] ²⁻ + (n)H ₂ O ₂ → [Cr ^{VI} (O) ₃ (O ₂)] ²⁻ → [Cr ^{VI} (O)(O ₂) ₃] ²⁻ → [Cr ^V (O ₂) ₄] ³⁻			(Eq. 16)
[Cr ^V (O ₂) ₄] ³⁻ + H ⁺ → [Cr ^{VI} (O ₂) ₃ (O)] ²⁻ + HO•			(Eq. 17)
[Cr ^V (O ₂) ₄] ³⁻ → [Cr ^{VI} O ₄] ²⁻ + O ₂ • ⁻ + ¹ O ₂		pH < 5	(Eq. 18)
[Cr ^V (O ₂) ₄] ³⁻ + (n)O ₂ • ⁻ + (n)H ⁺ → [Cr ^V (O ₂) _{4-n}] ³⁻ + (n)HO• + (n)O ₂			(Eq. 19)
Mn(II)/Mn(III)/Mn(IV): CHP			(Jacobsen et al., 1998; Kim et al., 2017)
Mn(III) + H ₂ O ₂ → Mn(IV) + OH ⁻ + HO•		pH = 7;	(Eq. 20)
Mn(IV) + H ₂ O ₂ → Mn(III) + HO ₂ • + H ⁺		γ-MnO ₂	(Eq. 21)
Mn ²⁺ + HO• → Mn(III) + OH ⁻			(Eq. 22)
Mn(III) + H ₂ O ₂ → [MnO ₂] ⁺ + 2H ⁺ → Mn ²⁺ + HO ₂ • + H ⁺		pH = 0-2	(Eq. 23)
Mn(IV) + H ₂ O ₂ → Mn ²⁺ + 2H ⁺ + O ₂			(Eq. 24)

Surfactants

Surfactants may be used to increase contaminant mobility or solubility, depending on concentration used relative to the critical micelle concentration (CMC). The CMC is an intrinsic property of each surfactant, and above this concentration all additional surfactant added to a solution will form micelles rather than monomers. Surfactant monomers increase contaminant mobility by lowering interfacial tension at the solution interface. Surfactant micelles increase contaminant solubility through micellar solubilization (AATDF, 1997). Additionally, surfactant molecules are comprised of a hydrophobic and hydrophilic portion, the relative strength of which is characterized by the hydrophile-lipophile balance number (HLB). Water-insoluble contaminants are solubilized by surfactants with a low HLB, whereas high HLB surfactants are effective for contaminants of higher water solubility (AATDF, 1997). Surfactants are further categorized as either anionic, cationic, nonionic, or zwitterionic based on the charge of the molecular head group. Anionic and nonionic surfactants are relatively nontoxic and demonstrate insignificant sorption to soil surfaces, making them ideal for environmental application (Lee et al., 2007). Zwitterionic surfactants contain both anionic and cationic heads, allowing for interaction between hydrophilic and hydrophobic interfaces. These surfactants are also relatively nontoxic but can adsorb to soil contents. Conversely, cationic surfactants are highly toxic and sorb strongly to soil surfaces, making them a poor choice for environmental application (Lee et al., 2007). As such, surfactants should be specifically selected for each site based on their HLB and dosed according to their CMC to achieve the desired effect. Improper surfactant selection can lead to increased site toxicity or decreased soil permeability.

through undesirable side reactions and emulsion effects. Compatible surfactant selection is especially significant when they are used to enhance chemical transformation methods such as ISCO. Surfactants must either be compatible with the oxidant or applied sequentially (Wang et al., 2013; Yang et al., 2017).

pH Amendments

Acidic or basic solutions may be added to the soil to lower or raise soil pH, respectively. These amendments may serve to activate or catalyze chemical reactions, alter contaminant speciation for manipulation of mobility or toxicity, or return the site to neutral conditions post-treatment. The most commonly used bases are various sodium or ammonium hydroxides, silicates, and carbonates, while sodium hydroxide is considered the most effective because of its low cost. Recent works have also utilized simulated concrete pore solution (SCPS) (Table 6) as an alkaline pH amendment capable of reducing the corrosion of steel in electrochemical systems (Williamson & Isgor, 2016). To minimize environmental impact from acidic pH amendments, organic acids such as citric acid should be used in place of strong acids. Furthermore, many organic acids such as citric acid dually function as chelating agents when used to address metal contamination (Nogueira et al., 2007).

Table 6. Example Recipe of Simulated Concrete Pore Solution

Reagent	Concentration (M)	Concentration (g/L)
Calcium Hydroxide	0.1	7.409
Sodium Hydroxide	0.1	3.9997
Potassium Hydroxide	0.2	11.2211
Calcium Sulfate	0.003	0.4082

(Williamson & Isgor, 2016)

Chelating Agents

Chelating agents form soluble metal chelate complexes by donating multiple electron pairs to the metal ion. These chemicals may be used to desorb metal contaminants from soil and suspend them into solution for extraction or reaction in the aqueous phase. Selection of a chelating agent should target chemicals that form strong complexes over the operational pH regime and exhibit high specificity for the COC, low affinity for sorption to soil surfaces, and relatively negligible toxicity. Chelate complexes remain highly stable and water-soluble over wide pH ranges, which increases their mobility for extraction. Natural organic chelating agents such as citric acid readily biodegrade and require no recapture and treatment when used in situ to enhance metal extraction or stabilize hydrogen peroxide (Cameselle & Pena, 2016; Merdoud et al., 2016; Nogueira et al., 2007).

Electrokinetics

In situ electrokinetic treatments can be used to address sites contaminated with metals and PAHs (Page & Page, 2002). Electrokinetic treatments impose a low-intensity direct current electrical field throughout the soil by gridded placement of alternately charged electrodes (Figure 3), typically for the extraction of inorganic contaminants (Reddy & Cameselle, 2009). Electrochemical treatments augment electrokinetic treatments by the injection of electrolytic solutions and enhancing agents to increase the efficacy of inorganic extraction and/or the removal or destruction of organic

contaminants (Reddy & Cameselle, 2009). The electrical field is carried by ions adsorbed to soil contents and suspended in solution to induce fluid transport throughout fine-grained soils via the following electrokinetic mechanisms: (1) electro-osmosis, the transport of pore fluid from anode to cathode; (2) electromigration, the transport of ions and their complexes to the oppositely charged electrode; and (3) electrophoresis, the transport of charged colloids to the oppositely charged electrode (Acar & Alshawabkeh, 1993). These systems overcome issues of low permeability by generating an advective plug flow throughout soil capillaries via an electrical gradient as opposed to a hydraulic gradient, allowing for operation in clays, silts, sediments, and other media resistant to conventional hydraulic distribution systems (Reddy & Cameselle, 2009). Electro-osmotic flow may be used to solubilize and transport contaminants and distribute chemical reagents that enhance contaminant desorption or transformation. Concurrently, the electromigrative flux desorbs and transports inorganic contaminants to the electrodes where they may be extracted by methods such as electroplating, precipitation, or ion exchange filters (Acar & Hamed, 1991). Electrochemical systems are typically used to address low-permeability soils contaminated with metals but are widely amenable to chemical enhancement, which allows for the added in situ desorption and destruction of most organic contaminants. As such, these systems are the only viable in situ treatment alternative for highly heterogeneous soils of low permeability, which contain mixtures of HMW-PAHs and metals.

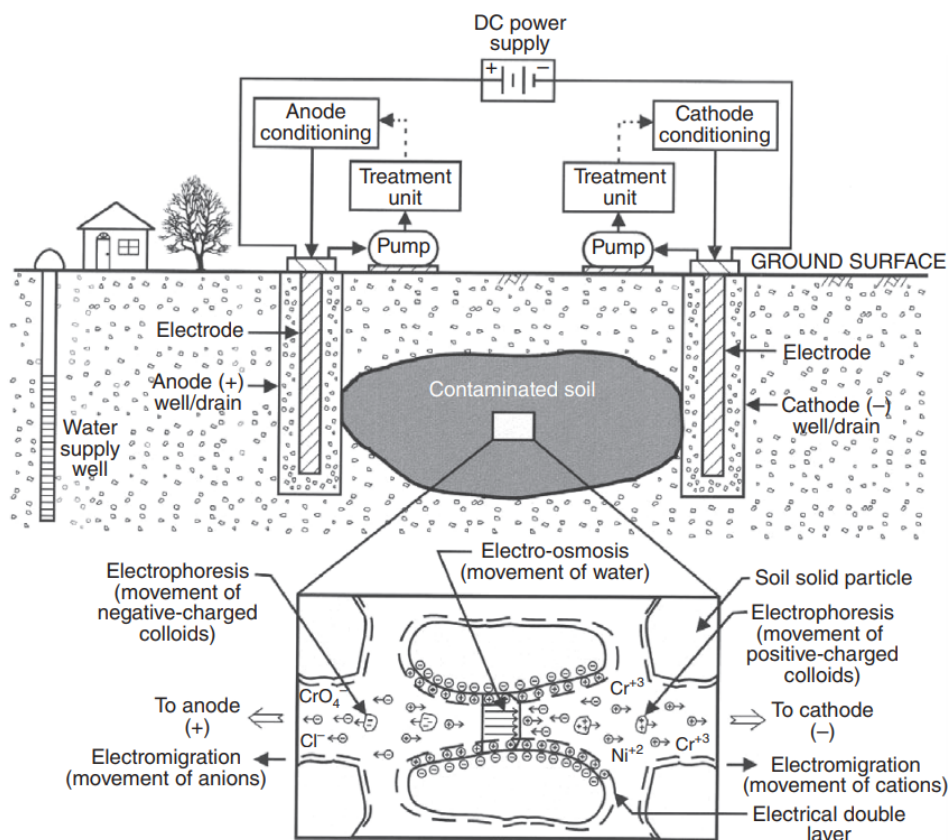


Figure 3. Schematic. Field-scale in situ electrochemical treatment with a diagram of electrokinetic transport mechanisms between clay particles.

As taken directly from Reddy and Cameselle (2009) with permission from John Wiley and Sons, Wiley Books: License Number 4703211191972.

Electrokinetics are a function of soil surface charge in clay-electrolyte systems. The original surface charge of clay particles is typically negative, determined by the isomorphous substitution of ions and reactions between surface functional groups with ions in the pore fluid (Sposito, 2016). The intrinsic surface charge of clay is considered the sum of permanent structural charge, dictated by isomorphous substitution, and the net proton charge, dictated by the relative concentration of H^+ and OH^- complexed by surface functional groups (Yeung, 2009). The net surface charge is further comprised of inner-sphere complex charge and outer-sphere complex charge, which consider sorptive processes with all other ions present in the pore fluid (Yeung, 2009). As such, the net surface charge of clay particles may fluctuate as a function of pore fluid composition, and depends primarily on electrolyte composition, ionic concentration, and soil pH. These interactions are best represented by the Gouy-Chapman-Stern-Grahame model of electrical double layer theory (Figure 4).

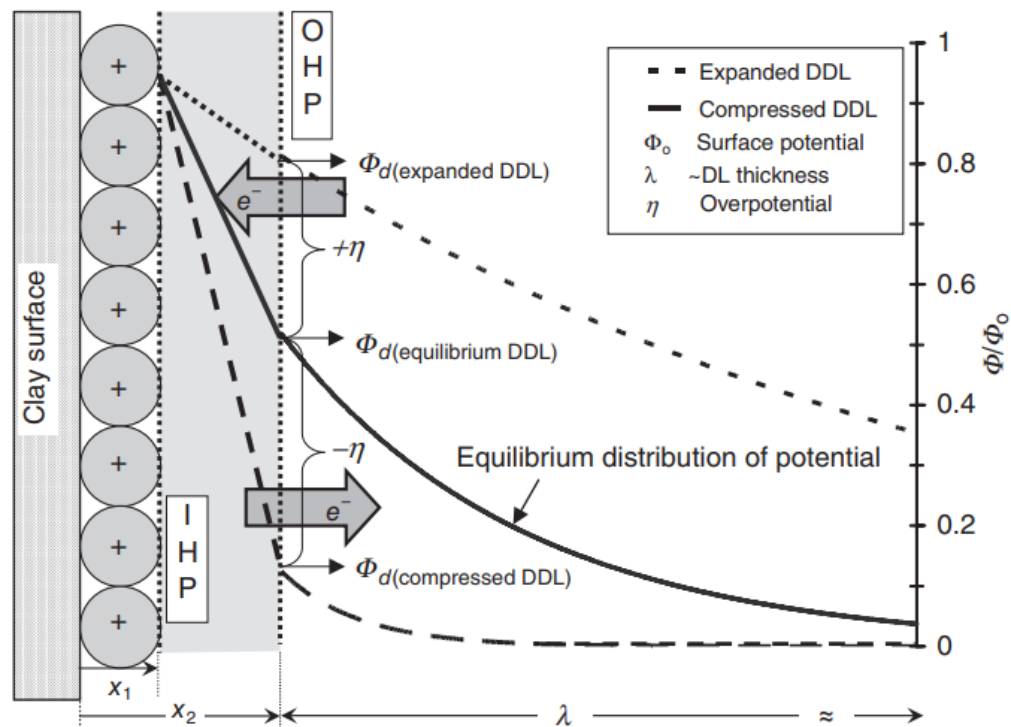


Figure 4. Schematic. The GCSG model interpretation of the electrical double layer theory with respect to a particle surface in a clay-electrolyte system.

As taken directly from Reddy and Cameselle (2009): Chapter 2, Pamukcu (2009) with permission from John Wiley and Sons, Wiley Books: License Number 4703211191972

According to the electrical double layer theory, hydrated particles in clay-electrolyte systems yield a fixed layer of specifically adsorbed counterions (Figure 4: X_1) and their solvation shells (Figure 4: X_2), together called the stern layer. The net surface charge of clay particles is approximated by measuring electrical potential across the stern layer, known as the zeta potential. Beyond the stern layer is a region of mobile charge called the diffuse layer (Figure 4: λ) in which counterions are only weakly attracted to the particle surface. This attraction decreases with distance from the stern layer, allowing ions to flow unimpeded by the intrinsic surface charge of clay particles, which has essentially

been neutralized (Pamukcu, 2009). It is the alignment of these electrical double layers in dense clay-electrolyte systems that allows for (1) the transport of ions and charge across particle surfaces; (2) the transfer of charge between particle surfaces and electrolytes in solution; and (3) the stern layer capacitance by which charge density is accumulated (Bard & Faulkner, 2000; Pamukcu, 2009). These phenomena throughout aligned electrical double layers induce relative motion between the clay and its pore fluid.

Electrokinetic phenomena are driven by the flow of electrical current throughout the electrical double layer by ionic and electrical conduction. Ionic conduction occurs throughout ions adsorbed to particle surfaces and electrolytes dissolved in solution. Electrical conduction is driven by stern layer capacitance and charge transfer across the solid-liquid interphase layers. Whereas electromigration is solely a function of ionic conductance, electro-osmosis is a surface-driven phenomenon inversely related to electrolyte concentration, and a function of both ionic and electrical conductance. Further, ionic conductance is a function of electrolyte concentration and is a reciprocally dynamic function of electromigration. Similarly, electron exchange across the stern layer not only drives electrical conduction, but also further stimulates sorptive fluctuations. As ionic conduction is partially a function of ions adsorbed to particle surfaces, these sorptive fluctuations alter electrokinetic mass transfer entirely (Pamukcu, 2009).

Electrokinetic mechanisms are a function of the electrical field strength, soil geophysical and geochemical properties, pore fluid composition and physicochemical properties, and all interactions therein that may influence characteristics of the electrical double layer (Yeung, 2009). For example, compression of the electrical double layer by high ionic concentration in the pore fluid inhibits electro-osmotic flow. Under the influence of an external electrical field, such compression induces a large spike in electrical potential across the stern layer (Figure 7: compressed DDL). This localized shift in electrical field intensity leads to electrostriction of the electrical double layer, which lowers stern layer capacitance, causing the release of electrons toward the bulk solution (Pamukcu, 2009). Such electron transfer generates faradaic current that stimulates cathodic redox reactions in the diffuse layer; alters pore fluid composition, particle surfaces, and sorptive processes; and influences transport retardation effects (Pamukcu, 2009). For this reason, particle surfaces in clay-electrolyte systems are often viewed as microelectrodes able to influence localized electrochemical diffusion across the solid-liquid interface. A mechanistic understanding of electrokinetic first principles is necessary to apply electrochemical treatments at the field scale where the electrochemical regime must be carefully engineered to preserve the efficiency of reagent and energy expenditure over time.

The simplest depiction of electrokinetic mass transport in clayey soils is given by adaption of the Nernst-Planck equation (Figure 5). The total mass flux of an ionic species over the field length between electrodes, $J_i(x)$, is described as a function of diffusive, migrative, and advective forces.

$$J_i(x) = - \underbrace{D_i^* \frac{\delta C_i(x)}{\delta x}}_{\text{Diffusion}} - \underbrace{u_i z_i C_i F \frac{\delta \Phi(x)}{\delta x}}_{\text{Migration}} - \underbrace{C_i v(x)}_{\substack{\text{Advection} \\ v_{adv} = v_{eo} \pm v_{em}}} \quad (\text{Eq. 25})$$

Figure 5. Equation. Nernst-Planck equation.

In equation 25, first, diffusion is simplified as a function of the ionic diffusion coefficient (D_i^*) and the ionic concentration gradient along the field length ($\delta C_i / \delta x$). Second, migration is simplified as a function of the ionic mobility (u_i), the ionic valence (z_i), the ionic concentration (C_i), Faraday's constant (F), and the electrostatic potential gradient along the field length ($\delta \Phi / \delta x$). Third, advection is simplified as a function of the C_i and the net advective velocity across the field length, $v(x)$, which includes both electro-osmosis and electromigration (Pamukcu, 2009). These forces are complex, as electromigrative forces may include both electrophoresis and electromigration, and advective forces include both electro-osmosis and electromigration. The inability to decouple fluid flow from its intrinsic ionic flux brings about the added significance of electrolysis reactions and localized electrochemical diffusion (Pamukcu, 2009).

Electrolysis

Ionic concentration gradients are inevitable during electrochemical treatments because of the CHP reactions and electrolysis reactions at the electrodes. Electrolysis may be exemplified by the electrolysis of water, including its oxidation at the anode (Equation 26) and its reduction at the cathode (Equation 27), which result in H_2O deprotonation to hydrogen ions and hydroxide anions.

Table 7. Equations 26–27

$2H_2O \rightarrow O_2 + 4H^+ + 4e^-$	Anode	$E^0 = -1.229 \text{ V}$	(Eq. 26)
$4H_2O + 4e^- \rightarrow H_{2(g)} + 4OH^-$	Cathode	$E^0 = -0.828 \text{ V}$	(Eq. 27)

The resulting ions are then transported throughout the soil at varying rates toward the oppositely charged electrode by electromigration, which develops acidic and basic fronts and alters soil pH. The fronts form at opposite ends of the system, forming strong chemical gradients. Because of the higher ionic mobility of H^+ than OH^- , the acid front typically dominates, and these ions converge near the cathode where they recombine to form water. The acidic pH regime dominant during electrochemical treatments promotes the desorption of metal cations, influences the dissociation of organic acids, and can determine which reactions occur in situ. Fluctuations in soil pH may negate or reverse the direction of electro-osmotic flow in cases where acidification or pH elevation beyond the clay's point of zero charge leads to reversal of the zeta potential (Yeung, 2009). Additionally, the sorption of hydrolysable metal cations onto negatively charged clay surfaces may induce similar effects on zeta potential and thus electro-osmosis (Hunter & James, 1992). For this reason, the pH must be controlled through chemical amendments in the electrode wells to control phenomena such as electro-osmosis in the soil. pH control in the electrode wells can also be used to influence the electrode effects and electrolysis of other compounds in addition to water.

The electrolysis of water in the electrode wells is the dominant electrolytic reaction, yet the electrical field can influence the speciation of all compounds in proximity to both the electrodes and the solid-liquid interface layer of energized clay particles. Both inorganic and organic contaminants can be transformed by electrolysis, as can the chemical reagents added to the electrode wells to enhance treatment. First, metals can be electrolytically transformed by the electrical field to promote solubilization or precipitation. Equations 28 and 29 in Table 8 demonstrate a generalized form in which metals (M_e) may be reduced to influence their speciation (Acar & Alshawabkeh, 1993).

Table 8. Equations 28–29

Equations	Eq. #
$M_e^{n+} + (n)e^- \rightarrow M_e$	(Eq. 28)
$Me(OH)_n + (n)e^- \rightarrow M_e + (n)OH^-$	(Eq. 29)

Electrolytic solubilization of metals can promote their effective transport by electromigration, after which electrolytic metal precipitation at the electrode wells is an effective means of metal contaminant removal. Conversely, metal precipitation by electrolytic reactions in the soil can yield ineffective electromigrative extraction. Secondly, electrolysis can transform and excite organic contaminants and treatment reagents through cation-anion annihilation.

The thermodynamics of the electrolytic transformation of contaminant/reagent molecule (M) in terms of Gibb's free energy (ΔG°) (Equation 30) can be described in terms of redox potential (ε°_{red} and ε°_{ox}) and Faraday's constant (F) (Equation 31) where the enthalpy of reaction (ΔH°) (Equation 32) in an electrochemical system is governed by the Nernst equation (Equation 33) (Hoytink, 1968; Romanias et al., 2014; Vasil'ev, 1970).

Table 9. Equations 30–33

Equations	Eq. #
$2M^+ + 2M^- \rightarrow 1M + 1M$	(Eq. 30)
$\Delta G^\circ = \{\varepsilon^\circ_{red} - \varepsilon^\circ_{ox}\}F$	(Eq. 31)
$\Delta H^\circ = \Delta G^\circ + T\Delta S^\circ = \Delta G^\circ - T\delta\Delta G^\circ/\Delta t = \{\varepsilon^\circ_{red} - \varepsilon^\circ_{ox}\}F - T\delta\{\varepsilon^\circ_{red} - \varepsilon^\circ_{ox}\}F/\Delta t$	(Eq. 32)
$\varepsilon_{cell} = \varepsilon^\circ_{cell} + 0.059\log_{10}(k_{M^-}/k_M)$	(Eq. 33)

The Nernst equation relates the standard electrode potential (ε_{cell}), temperature (T), and chemical activities (k_M) to the redox potential of an electrochemical reaction. Using this relation, the electrolytic reduction (Equations 34–37) or oxidation (Equations 38–40) of a molecule can be approximated for a given electrical potential. Such approximation further considers the temperature dependence of the redox potentials (Equation 41) and requires correction of the entropy based on electrostatic potential supplied (Equation 42) (Hoytink, 1968).

Table 10. Equations 34–42

Equation	Eq. #
$M + e^- \leftrightarrow M^-$	(Eq. 34)
$M^- + e^- \leftrightarrow M^{2-}$	(Eq. 35)
$M^- + HX \rightarrow MH^\bullet + X^-$	(Eq. 36)
$MH^\bullet + e^- \rightarrow MH^-$	(Eq. 37)
$M - e^- \rightarrow M^+$	(Eq. 38)
$M^+ + XY \rightarrow MY^\bullet + X^+$	(Eq. 39)
$MY^\bullet - e^- \rightarrow MY^+$	(Eq. 40)
$\delta\{\varepsilon^\circ_{red} - \varepsilon^\circ_{ox}\}/\Delta t = -0.008V \text{ deg. } C^{-1}$	(Eq. 41)
$\Delta H^\circ = \Delta G^\circ + 0.2Ev$	(Eq. 42)

By considering the solution temperature, electrical potential supplied, and the concentration of all known chemicals in the system, approximate predictions can be made for which electrolytic reactions will occur. This can be useful when determining reagent dosing, as adequate concentrations of reagents such as H_2O_2 must be selected such that they are not fully decomposed by electrolysis prior to their electrokinetic distribution. However, chemical concentrations in the environmental subsurface are often highly heterogenous and not fully known. This variability can lead to nonlinear and inaccurate prediction of electrochemical phenomena encountered at the field scale. Despite this uncontrollable circumstance, the electrode-well parameters such as pH, electrical intensity, and reagent/electrolyte concentration and composition may all be manipulated to influence successful contaminant removal based on optimization of the electrokinetic transport mechanisms electromigration, electrophoresis, and electro-osmosis.

Electromigration and Electrophoresis

Extraction of inorganic contaminants by electrokinetics occurs primarily by electromigration. Electromigration is defined as the transport of charged ions and their complexes toward the oppositely charged electrode. This mechanism serves to extract solubilized metal species from clayey soil as carried within the electro-osmotic flow (Figure 6).

$$v_{em} = u_i z_i n \tau F E_{x,t} \quad (\text{Eq. 43})$$

Figure 6. Equation. Equation 43.

Ion mobility is governed by the Nernst-Einstein-Townsend relation (Table 11, Equation 44), where the ionic diffusion coefficient (D_i^*) in electrochemical systems can be represented as a function of the molar limiting conductivity ($\Lambda_{m,i}^0$) for each electrolyte in solution (Table 11, Equation 45).

Table 11. Equation. Equations 44–45

Equation	Equation #
$u_i = \frac{D_i^* z_i F}{RT}$	(Eq. 44)
$D_i^* = \frac{RT}{z_i^2 F^2} \Lambda_{m,i}^0$	(Eq. 45)

Consequently, all aspects of electrokinetic transport in electrochemical treatment systems are dependent upon the diffusive flux of ions in pore solution, which dictate hysteresis by electrochemical gradients. Electrochemical diffusion within the bulk solution over time may be accurately predicted through numerical models that simultaneously solve the Nernst-Planck and Poisson's equations (Table 12, Equations 46 and 47) (Pamukcu, 2009). In this relationship, convection and ionic interactions are neglected such that charge density (ρ) becomes a function of the permittivity of the solvent (ϵ_s) and the electrostatic potential (Φ) with respect to time throughout the bulk fluid.

Table 12. Equations 46 and 47

Equation	Equation #
$\frac{\delta C_i}{\delta t} = \nabla(D_i^* \nabla C_i + u_i z_i F C_i \nabla \Phi)$	(Eq. 46)
$-\varepsilon_s \nabla^2 \Phi = \rho = \sum_i z_i F C_i$	(Eq. 47)

Evidently, the formation of ionic concentration gradients may yield spatial variation in conductivity, resulting in charge density accumulation and violating the local electroneutrality condition (Pamukcu, 2009). For this reason, diffusion potentials serve to eliminate charge separation and preserve electrical neutrality in the bulk fluid throughout regions of limited conductivity (Newman & Thomas-Alyea, 2004). However, electroneutrality within the electrical double layer (Figure 4) is a function of the Debye screening length (λ_D) relative to the field length (L) (Chu, 2005). Using a dimensionless form of Poisson's equation (Figure 7, Equation 48), it can be demonstrated that charge density accumulates along the stern layer and in proximity to the electrodes violating electroneutrality, while remaining negligible throughout the diffuse layer in field-scale clay-electrolyte systems where $\lambda_D \ll L$ (Chu, 2005; Pamukcu, 2009). Such charge density accumulation effectuates electromigration and consequently alters the electrical field.

$$-\varepsilon \nabla^2 \Phi = \sum_i z_i c_i \quad (\text{Eq. 48})$$

Where: $\varepsilon = \frac{\lambda_D}{L}; \Phi = \frac{\phi}{RT/F}; c_i = \frac{C_i}{C_{eq}}; \lambda_D = \sqrt{\frac{\varepsilon_s RT}{F^2 C_{eq}}}$

Figure 7. Equation. Equation 48.

Electromigration is unique because of its impact on bulk fluid current density. The average conductance of bulk fluid ions is at least one magnitude higher than conductance along the particle surfaces in natural clayey soil systems (Shang et al., 1994). Most electrical conductance occurs via electrolytes in solution, therefore their continuous electromigrative flux results in a constantly changing electrostatic potential. As electrolytes progress toward the electrodes and are extracted from the clay-electrolyte system, potential drops occur, therefore lowering the efficacy of electrokinetic treatments over time. The multivariate dependency of electromigration is represented by Figure 8, Equation 49, in which the electrical field strength is demonstrated to be a function of bulk current density (j_b), the distribution of charge-carrying ions by electrochemical diffusion, and the bulk conductivity (σ_b), as a function of time along the field length (Pamukcu, 2009).

$$E(x, t) = \frac{j_b(t) + F \sum_i z_i D_i^* \frac{\delta C_i(x, t)}{\delta x}}{\sigma_b(x, t)} \quad (\text{Eq. 49})$$

Figure 8. Equation. Equation 49.

Furthermore, the electromigrative flux of ions may be augmented or retarded by electro-osmosis, which can impact the extraction of metals by microscale advection. As electromigration occurs within the diffuse layer, and to some extent the bulk fluid, flow of the soil pore fluid can also impact the electrical field strength through an alternative mechanism of ion transport.

Electro-osmosis

Electro-osmosis depends upon the electromigration of cationic electrolytes, which distribute water carried in their solvation shells. This transport occurs primarily within the diffuse layer, imparting viscous drag on the bulk solution to induce advective flow. It is this advective flow that allows for the distribution of H_2O_2 and other neutrally charged species throughout electrochemical treatment systems. Electro-osmotic H_2O_2 distribution allows for in situ CHP reactions to be catalyzed by the naturally occurring soil contents and contaminants. Electro-osmotic flow homogenously distributes chemical amendments throughout clay systems despite negligible hydraulic conductivity. In clayey soils where k_h is negligible and electrolyte concentrations are low, electro-osmosis serves as the dominant fluid transport mechanism (Reddy & Cameselle, 2009). For this reason, Darcy's law for fluid flow through a porous medium in response to a hydraulic gradient is not appropriate for representing electro-osmotic flow through clayey soils. Rather, electro-osmotic velocity, v_{eo} , may be represented by the Helmholtz-Smoluchowski (H-S) theory (Figure 9, Equation 50) as a function of ε_s , the viscosity of the pore fluid (η), the zeta potential of the soil particles (ζ), and $E_{X,t}$. Electro-osmotic velocity may also be denoted as a function of the coefficient of electro-osmotic conductivity (k_{eo}) or adapted to a measure of volumetric electro-osmotic flow (Q_{eo}).

$$v_{eo} = \frac{\varepsilon_s \zeta}{\eta} \cdot \frac{\delta \Phi}{\delta x} = k_{eo} E_X \rightarrow Q_{eo} = v_{eo} A \quad (\text{Eq. 50})$$

Figure 9. Equation. Equation 50.

When horizontal electrode configurations are utilized as in Figure 6, there exists little potential for deleterious contaminant dispersion in comparison to conventional hydraulic systems. Electro-osmosis occurs as a microscopic plug flow, driven by electrical conductance at the stern layer in the direction of the electrical field (Pamukcu, 2009). For this reason, electro-osmosis is often assumed to be majorly one-dimensional and uniform throughout clays between the electrodes. However, in macroscopic systems, soil heterogeneities as well as chemical and ionic gradients occurring in pore fluid may alter electro-osmotic flow. This assumption with use of the H-S equation often results in nonlinear predictions and an inability to assume steady state conditions, creating challenges for those looking to implement electrochemical treatment at the field scale (Pamukcu, 2009). Inadequate optimization may result in unintended side reactions, shifts in electrical double layer thickness, shifts in electrolyte composition, loss of conductivity, and reverse of either electromigrative or electro-osmotic flow. For this reason, it is important to learn from successful past implementations of electrochemical treatment for proof of concept and initial parameter selection for the electrochemical regime. Refer to Appendix B for additional information related to electrochemistry and the corresponding reactions and principles.

Past Implementations of Electrokinetic Treatment Technologies

Numerous laboratory and field-scale studies have demonstrated the ability for electrochemical treatments to address chromium, manganese, or PAH contamination individually. Gent (2004) demonstrated the ability for pH-amended electrokinetics to extract chromium from clayey soil at the field scale. The site consisted of 125m³ of unspecified soil contaminated to a depth of 3 m with 180–1100 mg/kg chromium. By maintaining a pH of 4 using citric acid as an enhancing agent, chromium was removed from 78% of the soil over 6 months. Approximately 5% of the total chromium was extracted in the electrode wells, whereas the remaining chromium was concentrated around the cathode for targeted excavation. Surprisingly, the authors found their field-scale implementation to be more effective than initial bench-scale results (Gent, 2004). The Gent (2004) study supports the hypothesis that electrochemical treatment at an acidic pH can transport chromium in situ, yet the authors' results leave room for potential improvement via the addition of CHP systems. Further, Alcántara et al. (2008b) demonstrated the ability for EK-CHP to destroy 99% of the low-molecular-weight (LMW) PAH phenanthrene in clayey soils in only two weeks at the bench scale. Additionally, they demonstrated the ability for 10% H₂O₂ added to the anode and cathode reservoirs to maintain low pH systemwide absent of acid amendments. They found this regime more effective than the addition of 10% H₂O₂ to only one reservoir with sulfuric acid added to maintain pH (Alcántara et al., 2008b). The study by Alcántara et al. (2008b) suggests that distribution of H₂O₂ through both reservoirs may yield higher chromium extraction efficiency than that achieved by Gent (2004), who utilized acid absent H₂O₂. Finally, Reddy and Karri (2008) investigated the ability for electrochemical treatment with H₂O₂ to concurrently extract heavy metals and LMW-PAHs. In their work, nickel and phenanthrene were used as model contaminants. Negligible nickel was removed, while up to 56% phenanthrene destruction was achieved (Reddy & Karri, 2008). These poor results likely stem from the low iron concentrations in the soil (~693–1300 mg/kg) and the lack of pH control at the cathode leading to precipitation of nickel. However, combined interpretation of these studies suggests that pH-controlled EK-CHP should succeed in mineral-rich Illinois soils for the concurrent removal of HMW-PAHs and chromium with proper control of the electrochemical regime.

CHAPTER 3: METHODOLOGY

MATERIALS

Soil Characteristics

Experiments were conducted using kaolinite clay obtained from the Old Hickory Clay Company (Kentucky clay No. 5, Mayfield, Kentucky). Kaolinite clay was specifically selected because of its high specific surface area and low cation-exchange capacity. The relatively simple composition of kaolinite yields an ideal model clay for interpretation and optimization of the electrochemical mechanisms. Table 13 summarizes the index and mineralogy properties for the kaolinite used.

Table 13. Index Properties and Mineralogy of Kaolinite Clay

Specific Surface Area (m ² /g)	Method: drying-based single point	12
Cation Exchange Capacity (meq/100g)	Method: ammonium displacement	5.5
*Specific Gravity		2.58
*Particle Size Distribution (% less than)		
5μm		86
2μm		74
1μm		60
0.5μm		48
Median Particle Diameter (μm)		0.67
*Loss on Ignition (%)		9.79
*Chemical Analysis (%)		
SiO ₂		56.95
Al ₂ O ₃		29.01
Fe ₂ O ₃		0.88
TiO ₂		2.26
CaO		0.11
MgO		0.26
Na ₂ O		0.80
K ₂ O		0.69

(Akin & Likos, 2017a, 2017b); *Values specified by clay supplier.

Chemical Reagents

All reagents were prepared using ACS Grade chemicals and type 1 ultrapure water (18.2 M Ω ·cm at 25°C) purified by a Milli-Q® Advantage A10 Water Purification System. The following chemicals were utilized: (1) VWR Chemicals BDH®: Brij™35 (Polyoxyethylene [23] lauryl ether), citric acid monohydrate, hexane, hydrogen peroxide, potassium hydroxide, and sodium sulfate; (2) Thermo Fisher Scientific: ammonium molybdate, chromium(VI)oxide, manganese(IV)oxide, and potassium iodide; (3) J.T. Baker: calcium hydroxide, calcium sulfate, nitric acid, sodium hydroxide, soluble potato starch, and sulfuric acid; (4) Cotronics Corporation: RESCOR™ CER-CAST Ceramic 780 alumina oxide; (5) Arcos Organics: pyrene; (6) Sigma Aldrich: sodium thiosulfate; (7) Research Products International: trisodium citrate; and (8) A-L Compressed Gases, Incorporated: compressed argon gas (99.985%) and ultra-pure helium gas (>99.999% He).

Bench-scale Electrochemical Reactor

Bench-scale reactors resembling field-scale in situ electrokinetic systems (Figures 10–12) were designed and fabricated to assess the electrochemical treatment of soils co-contaminated with HMW-PAHs and metals. Each reactor consists of two 350 mL chlorinated polyvinyl chloride (CPVC) electrode wells situated 20 cm apart, from the centroid of powered-electrode-to-powered-electrode, in a high-density polyethylene (HDPE) soil cell with an initial working volume of 8.5 L. Class A/B glass fiber filters (Φ 1 μ m) were used to prevent soil intrusion into the electrode wells. Molded superfine graphite rods (0.5"OD \times 12"L; Graphtek™ LLC.; Resistivity: 0.00050 ohm/inch) were selected for their corrosion resistance, cost-efficacy, and low affinity for hydrogen peroxide decomposition relative to other materials and were utilized for all electrodes (Minghua et al. 2018; Rueffer et al., 2011). Electrolytic solutions containing various salts, surfactants, and/or oxidants were leveraged to distribute electrical current, facilitate contaminant removal, adjust pH, and retain/rehabilitate post-treatment soil integrity. The level of electrolytic solution in each electrode well was maintained by automated pumping to the anode well and overflow to sample collection from the cathode well, thereby isolating electro-osmotic flow by preventing differences in piezometric head. A direct current power supply (Dr. Meter 30 V/5A DC) was used to impose a low-intensity electrical field (1.5 V/cm to 3 V/cm) throughout the soil between electrodes for driving electrokinetic transport of the electrolytic solution and contaminants. In experiments 4–6, experimental surcharge plates were utilized to prevent soil swelling from gas generation, informed by the observations and challenges in experiments 1–3. Experiments 4 and 5 used a prefabricated concrete surcharge plate lined with HDPE. Experiment 6 used a surcharge plate formed in place from reaction-bonded alumina oxide ceramic (RESCOR™ CER-CAST Ceramic 780; 8 lb).

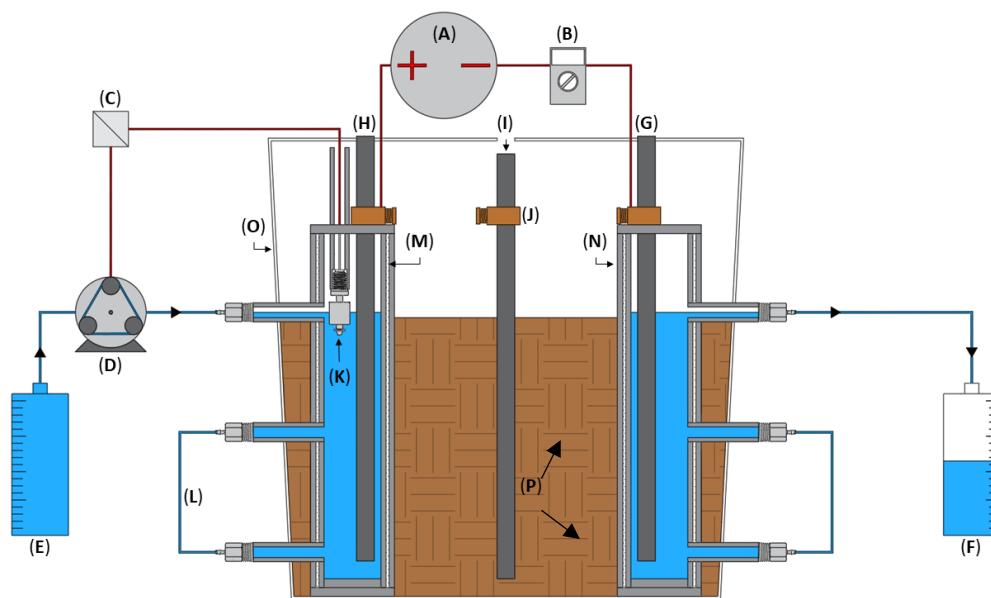


Figure 10. Schematic. Cross-sectional schematic of the bench-scale electrochemical reactor.
(A): Direct current power supply; (B): Digital multimeter; (C): Power relay; (D): Peristaltic pump;
(E): Anode-well solution reservoir; (F): Reactor outflow reservoir; (G): Cathode; (H): Anode;
(I) Auxiliary electrode; (J): Copper grounding rod clamp; (K) Normally closed float switch; (L): Tygon
tubing sight glass; (M): Glass fiber filter; (N) Nested CPVC Pipes referred to as electrode wells;
(O): HDPE soil cell; and, (P) Contaminated soil.

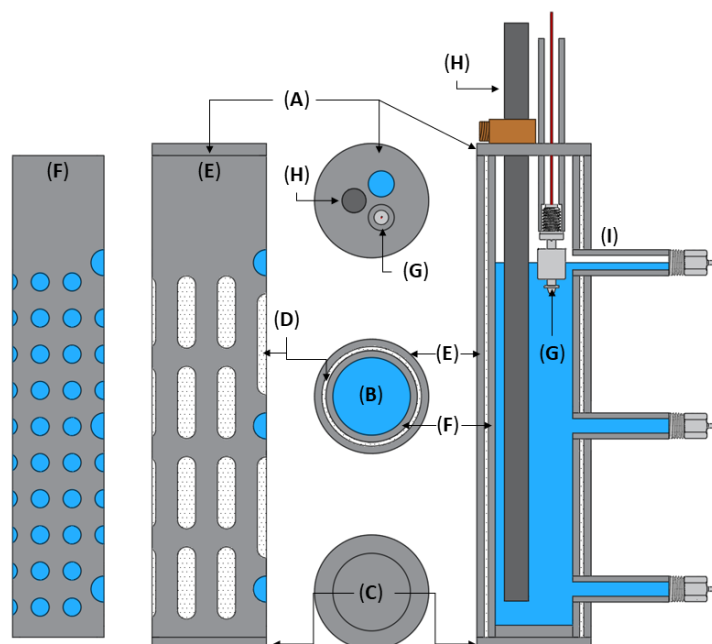


Figure 11. Schematic. Parts and detailed schematic of the modular electrode-well components.
(A): Removable cap with access ports; (B): Electrode-well reservoir; (C): Well bottom connected to
the outer pipe only; (D): Glass fiber filter; (E): Outer CPVC pipe; (F): Inner CPVC pipe;
(G): Normally closed float switch; (H): Electrode; (I) Electrode-well inflow/outflow.

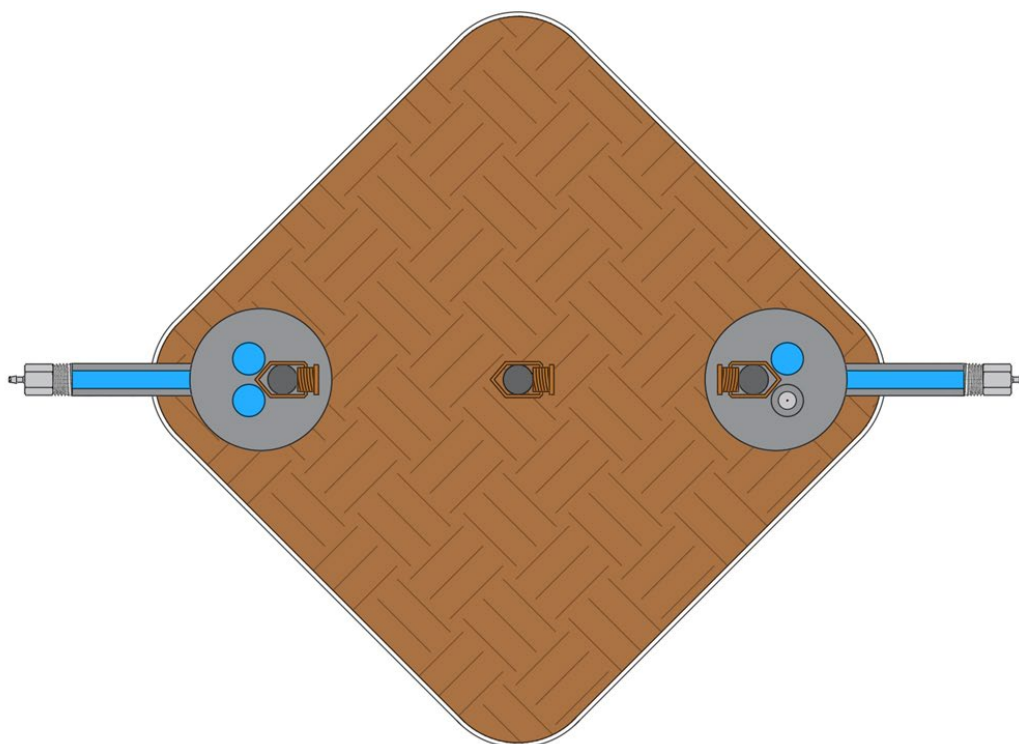


Figure 12. Schematic. Top-down schematic of the bench-scale electrochemical reactor.

EXPERIMENTAL DESIGN

Soil Spiking

Six bench-scale experiments were carried out to investigate the efficacy of electrochemical treatment toward removing HMW-PAHs and metals from clayey soil. Table 14 provides a summary of the pretreatment soil properties for each experiment.

Table 14. Summary of Initial Soil Properties

Experiment	Contaminant(s)	Concentration (mg/kg)		Avg. pH	Avg. Moisture Content (%)
		Dry	Wet		
1	Pyrene	500	300	5.5	40.1
2	Pyrene	500	300	5.8	40.9
3	Pyrene	500	300	5.9	40.5
4	Pyrene	500	300	5.8	38.1
5	Manganese	1,580	1,235	3.8	21.8
6	Pyrene, Chromium	500, 260	300, 163	2.5	37.2

Spiked Soil :10 kg—Dry kaolinite; Kentucky clay No. 5; Volume: ~8530 cm³

For experiments 1–4, 10 kg of dry kaolinite was contaminated with 500 mg/kg pyrene. Five batches of 2 kg kaolinite powder were mixed with 1 L of 1 g-pyrene/L-hexane solution in a planetary mixer at

135 rpm until uniformly saturated, followed by manual grinding to ensure passage through a No. 4 sieve (4.76 mm). The laboratory contaminated kaolinite batches were stored in shallow pans in a fume hood and mixed daily for 10 days to evaporate the hexane. After 10 days, Milli-q water was added to each batch, and the pans were covered for 24 hours to allow moisture equilibration at the desired water content (40% w/w), thereby achieving an initial wet concentration of 300 mg/kg pyrene.

For experiment 5, 10 kg of dry kaolinite was contaminated with 2.5 g/kg of MnO_2 , resulting in 1,580 mg/kg manganese. Five 2 g batches were mixed with 2 L of 1.25 g- MnO_2 /L-7% HNO_3 solution in a planetary mixer, followed by manual grinding. The batches were stored in shallow pans and heated at 120°C for 48 hours, mixing every 12 hours to evaporate the HNO_3 . After cooling to ambient temperature, Milli-q water was added to each batch, and the pans were equilibrated at the soil's optimum water content 21.8% w/w to achieve an initial wet concentration of 1,235 mg/kg.

For experiment 6, 10 kg of dry kaolinite was contaminated with 500 mg/kg of CrO_3 , resulting in 260 mg/kg hexavalent chromium. Five 2 kg batches were contaminated with 2 L of 250 mg- CrO_3 /L-7% HNO_3 consistent with experiment 5. After drying and cooling, the batches were contaminated with pyrene consistent with experiments 1–4 and wetted to achieve an initial water content of 40% w/w with initial contaminant concentrations of 163 mg/kg chromium and 300 mg/kg pyrene.

Following spiking for each experiment, the total soil volume was loaded into the reactor in five layers by categorized batch, each tamped with a carbon rod to minimize voids and ensure uniformity.

Electrochemical Regime

In this work, the electrochemical treatment utilizes electro-osmosis to facilitate the advective distribution of H_2O_2 and various enhancing agents homogeneously throughout clayey soils as a microfluidic plug flow while electromigration transports metal contaminants for extraction. Included in Table 15 is a summary of the electrochemical regime used in each experiment. Further detail is provided for each experiment in Chapter 4 and Appendix C.

Table 15. Summary of Electrochemical Regime by Experiment

Experiment	Duration (Days)	Initially Supplied		Electrical Potential	pH Adj.	Surcharge
		Anode Well	Cathode Well			
1	14	– 10% H_2O_2 & 0.1 M Citrate Buffer	– 10% H_2O_2 & 0.1 M Citrate Buffer	30 V 1.5 V/cm	No	No
2	7	– 5 g/L Brij™35 & 0.1 M Citrate Buffer	– 5 g/L Brij™35 & 0.1 M Citrate Buffer	30 V	No	No
	7	– 10% H_2O_2 & 0.1 M Citrate Buffer	– 10% H_2O_2 & 0.1 M Citrate Buffer	1.5 V/cm		
3	14	– 5 g/L Brij™35 & 0.1 M Citrate Buffer	– 5 g/L Brij™35 & 0.1 M Citrate Buffer	30 V 1.5–3 V/cm	No	No
4	2	– 10% H_2O_2 &	– 10% H_2O_2 &	30 V	Yes	Yes

Experiment	Duration (Days)	Initially Supplied		Electrical Potential	pH Adj.	Surcharge
		Anode Well	Cathode Well			
		0.1 M Citrate Buffer	0.1 M Citrate Buffer	1.5 V/cm		
	12	– 3% H ₂ O ₂ & 0.1 M Citrate Buffer	– 3% H ₂ O ₂ & 0.1 M Citrate Buffer			
5	14	– 10% H ₂ O ₂ & 0.1 M Citrate Buffer	– 10% H ₂ O ₂ & 0.1 M Citrate Buffer	30 V	Yes	Yes
	7	– 10% H ₂ O ₂ & 0.1 M SCPS	– 10% H ₂ O ₂ & 0.1 M SCPS	1.5 V/cm		
6	28	– 10% H ₂ O ₂ & 0.1 M Citrate Buffer	– 10% H ₂ O ₂ & 0.1 M Citrate Buffer	30 V 1.5–3 V/cm	Yes	Yes

Selection of Contaminants

Model contaminants were selected to represent Illinois contaminants of concern (COC) for use in bench-scale experimentation. Pyrene was selected as a model HMW-PAH contaminant because of its similar chemical attributes to benzo(a)pyrene, the most prevalent yet incredibly toxic COC. Hexavalent chromium was selected as a model toxic metal contaminant because of its prevalence, multiphase behavior, and challenging interactions with HMW-PAHs. Manganese was selected as a model nontoxic metal contaminant because of its prevalence in Illinois as both a common earth element and cause for regulatory exceedance.

Selection of Chemical Reagents

States such as Illinois, and more so California, regulate waters more broadly than is required by the federal Clean Water Act (ELI, 2013). For this reason, both Illinois and California underground injection restrictions were assessed to ensure not only Illinois regulatory acceptance, but also that the most environmentally friendly chemical reagents were selected. Hydrogen peroxide, citric acid, sodium citrate, calcium hydroxide, sodium hydroxide, and ethoxylated surfactants are included in the Los Angeles, California, Water Boards' list of authorized injection material amendments (State of California, 2019). For this reason, a nonionic polyoxyethylene surfactant (Brij™35) and the simulated concrete pore solution (SCPS) reagents outlined in Table 5 were chosen as augmentations to stabilized hydrogen peroxide (SHP) and catalyzed hydrogen peroxide propagation (CHP) systems because both reagents show promise for field implementation.

It was chosen to utilize SHP solutions while relying upon the metal oxide minerals and contaminants present in the soil to yield CHP reactions, as opposed to supplying external catalysts, for several reasons. First, iron oxides such as ferrihydrite, goethite, hematite, and magnetite can catalyze the decomposition of H₂O₂ to yield HO•. This form of catalysis functions from pH 3–7, as a function of iron speciation (Fe²⁺ > Fe³⁺), iron oxide surface area, concentration, and H₂O₂ concentration (Kwan & Voelker, 2003). Furthermore, Watts and Teel (2005) suggested that externally supplied soluble iron yields too rapid a rate of H₂O₂ decomposition in soils, disallowing for its transport down gradient and the necessary oxidant-contaminant contact time.

Brij™35 was investigated for its potential to supplement contaminant desorption for improving both contaminant-oxidant contact and contaminant extraction via the electrophoresis of contaminant colloids formed by micellar solubilization. Past treatments had success in augmenting HMW-PAH removal by enhancement with Brij™35. Soil washing experiments using Brij™ 35 found it to be the most effective augmentation for the removal of benzo(a)pyrene (BaP) from soil. In their work, Madadian et al. (2014) found 5 g/L Brij™35 to remove 85.81% and 79.94% of BaP from the coarse and fine soil fractions, respectively, while removing 81.66% of total PAHs considering the copresence of the LMW-PAHs anthracene and naphthalene (Madadian et al., 2014). Similarly, augmentation of electrokinetics with 10 g/L Brij™35 achieved 84% (BaP) removal, the highest removal relative to enhancement with the other surfactants Mergol, Tergitol, Tween 20, Tween 80, and Tyloxapol (Alcántara et al., 2008a). Finally, Gomez et al., (2009) utilized a two-stage electrochemical treatment approach in which electrokinetic extraction augmented with anodic pH control (pH = 7) and 1% Brij™35 was followed by electrochemical oxidation to treat the liquid waste stream. In 33 days, they were able to extract 76% of the BaP (Gómez et al., 2009). The extracted BaP was then completely destroyed in only 16 hours by an electrochemical oxidation reactor that utilized graphite rods for the active electrodes (Gómez et al., 2009).

Laboratory Soil Sampling for Analyses

Pretreatment: Figure 13 portrays the pretreatment sampling scheme described in the “Soil Spiking” section, used to characterize each laboratory spiked soil layer prior to loading the reactor. In single contaminant experiments (experiments 1–5), each point was used for a single parameter measurement to achieve high spatial variability between samples. In the co-contaminant experiment (experiment 6), the pH samples were subsequently used for pyrene analysis such that metals analysis could be performed without increasing the mass of soil removed pretreatment.

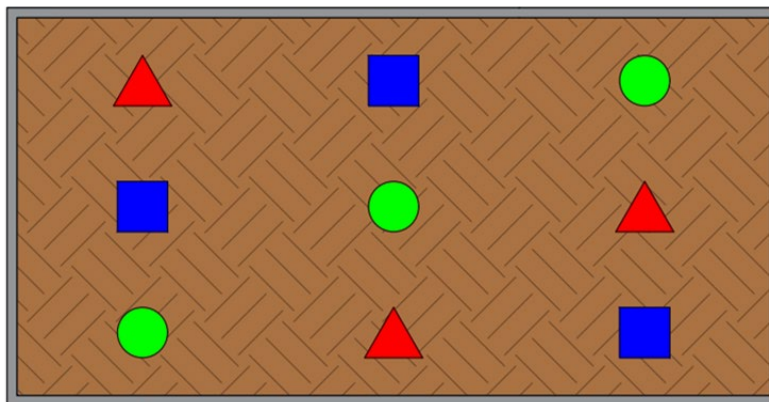


Figure 13. Plan. Pretreatment batch sampling plan for soil characterization. Sample points: red triangle = pH/secondary contaminant; blue square = moisture content; and green circle = contaminant concentration.

Post-treatment: Samples were sequentially collected from the reactor in four layers, anode to cathode, top to bottom, according to the coordinate system in Figure 14. Accordingly, 64 samples were collected for each measured parameter at 5 cm spacing in three-dimensions between the electrodes. This sampling system allowed for a 3D delineation of the post-treatment contaminant

concentrations, pH, and moisture content. The results and plots in Chapter 4 reference these coordinates as sample names; for example, X,Y,Z: 2.5, +5, 17.5, refers to the section closest to the anode well, offset 5 cm to the left of the electrodes, and in the bottom layer.

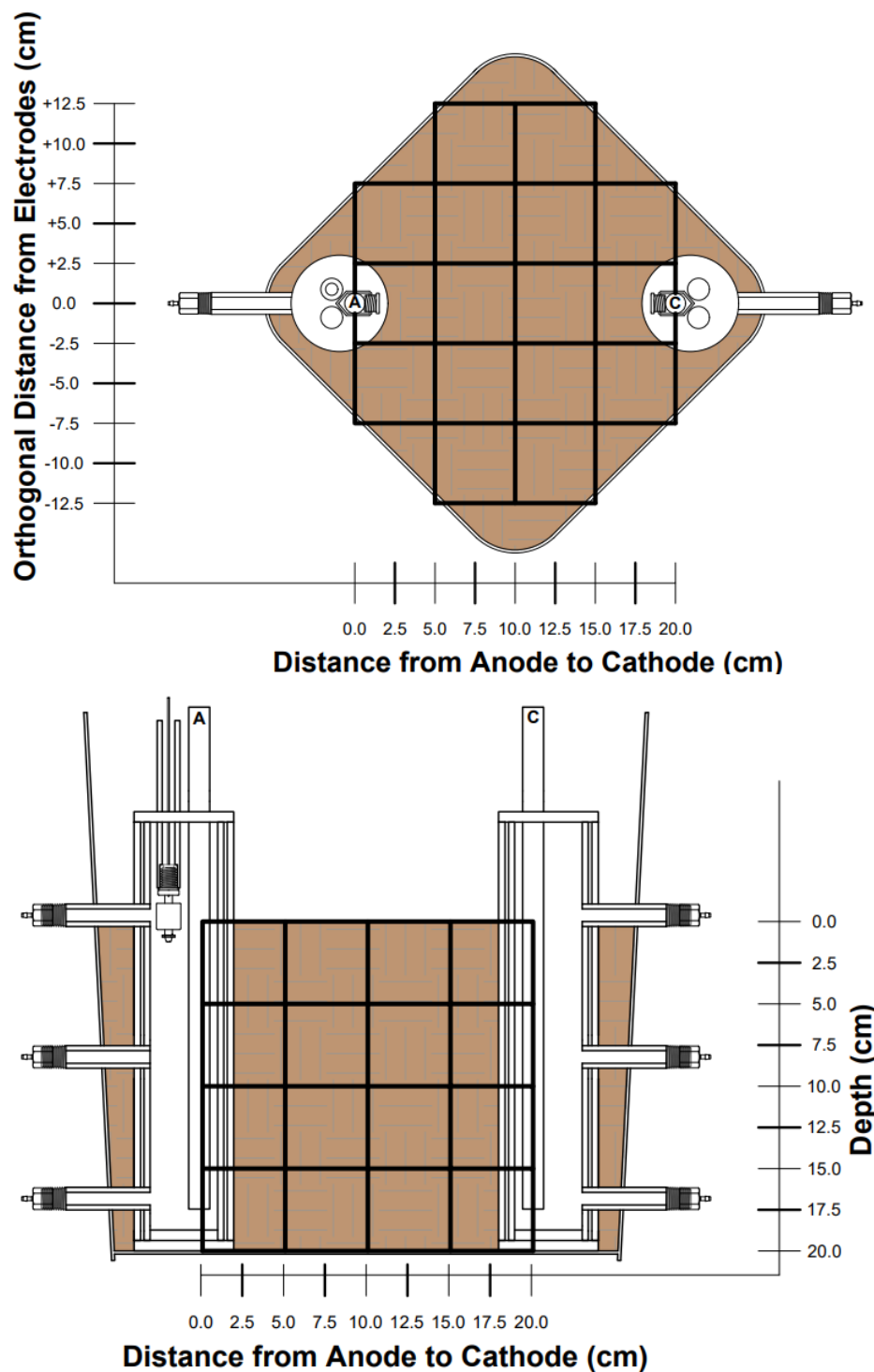


Figure 14. Schematic. Post-treatment reactor sampling plan with relative coordinate system defined to scale. Top image = Top-down view. Bottom image = Cross-sectional view.

ANALYTICAL METHODS

Auxiliary Methods

Sample Preparation: When required for sample preparation, mechanical mixing entailed vortexing sample vials at 2750 ± 250 rpm for 1 minute at a time, and centrifugation was performed for 50–10 minutes at 4200 rpm with an Eppendorf® Centrifuge 5804R at 20°C with unitless acceleration and braking speeds set to 9 and 5.

Soil Moisture Content: Soil moisture content was determined pre- and post-treatment following ASTM D2216-19 “Standard Test Methods for Laboratory Determination of Water (Moisture) Content of Soil and Rock by Mass.”

Reactor Performance Checks

Electrical current and electrostatic potential were measured daily between the powered-to-powered and auxiliary-to-powered electrodes by Morpilot® auto-ranging digital multimeter. Hydrogen peroxide concentrations in the electrode wells and reactor outflow were determined daily by sodium thiosulfate iodometric titration. The pH and temperature of electrode-well solutions and reactor outflow were measured daily with a VWR® sympHony™ B10P Benchtop Meter with a VWR® 89231-596 pH Electrode and Integrated Temperature Sensor. Soil pH was measured pre- and post-treatment, and pH of the electrode-well solutions and reactor outflow were measured daily (USEPA Method 9045D; USEPA, 2021a). Liquid sample aliquots of 10–20 mL were removed from the electrode wells for daily analyses. They were either replaced automatically with fresh solution at the anode well or manually with 10 mL fresh solution or solution recovered from the reactor outflow at the cathode well, depending on residual H_2O_2 concentration in the overflow (i.e., > 8%).

Polycyclic Aromatic Hydrocarbons and Degradation Product Analysis

Sample Preparation: Both aqueous samples taken during treatment and the post-treatment soil samples were prepared for gas chromatography mass spectrometry (GCMS) analyses by hexane solvent extraction with mechanical mixing by vortex, either one time, or twice daily over 4 days, respectively (extraction efficiency > 99%). Organic contaminants were extracted from 10 g wet soil samples with the addition of 10 mL Milli-Q water and 10–20 mL hexane, vortexing and centrifugation, and dilution with additional hexane. GCMS analyses followed an adapted EPA Method 8270D (SW-846): “Semi Volatile Organic Compounds” to determine pyrene concentrations and detect pyrene degradation products.

GCMS Parameters: Pyrene concentrations of both aqueous sample solution and soil extracts were determined by GCMS analysis. An Agilent Technologies 7820A GC system with an Agilent Technologies 5977B MSD fitted with an Agilent 190915-433 HP-5ms GC Column, 30 m, 0.25 mm, 0.25 μm nominal was used. Operational conditions included an initial temperature of 100°C held for 4 minutes, a rate of 8°C/min, and a final temperature of 280°C held for 4 minutes. The temperatures of the injector and the detector were 280°C.

GCMS Quality Control: A blank was run at the start and end of analysis as well as between each sample to eliminate residual pyrene from the column between runs. The GCMS was routinely baked and calibrated as needed.

Metals Analysis

Sample Preparation: Sample preparation for inductively coupled plasma mass spectrometry (ICPMS) analyses followed an adapted USEPA Method 3050B (SW-846): “Acid Digestion of Sediments, Sludges, and Soils” (USEPA, 2021b). One gram of wet soil sample was distributed in capped Hach vials placed in aluminum reaction blocks on a hot plate. The vials were heated at $95\pm5^{\circ}\text{C}$ for 30 to 60 minute intervals, following the sequential additions of 6 mL 1:1 ($\text{H}_2\text{O}:\text{HNO}_3$), 4 mL 70% HNO_3 , and 1 mL of 30% H_2O_2 . A fourth heating period was applied to samples in which effervescence was still occurring, or brown gas was present, such that complete metal oxidation to water-soluble nitrate salts was achieved. Digested samples were vacuum filtered through 0.22 μm pore diameter glass fiber filters and diluted with 1% HNO_3 to a 1000-fold dilution factor. Metals analyses followed an adapted USEPA Method 6020B: “Inductively Coupled Plasma—Mass Spectrometry” for use with kinetic energy discrimination (KED; also known as collision mode) to minimize polyatomic interferences (USEPA, 2021c).

Description of ICPMS Method: The total concentrations of 17 inorganic elements (As, Cd, Cr, Cu, Mn, Ni, Se, Ag, U, V, Zn, Ba, Be, Co, Pb, Tl, and Th) were determined by a PerkinElmer NexION™ 350X ICPMS with the collision reaction cell set to KED mode. Argon gas (99.985%) was used for plasma, auxiliary, and nebulizer gas flow. Ultra-pure helium gas (> 99.999% He) was used in the collision cell for KED. Table 16 shows additional ICPMS program conditions.

Table 16. ICPMS Program Conditions

Nebulizer Gas Flow	(L/min)	0.835
Auxiliary Gas Flow	(L/min)	1.2
Plasma Gas Flow	(L/min)	18
ICP RF Power	(Watts)	1600
Analog Stage Voltage	(Volts)	-1675
Pulse Stage Voltage	(Volts)	1050
Discriminator Threshold	(Pulses)	12
Deflector Voltage	(Volts)	-12
Quadrupole Rod Offset	(Volts)	12
Cell Entrance Voltage	(Volts)	0
Cell Exit Voltage	(Volts)	-38
Cell Rod Offset	(Volts)	-15
Axial Field Voltage	(Volts)	475
RP _a		0
RP _q		0.25
Cell Gas A	(mL/min)	2

Quality Control: Samples were measured with 40 sweeps/reading, 1 reading/replicate, and 3 replicates. Quality control checks were performed at the beginning and end of each run, and after every tenth measurement, with 2–4 standard concentrations. Internal indium standards were added to each blank, standard, and sample. Sample cross-contamination was prevented by a 60 second wash cycle, 60 second sample flush, and 30 second read delay. The washing solution varied between 1% and 10% HNO₃, depending on concentrations present in the samples (i.e., highly contaminated samples required 10% acid to remove contamination from the ICPMS cones between runs), whereas highly diluted samples required only 1% acid to restore baseline conditions. Samples were only analyzed after satisfying calibration with $R^2 > 0.99$ for all 17 metals.

Unconfined Compressive Strength

Soil specimen preparation for unconfined compressive strength (UCS) tests was performed with a Harvard Miniature Compaction Apparatus (Humboldt Mfg. Co., Elgin, Illinois). The soil was passed through a No. 4 (4760 micron) sieve, and 160 g soil specimens were compacted at target optimum moisture content (21.8% w/w) in eight 20 g layers, using a 20 lb dynamic compaction hammer to apply 25 blows per layer. Compacted soil specimens were extracted from the mold and trimmed to 1.2625" (33 mm) ID by 2.816" (71 mm) H, prior to oven drying at 110°C for 24 hours. Dry conditions were used as a reference with the goal of comparing the strength of the soils before and after electrochemical treatment. Therefore, all samples had the same water content so that water content or suction did not interfere with soil strength measurements. UCS tests were performed on dried specimens with a GEOTAC GeoJac™ Digital Load Actuator with the GEOTAC Sigma-1™ Automated Load Test System Software at a strain rate of 0.4%/min.

CHAPTER 4: RESULTS AND DISCUSSION

OVERVIEW

The electrochemical treatment of clayey soils co-contaminated with HMW-PAHs and metals was evaluated, and six investigative bench-scale experiments were performed. The removal of pyrene contamination as a model HMW-PAH was evaluated in four experiments to better understand the electrochemical phenomena present prior to the addition of metal co-contaminants. The first three experiments evaluated different chemical regimes, and the fourth experiment utilized the best-performing chemical regime with the addition of pH control in the cathode well and a surcharge load applied to the soil surface. The fifth experiment evaluated the removal of manganese contamination as a model nontoxic metal. This experiment was performed using the same electrochemical regime applied in experiment 4 to explore the feasibility of metal removal under the same electrochemical conditions as the previously explored pyrene treatment. One major difference between experiment 5 and the others was the initial moisture content. Use of a nontoxic contaminant allowed for the performance of unconfined compressive strength (UCS) testing on the pre- and post-treatment manganese contaminated kaolinite. This additional test was performed in experiment 5 to assess the treatment's impact on soil structural integrity. For this reason, the initial moisture content was changed from 40% to 21.8%—the kaolinite's optimum moisture content—for the benefit of added geotechnical analyses. Additionally, experiment 5 proceeded for a week longer than experiments 1–4 such that pH correction and soil strength reinforcement by calcium replenishment could be attempted using electrokinetically distributed simulated concrete pore solution (SCPS). Experiment 6 was the only co-contamination experiment evaluated. In this experiment, pyrene and hexavalent chromium were evaluated in an attempt to overcome their highly recalcitrant interactions. Experiment 6 proceeded for 28 days in a highly explorative fashion, intended to work toward optimizing the electrochemical regime. These experiments are independently discussed in greater detail in the following sections.

EXPERIMENT 1: PYRENE TREATMENT WITH H_2O_2 AND CITRATE BUFFER

First, the destructive treatment of 300 mg/kg pyrene over 14 days using electro-osmotically supplied H_2O_2 was evaluated. An electrostatic potential gradient of 1.5 V/cm was used to distribute an electrolytic treatment solution of 10% H_2O_2 with 0.1 M citrate buffer. Figure 15 displays the post-treatment pyrene concentration distribution in three-dimensions between the electrode wells. Pyrene removal was highest in the lower soil layers, whereas pyrene accumulation was apparent in the uppermost soils near the anode well. A strong correlation between treatment efficiency and soil depth was observed, which demonstrates negligible pyrene destruction in the uppermost layer (Figure 16). This occurrence is attributed to the deleterious soil swelling effects caused by gas generation from the violent catalyzed hydrogen peroxide (CHP) reactions. As evident from Figure 15, the uppermost soil layer nearest the cathode well could not be sampled because of the swelling effects, which caused soil migration away from the area and accumulation near the anode well. The changes in soil structure post-treatment are readily visible in Figure 38. Further apparent is lesser pyrene removal at the reactor edges, where the orthogonal distance from electrodes is greatest. The greatest pyrene removal occurred along the shortest field length, with a symmetrical decline in

treatment efficiency with respect to orthogonal distance in either direction (Figure 17). Inward constriction of the soil along all nonconductive boundaries likely also contributed to lower pyrene removal along the reactor edges and the anode well. This observation is supported by the large visible voids (Figure 38), as electro-osmosis is a surface-driven property dependent upon the presence of a microcapillary lined with charged electrical double layers. Without electro-osmotic flow, the H_2O_2 is not distributed through the soil for the degradation of pyrene.

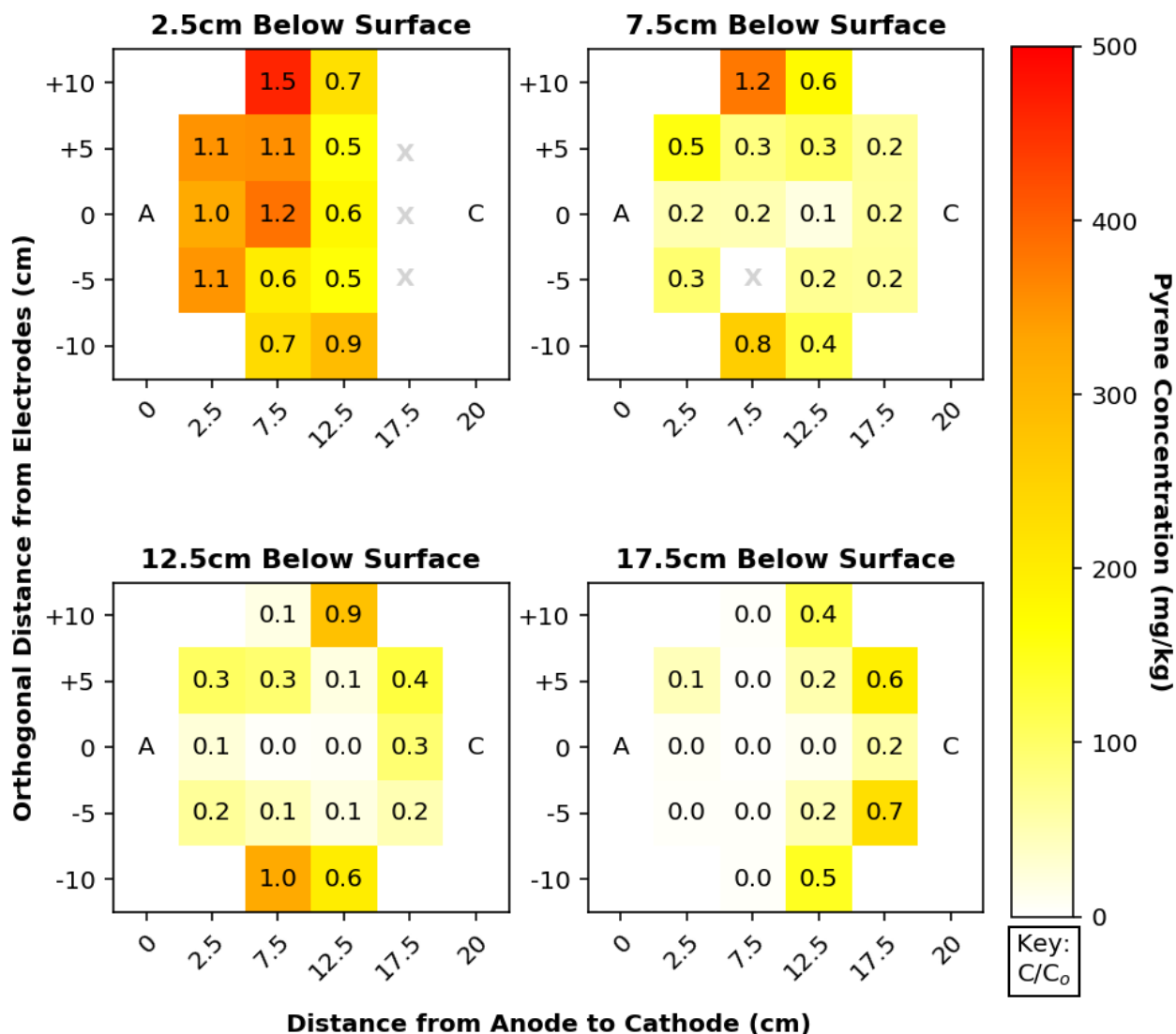


Figure 15. Graph. Final pyrene concentration distribution by depth below soil surface (experiment 1). The numbers shown for each sample point indicate the treated concentration normalized by the initial concentration (C/C_0).

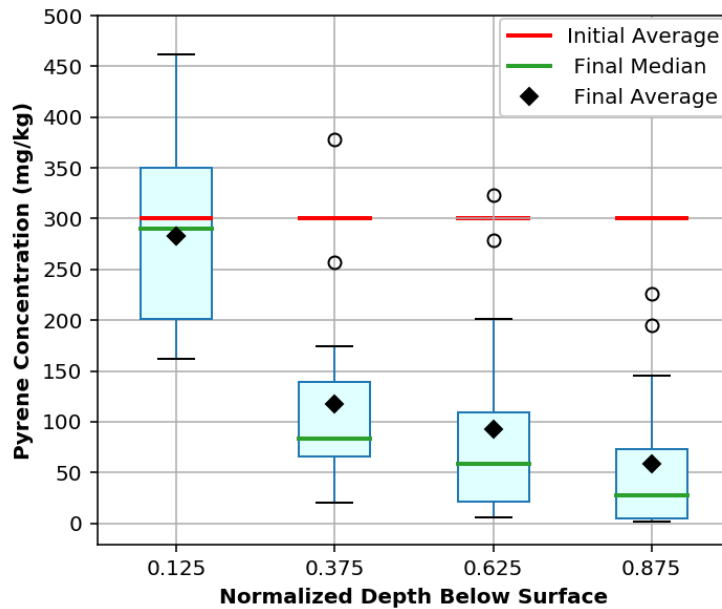


Figure 16. Graph. Final pyrene concentration distribution by normalized depth below the soil surface (depth/total depth) (experiment 1). The lower horizontal lines (inside of box) represent the final median values and the upper horizontal lines represent the initial averages for each box and whisker column.

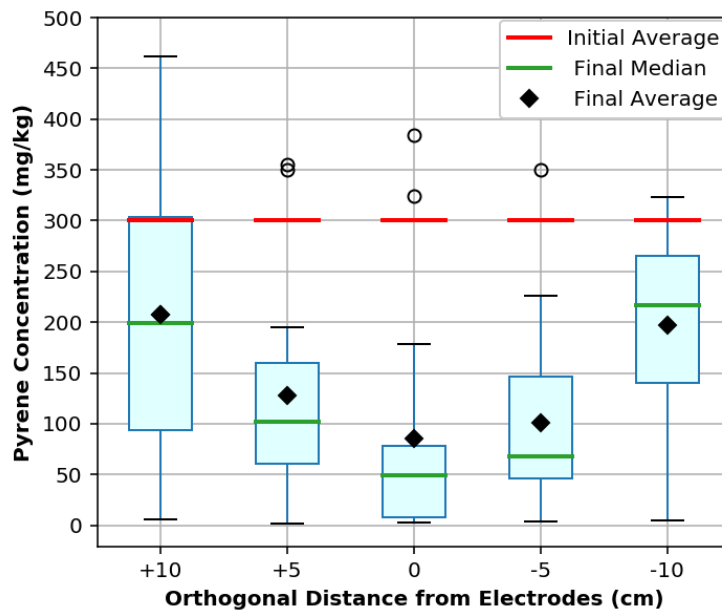


Figure 17. Graph. Final pyrene concentration distribution by orthogonal distance from electrodes (experiment 1). The lower horizontal lines (inside of box) represent the final median values and the upper horizontal lines represent the initial averages for each box and whisker column.

The significance of electro-osmotic flow and the development of an electrolytic acid front were demonstrated. The interstitial fluid migrated from anode to cathode in response to the electrical field

(Figure 18). The destruction of pyrene near the cathode well (Figure 15) further corroborates the theory that electro-osmosis can facilitate advective H_2O_2 transport through the soil as a plug flow. Secondly, a high degree of soil acidification occurred (Figure 19). The decrease in pH was greatest near the anode, where H^+ is generated by the electrolysis of water. To a lesser degree, the remaining soil was acidified essentially homogeneously with respect to each orthogonal band per soil depth. Surprisingly, despite pH reaching up to 13.0 in the cathode well, no back diffusion of OH^- into the soil was apparent. Oppositely, the anode well pH reached a minimum of 0.7. This pH gradient likely augmented the electro-osmotic flow rate via electrochemical diffusion. A large flux of H^+ from anode to cathode would support the advective microscale transport of H_2O . Further, the pH influenced electrodeposition onto the electrodes. As shown by Figure 39, the post-treatment anode was free of any attached ions, whereas the cathode was caked in irreversibly attached sodium crystals remnant from the citrate buffer. Electrodeposition onto the cathode progressively increased electrical resistance and decreased the efficiency of current transmission between electrodes over time. For this reason, pH control at the cathode is necessary to preserve the efficiency of energy expenditure over time.

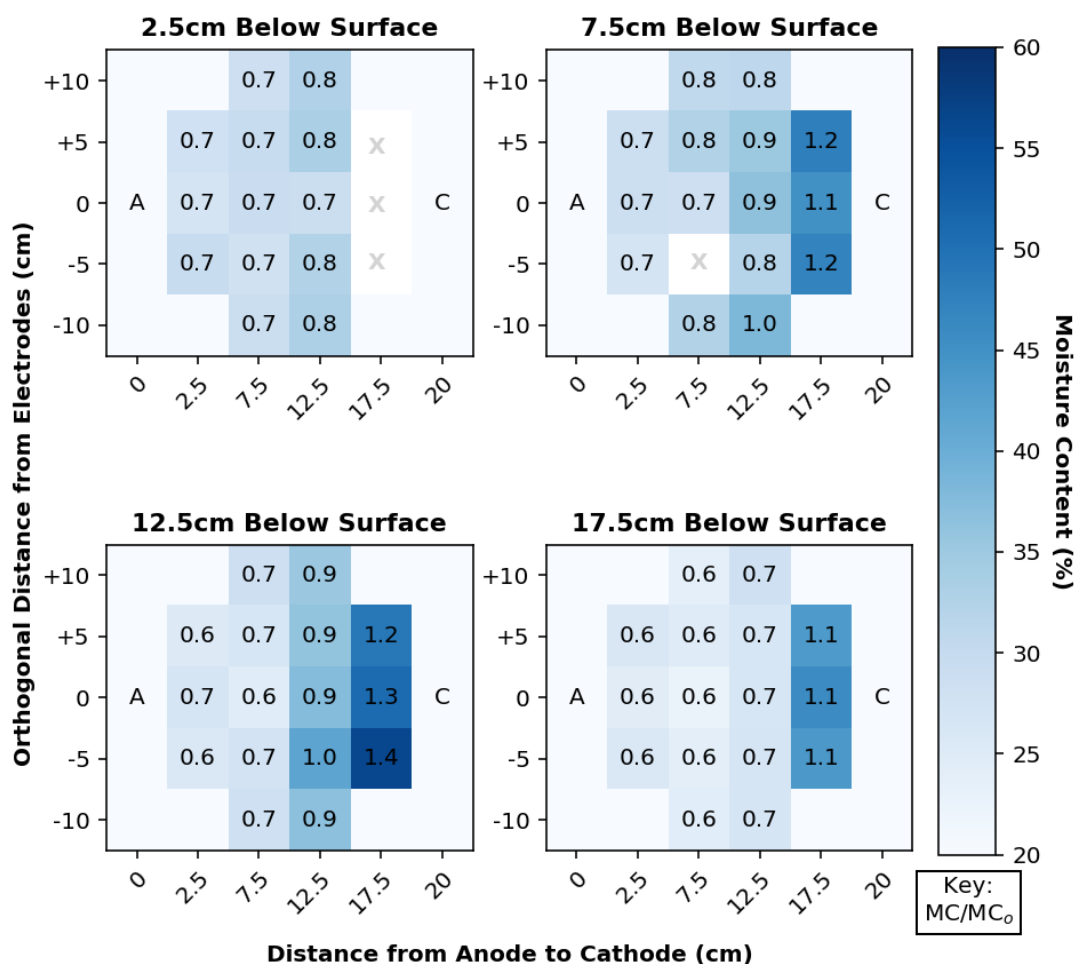


Figure 18. Graph. Final moisture content (MC) distribution by depth below soil surface (experiment 1). The numbers shown for each sample point indicate the final MC normalized by the initial MC (MC/MC₀).

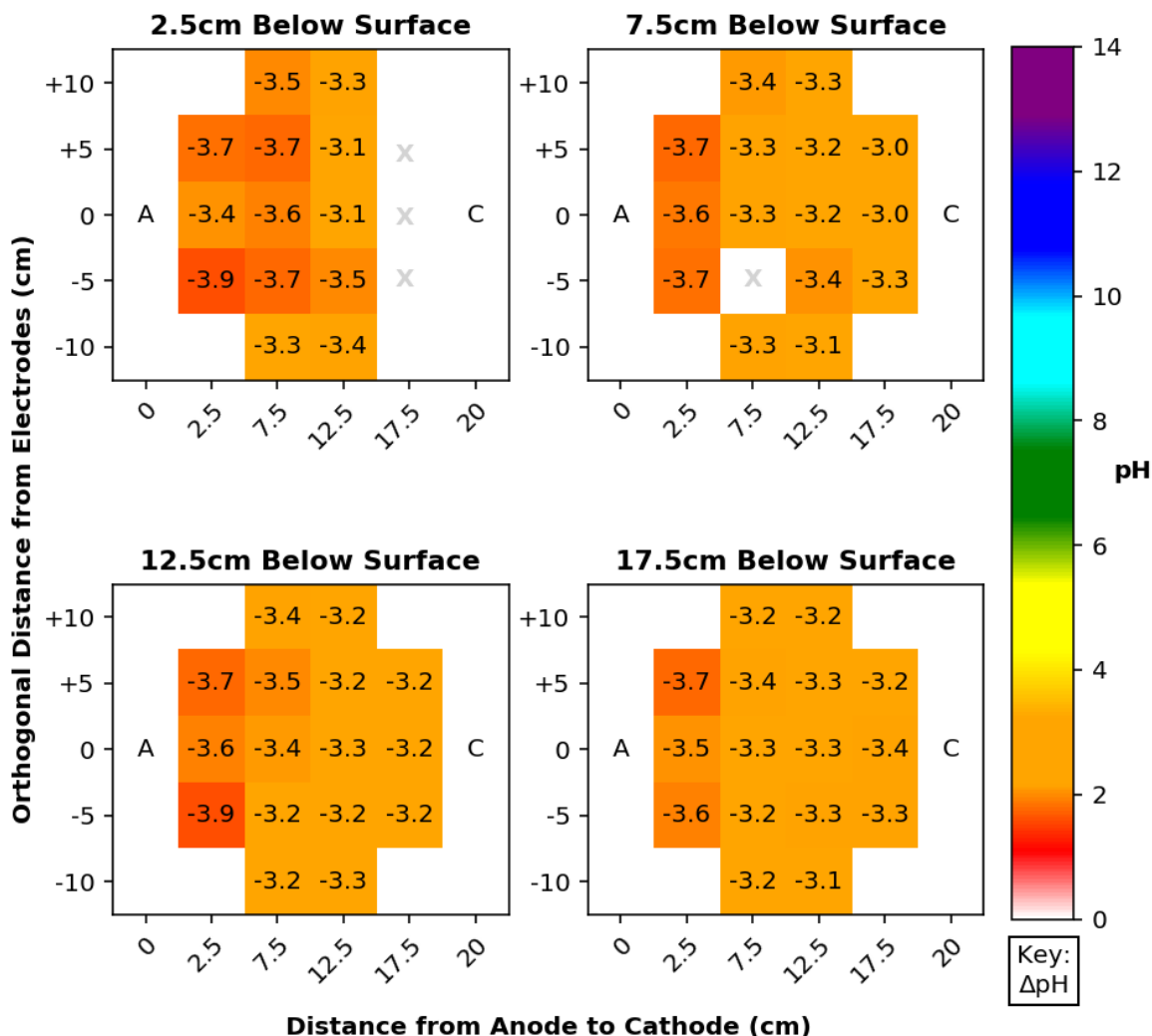


Figure 19. Graph. Final pH distribution by depth below soil surface (experiment 1). The numbers shown for each sample point indicate the change in pH from the initial conditions (Δ pH).

Experiment 1 was highly successful in the removal of pyrene from clayey soil in only 14 days. An average pyrene removal of $58.0 \pm 38.6\%$ was achieved, with a maximum of 99.4%. Distribution of H_2O_2 throughout soils of negligible hydraulic conductivity by electro-osmosis is a promising approach to addressing HMW-PAH contamination. The minimum pyrene removal of -48.2% occurred because of soil swelling near the anode, indicating transport as opposed to destruction. Following this experiment, it was hypothesized that the application of a surcharge load during treatment to prevent deleterious soil swelling could greatly improve treatment efficiency.

EXPERIMENT 2: PYRENE TREATMENT WITH A NONIONIC SURFACTANT, H_2O_2 , AND CITRATE BUFFER

The extraction/destruction-based treatment of 300 mg/kg pyrene over 14 days using two sequential week-long chemical regimes was evaluated. An electrostatic potential gradient of 1.5 V/cm was used.

An electrolytic treatment solution of 5 g/L Brij™35 (polyoxyethylene[23] lauryl ether) with 0.1 M citrate buffer was supplied to the electrode wells for the first 7 days, followed by 10% H₂O₂ with 0.1 M citrate buffer for the second week. The lowest pyrene removal occurred near the cathode well (Figure 20). A strong correlation was demonstrated between lower pyrene removal and greater orthogonal distance from the electrodes (Figure 21), consistent with experiment 1. Converse to experiment 1, little correlation between depth and treatment efficiency was observed. Rather, pyrene removal increased with proximity to the anode well (Figure 22). These findings may be attributed to two mechanisms. First, addition of the nonionic surfactant contributed to both pyrene desorption and micellar solubilization to form colloids, increasing the efficacy of transport from anode to cathode by electro-osmosis and electrophoresis, respectively. Second, the electrokinetic transport toward the cathode likely resulted in surfactant accumulation near the cathode well, which quenched the available HO• through competing side reactions and prevented pyrene destruction in the region. The second mechanism is supported by the finding that no residual surfactant remained in the soil post-treatment due to the second week of flushing with 10% H₂O₂. These findings indicate that H₂O₂ addition following Brij™35 soil flushing is an effective means of overcoming the common issue of residual surfactant contamination following soil flushing treatments.

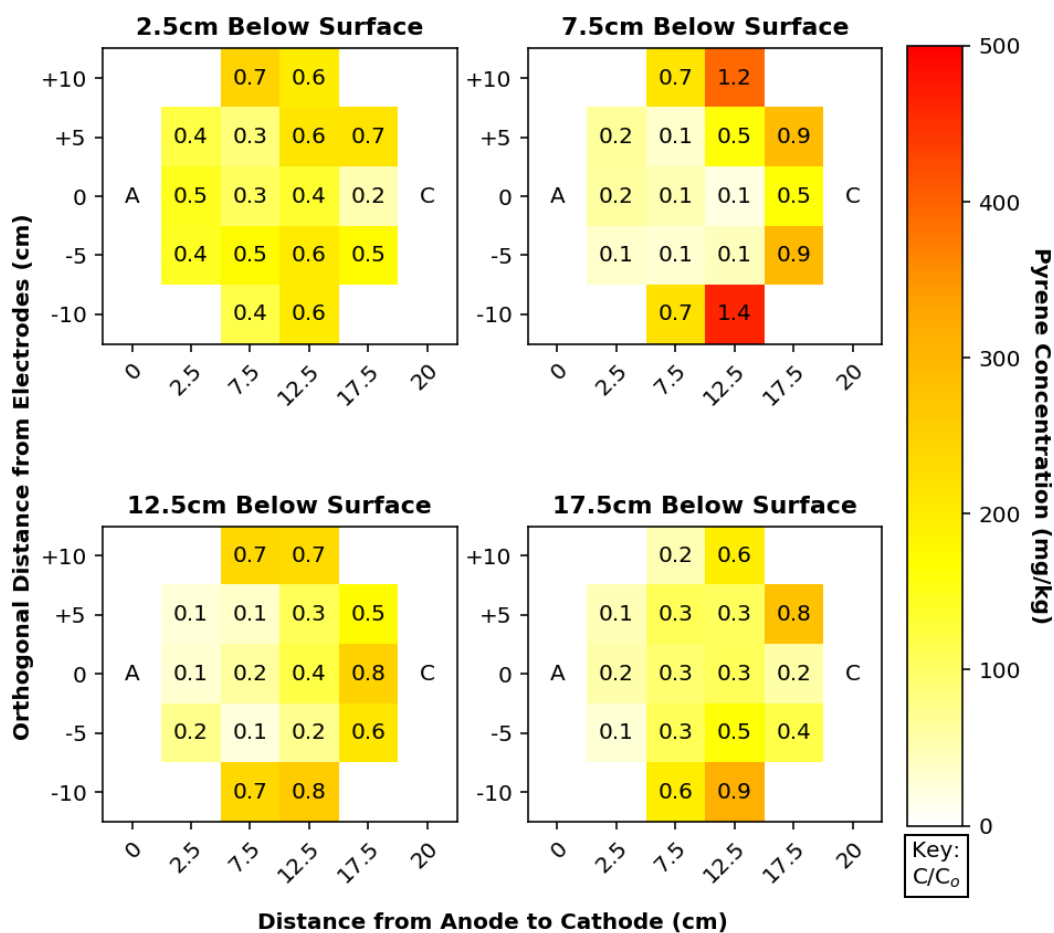


Figure 20. Graph. Final pyrene concentration distribution by depth below soil surface (experiment 2). The numbers shown for each sample point indicate the treated concentration normalized by the initial concentration (C/C_0).

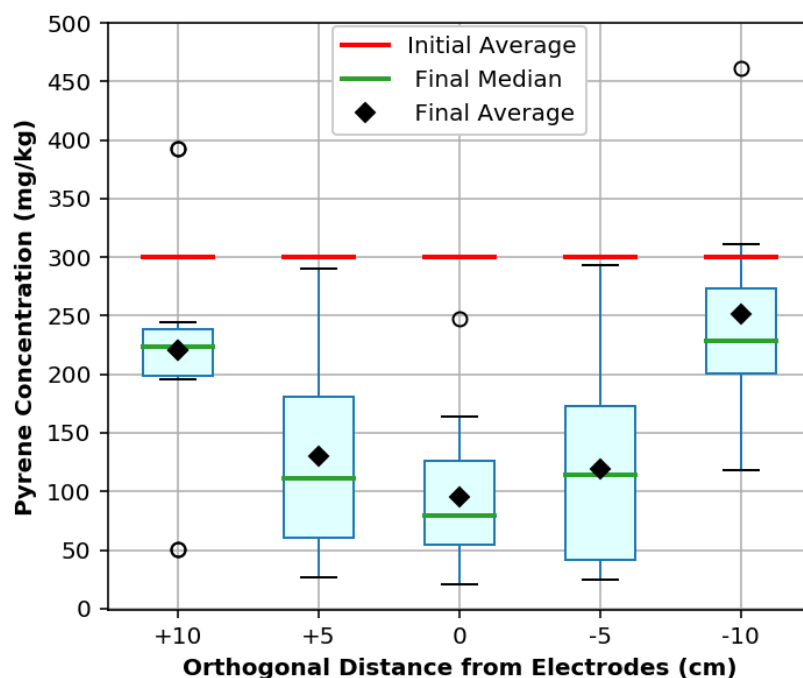


Figure 21. Graph. Final pyrene concentration distribution by orthogonal distance from electrodes (experiment 2). The lower horizontal lines (inside of box) represent the final median values and the upper horizontal lines represent the initial averages for each box and whisker column.

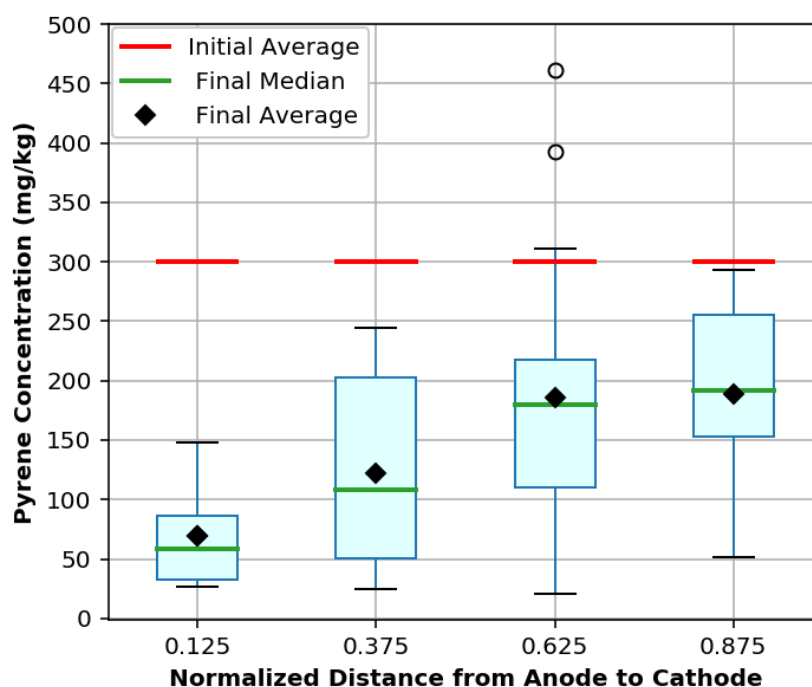


Figure 22. Graph. Final pyrene concentration distribution by normalized distance (distance/total distance) from anode to cathode (experiment 2). The lower horizontal lines (inside of box) represent the final median values and the upper horizontal lines represent the initial averages for each box and whisker column.

The observed electro-osmotic flow and soil acidification were both consistent with experiment 1. The electro-osmotic flow proceeded from anode to cathode, as shown in Figure 23. It is readily apparent that density effects were not present in the electro-osmotic flow regime, as the greatest moisture content was detected in the upper soil layers. As such, electro-osmotic flow between electrodes as a method of soil flushing throughout clayey soils with minimal risk of downwards contaminant dispersal is well supported.

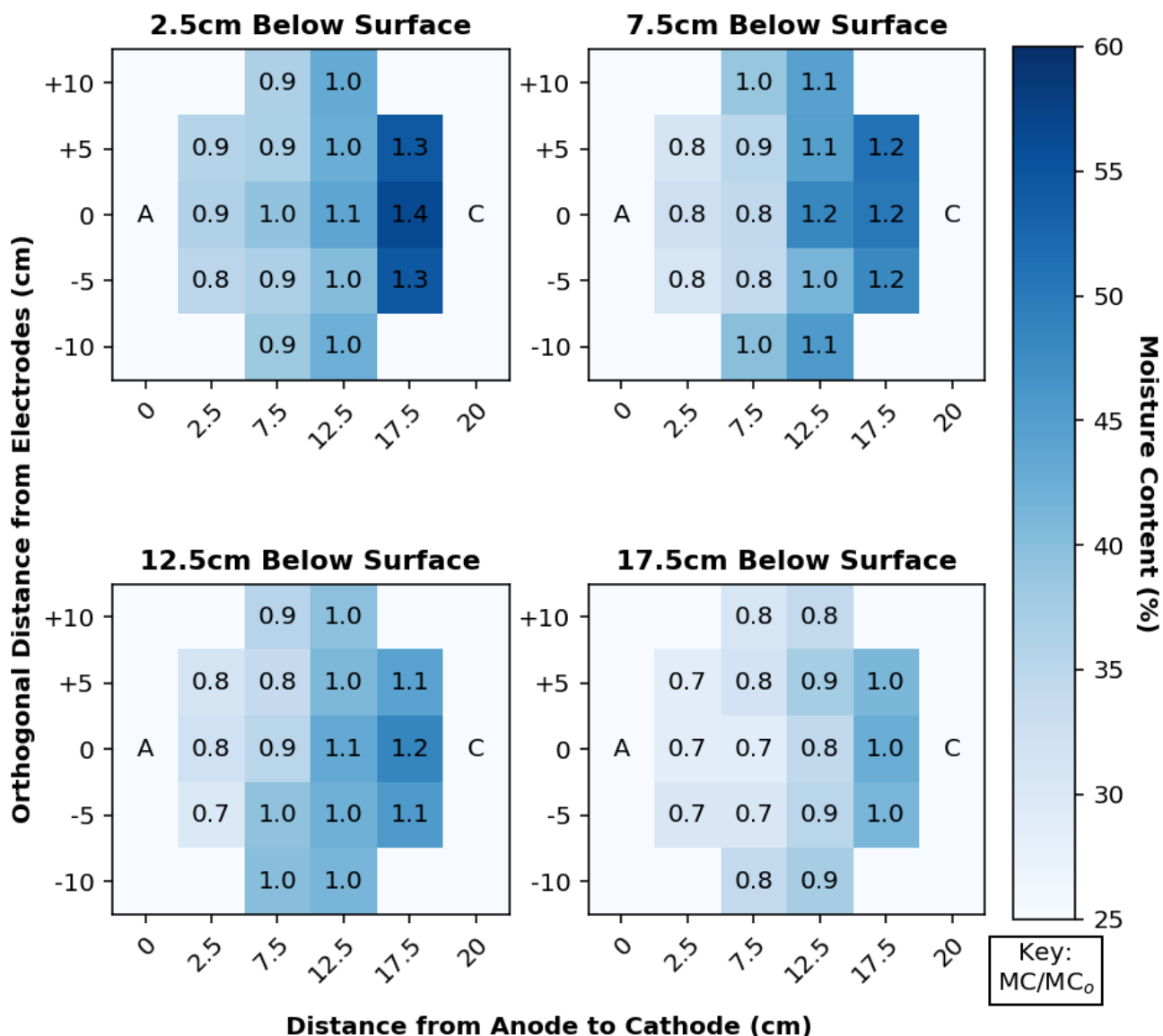


Figure 23. Graph. Final moisture content distribution by depth below soil surface (experiment 2). The numbers shown for each sample point indicate the final MC normalized by the initial MC (MC/MC_0).

Second, homogenous soil acidification induced by the acid front was demonstrated (Figure 24). H^+ generated by electrolysis at the anode proceeded toward the cathode via electromigration at a rate greater than the counter flux of OH^- from the cathode well. Consistent with the results of Alcántara et al. (2008b) the addition of H_2O_2 to both the anode and cathode wells served as a viable approach for negating the progression of a basic front, which has historically impeded the success of electrokinetic treatments (Alcántara et al., 2008b).

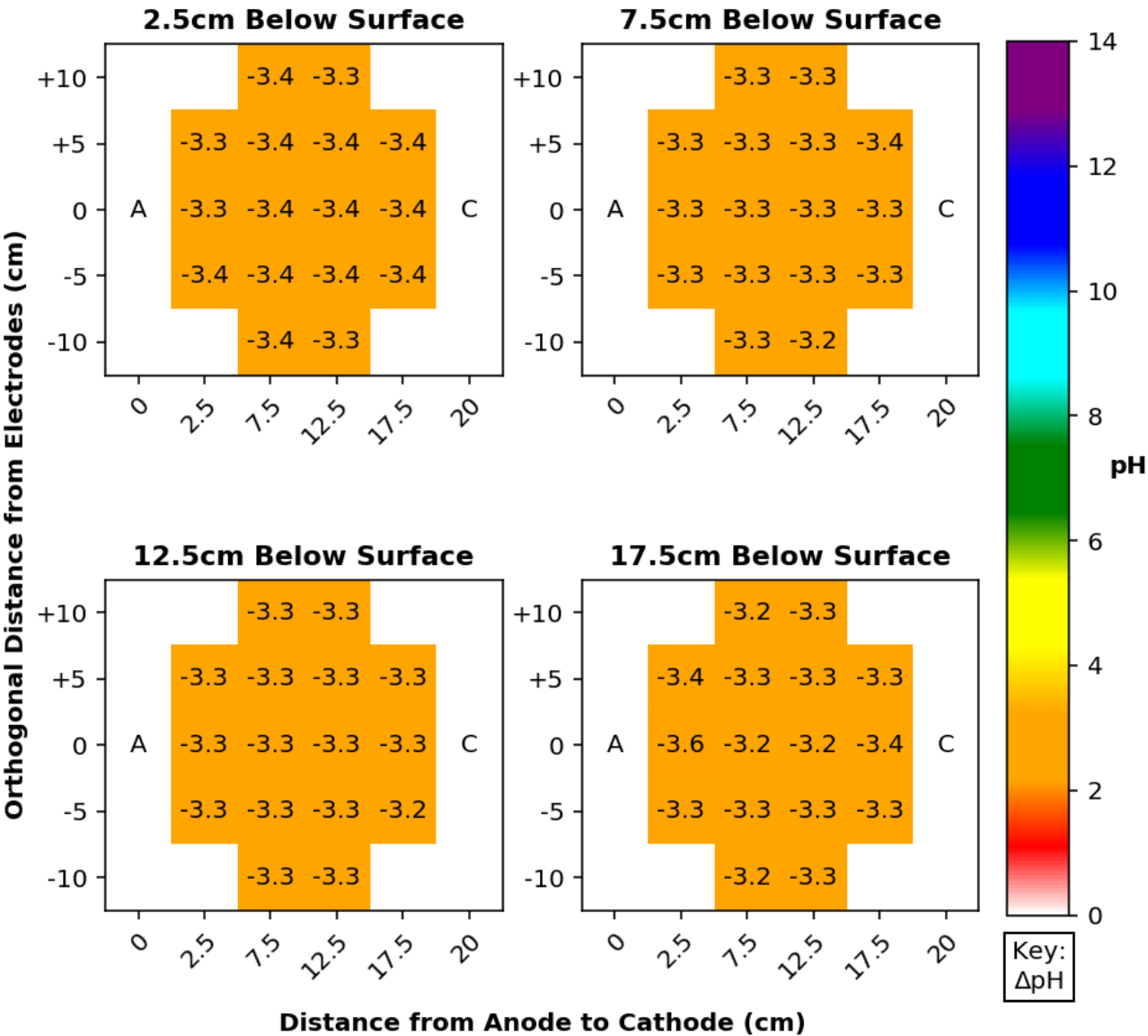


Figure 24. Graph. Final pH distribution by depth below soil surface (experiment 2). The numbers shown for each sample point indicate the change in pH from the initial conditions (ΔpH).

The addition of Brij™35 caused two significant changes to the post-treatment electrodes that were not observed during experiment 1. First, disintegration of the anode occurred (Figure 40). The electrodes are composed of a superfine graphite powder, molded by compression. The surfactant lowered the surface tension between graphite particles, which resulted in physical separation. Conversely, no disintegration of the cathode occurred. This observation suggests a pH dependency of the surfactant in which alkaline pH prevented necessary hydrogen bonding. Secondly, no electrodeposition was present on the cathode, which means that nonionic surfactant addition at the cathode could prove beneficial for prevention of electrodeposition-based loss in electrical efficiency.

The results of this experiment suggest the successive addition of nonionic surfactants and H₂O₂ is a promising augmentation to electrokinetic systems for the removal of HMW-PAHs. An average pyrene removal of $56.8 \pm 28.4\%$ was achieved, with a maximum of 93.8%. Despite lower average and maximum removal, the standard deviation was 10.2% lower than in experiment 1, suggesting an increased homogeneity of treatment. As Brij™ 35 has been demonstrated by others as a highly successful enhancing agent for the removal of benzo(a)pyrene (BaP), this approach is worth further investigation to address soils co-contaminated with higher molecular weight PAHs (Alcántara et al., 2008a; Gómez et al., 2009; Madadian et al., 2014).

EXPERIMENT 3: PYRENE TREATMENT WITH A NONIONIC SURFACTANT

The extraction-based treatment of 300 mg/kg pyrene over 14 days using a nonionic surfactant was evaluated. An electrostatic potential gradient of 1.5 V/cm was used to distribute an electrolytic treatment solution of 5 g/L Brij™35 with 0.1 M citrate buffer. The lowest pyrene removal was observed in the lower soil depths (Figure 25). Further, pyrene removal was homogenous in all layers except for the uppermost region (Figure 26). These findings are attributed to the clogging of soil pores in the lower extents by the residual surfactant. Unlike experiment 2, in this case there was no successive H₂O₂ applied to degrade the Brij™35. Surfactant accumulation in the soil was homogeneously apparent post-treatment during centrifugation and GCMS analyses, in which saponified emulsions (Figure 41) and numerous long-chain hydrocarbons were detected, respectively. Clogging of the lower soil pores was similarly apparent (Figure 42) and was also demonstrated by the soil moisture content (Figure 27). The use of Brij™35 for 14 days resulted in low pyrene removal of $23.8 \pm 26.5\%$, on average. Additionally, the post-treatment electrode properties were disadvantageous. The anode almost entirely disintegrated because of the Brij™35 addition (Figure 43), and a significant quantity of electrodeposition occurred on the cathode. It was found that the use of a nonionic surfactant without successive H₂O₂ addition is not able to prevent sodium attachment to the electrode. This electrochemical regime should be avoided because of the residual surfactant contamination, low pyrene removal, and deleterious impacts on both electrodes.

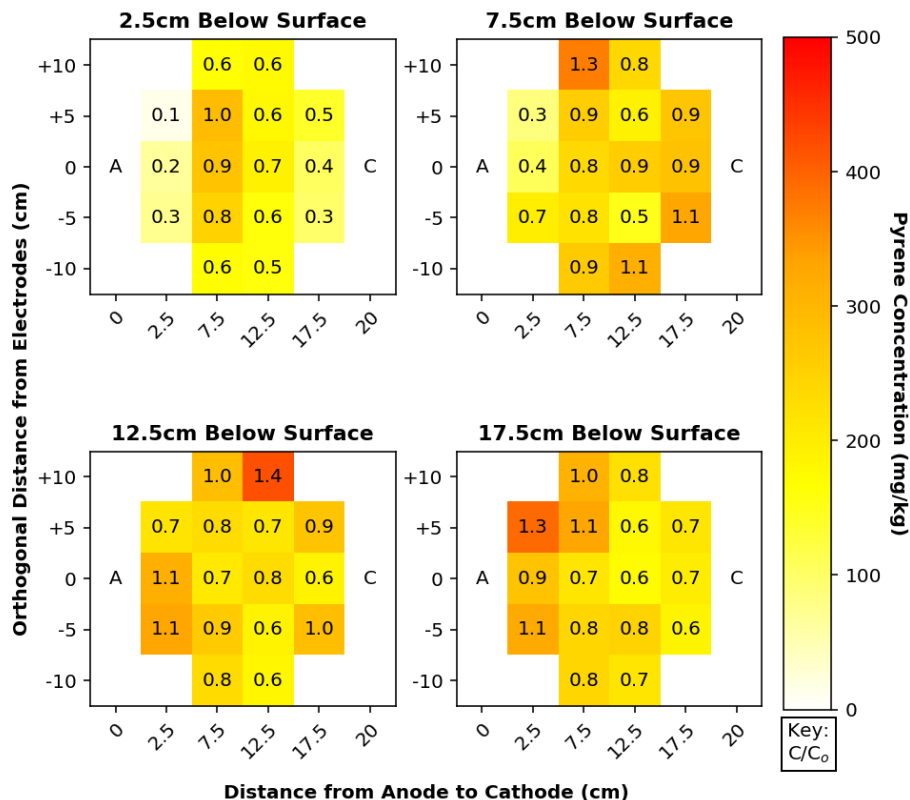


Figure 25. Graph. Final pyrene concentration distribution by depth below soil surface (experiment 3). The numbers shown for each sample point indicate the treated concentration normalized by the initial concentration (C/C_0).

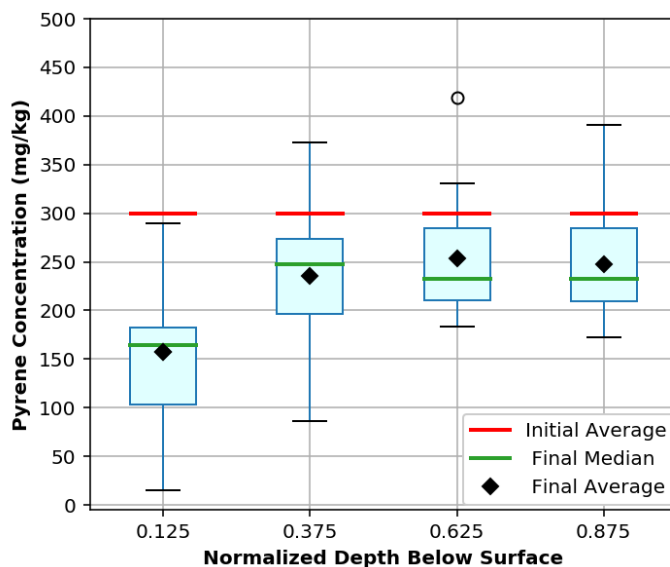


Figure 26. Graph. Final pyrene concentration distribution by normalized depth below the soil surface (depth/total depth) (experiment 3). The lower horizontal lines (inside of box) represent the final median values and the upper horizontal lines represent the initial averages for each box and whisker column.

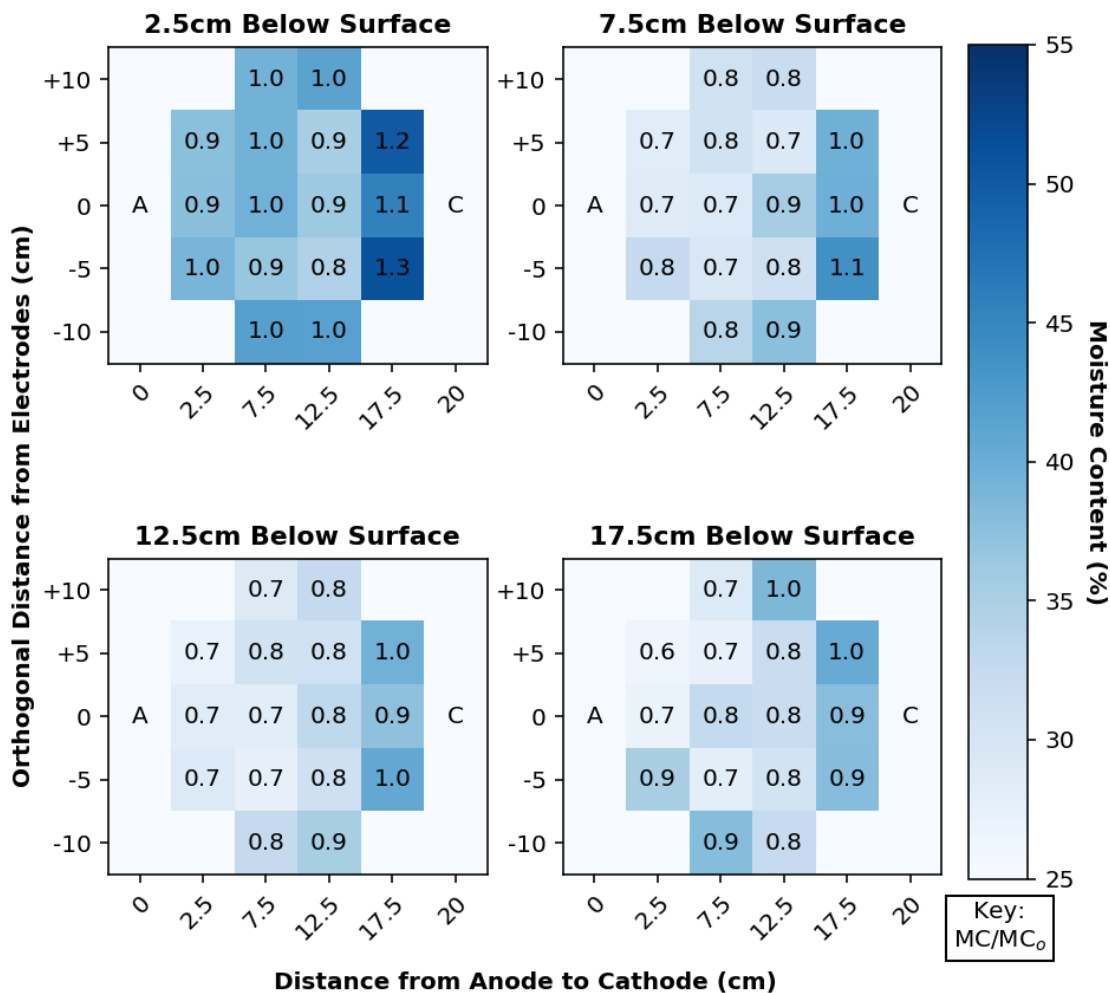


Figure 27. Graph. Final moisture content distribution by depth below soil surface (experiment 3). The numbers shown for each sample point indicate the final MC normalized by the initial MC (MC/MC_0).

EXPERIMENT 4: PYRENE TREATMENT WITH A SURCHARGE, H_2O_2 , CITRATE BUFFER, AND CATHODE-WELL pH AMENDMENTS

The destructive treatment of 300 mg/kg pyrene over 14 days using electro-osmotically supplied H_2O_2 was evaluated. A surcharge load was applied to prevent swelling, and cathode-well pH amendments were used to reduce cathodic electrodeposition. A 2-day purge of highly concentrated H_2O_2 intended to desorb the pyrene was followed by a lower H_2O_2 concentration to minimize gas generation. An electrostatic potential gradient of 1.5 V/cm was used to distribute an electrolytic treatment solution of 10% H_2O_2 with 0.1 M citrate buffer for the first 2 days, followed by 3% H_2O_2 with 0.1 M citrate buffer for the following 12 days. Citric acid was supplied to the cathode well once daily to lower the pH to 3.8 ± 0.2 and encourage CHP reactions. Unlike experiment 1, pyrene did not accumulate in the uppermost layer near the anode well. Rather, little correlation was apparent between pyrene removal and depth (Figure 28). However, the trend for lower pyrene removal with respect to greater orthogonal distance was present, consistent with previous experiments. Furthermore, the highest

pyrene removal occurred near the central auxiliary electrode across all depths. The correlation between pyrene removal and distance from anode to cathode is masked by the competing trend of orthogonal distance, in which the highly concentrated ± 10 cm sample locations skew the trendline (Figure 29). The post-treatment soil surface indicated significant gas generation as evident from sponge-like voids (Figure 44). It was clear that the application of surcharge prevented soil swelling, yet the lower H_2O_2 concentration still caused significant off gassing. The effects of gas generation were potentially exacerbated by the accumulation of gas below the surcharge plate; thus, it was hypothesized a semiporous material for the surcharge load may yield better results.

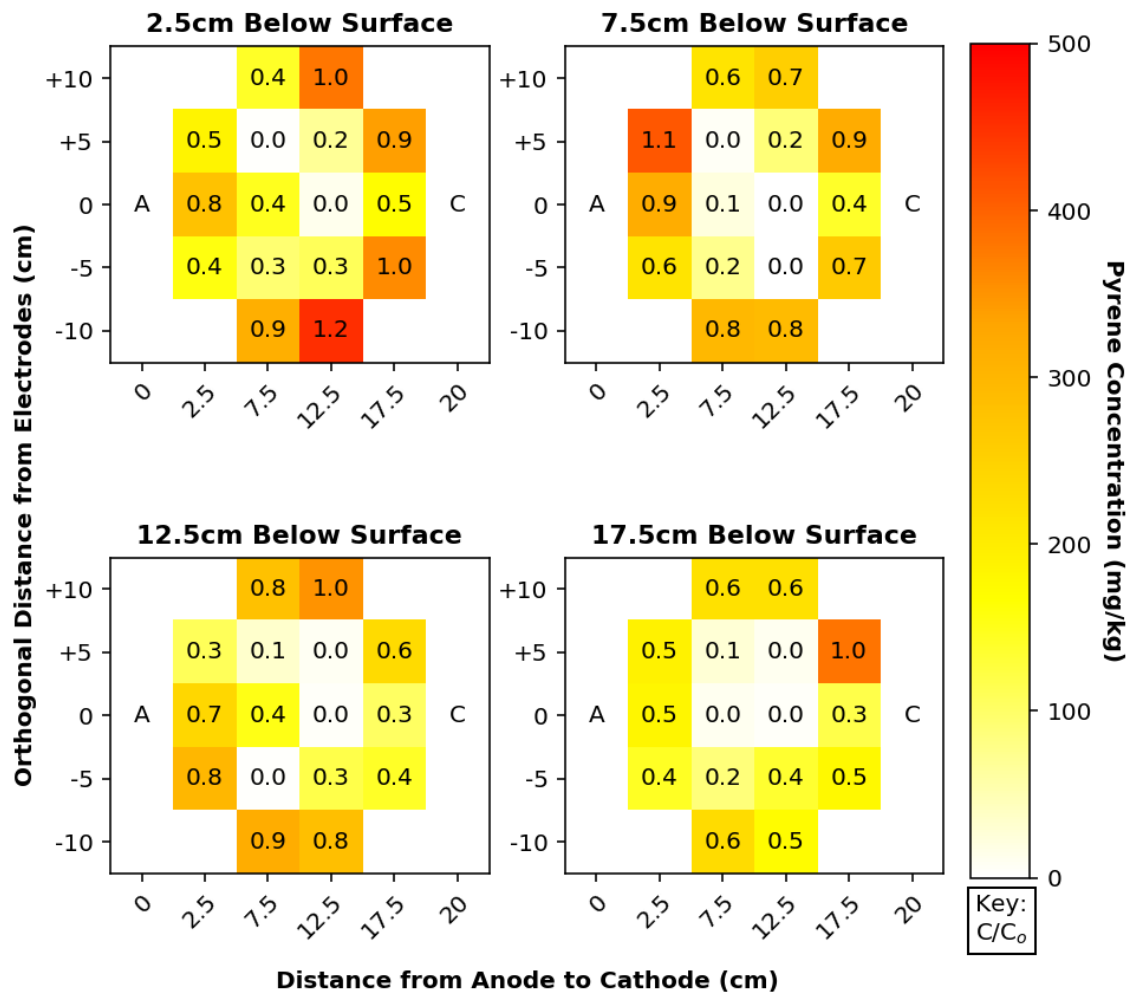


Figure 28. Graph. Final pyrene concentration distribution by depth below soil surface (experiment 4). The numbers shown for each sample point indicate the treated concentration normalized by the initial concentration (C/C_0).

Several phenomena occurred in this experiment worth noting. Oxidative destruction was the predominant pyrene removal mechanism, as extraction would have resulted in more negative minimum removals. Furthermore, a strong correlation between lower moisture content and lower pyrene concentration was observed (Figure 29). This correlation suggests that the pyrene was successfully desorbed into the aqueous phase, as soils containing more liquid contained more pyrene.

Secondly, the use of a lower H_2O_2 concentration with added pH amendments to the cathode well resulted in substantial electrodeposition on the cathodes (Figure 45). This electrodeposition occurred despite past evidence that acidic pH prevents deposition on the electrodes, suggesting higher H_2O_2 concentrations present in the anode well may have a stronger influence than the pH. Consequently, considering the lower treatment efficiency (52.6%) than experiment 1 (58.0%), the use of 10% H_2O_2 should be used in addition to the surcharge load.

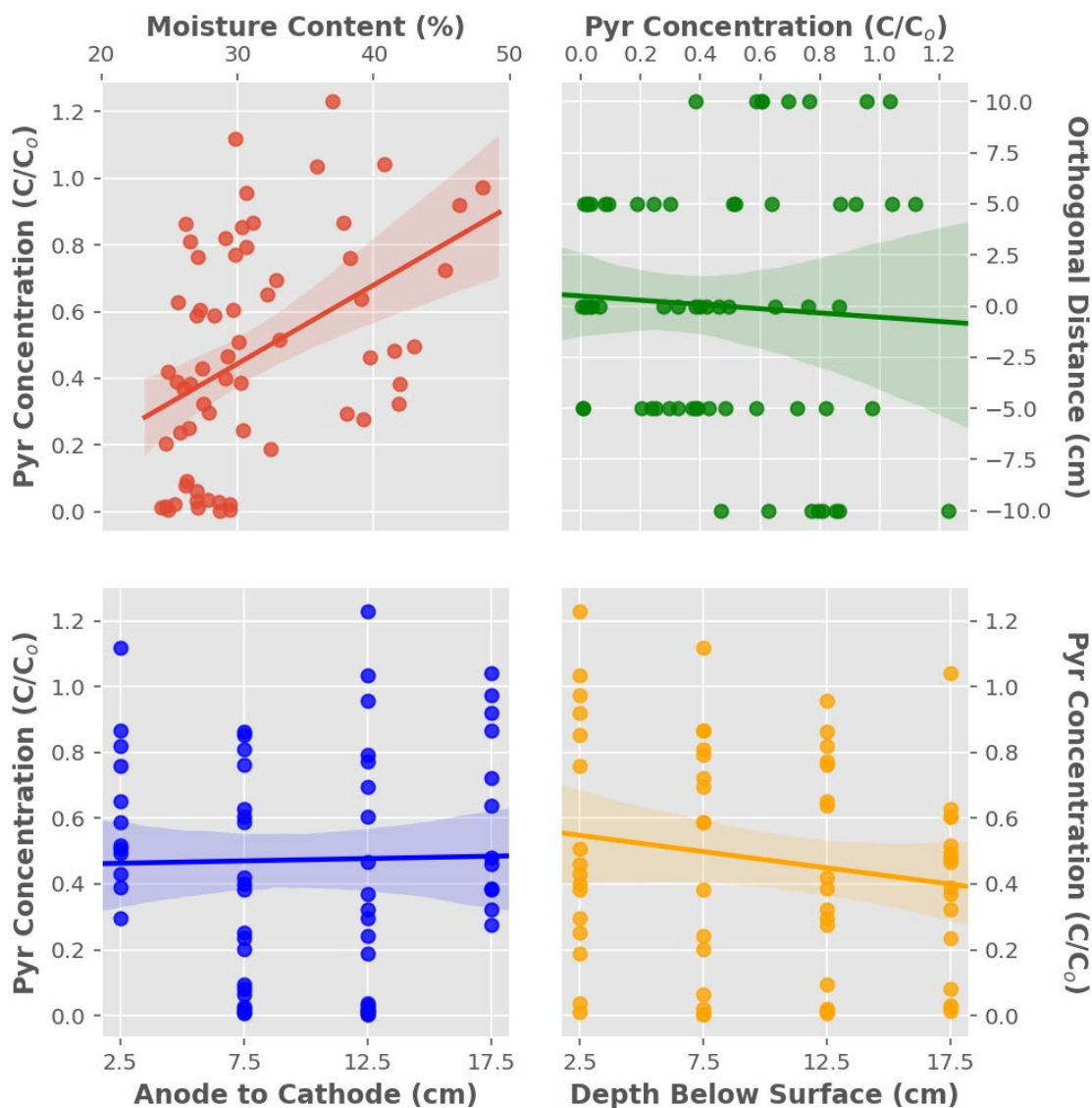


Figure 29. Graph. Pyrene concentration as a function of moisture content and each spatial dimension (experiment 4). The shaded regions represent the 95% confidence intervals of the linear regressions.

EXPERIMENT 5: MANGANESE TREATMENT WITH A SURCHARGE, H_2O_2 , SCPS, CITRATE BUFFER, AND CATHODE-WELL pH AMENDMENTS

The extraction-based treatment of 1,235 mg/kg manganese over 21 days by electrokinetics augmented with electro-osmotically supplied H_2O_2 and simulated concrete pore solution (SCPS) was

evaluated. Consistent with experiment 4, a surcharge load and cathode-well pH amendments were applied. An electrostatic potential gradient of 1.5 V/cm was used. An electrolytic treatment solution of 10% H₂O₂ with 0.1 M citrate buffer was supplied to the electrode wells for the first 14 days, followed by 10% H₂O₂ with 0.1 M SCPS for the third week. Citric acid was supplied to the cathode well once daily to lower the pH to 4.2 ± 0.4 for the first 14 days. The manganese was successfully transported from the anode toward the cathode by electromigration (Figures 30 and 31). With an average manganese removal of 42.3%, over 66% of the remaining manganese was present at a 0.875 normal distance from anode to cathode. Also, over 94% of the manganese at a 0.125 normalized distance from anode to cathode was removed, reaching a minimum of 4.6 mg/kg. Significant cathodic electrodeposition occurred yet was different in crystalline structure than that encountered in past experiments (Figure 46). Similarly, large concretions were present in the cathode well (Figure 47). These structures were determined to be primarily composed of manganese from analysis of acid-leached extracts. These results are highly promising, suggesting the manganese could have been entirely removed had the treatment proceeded for a longer duration.

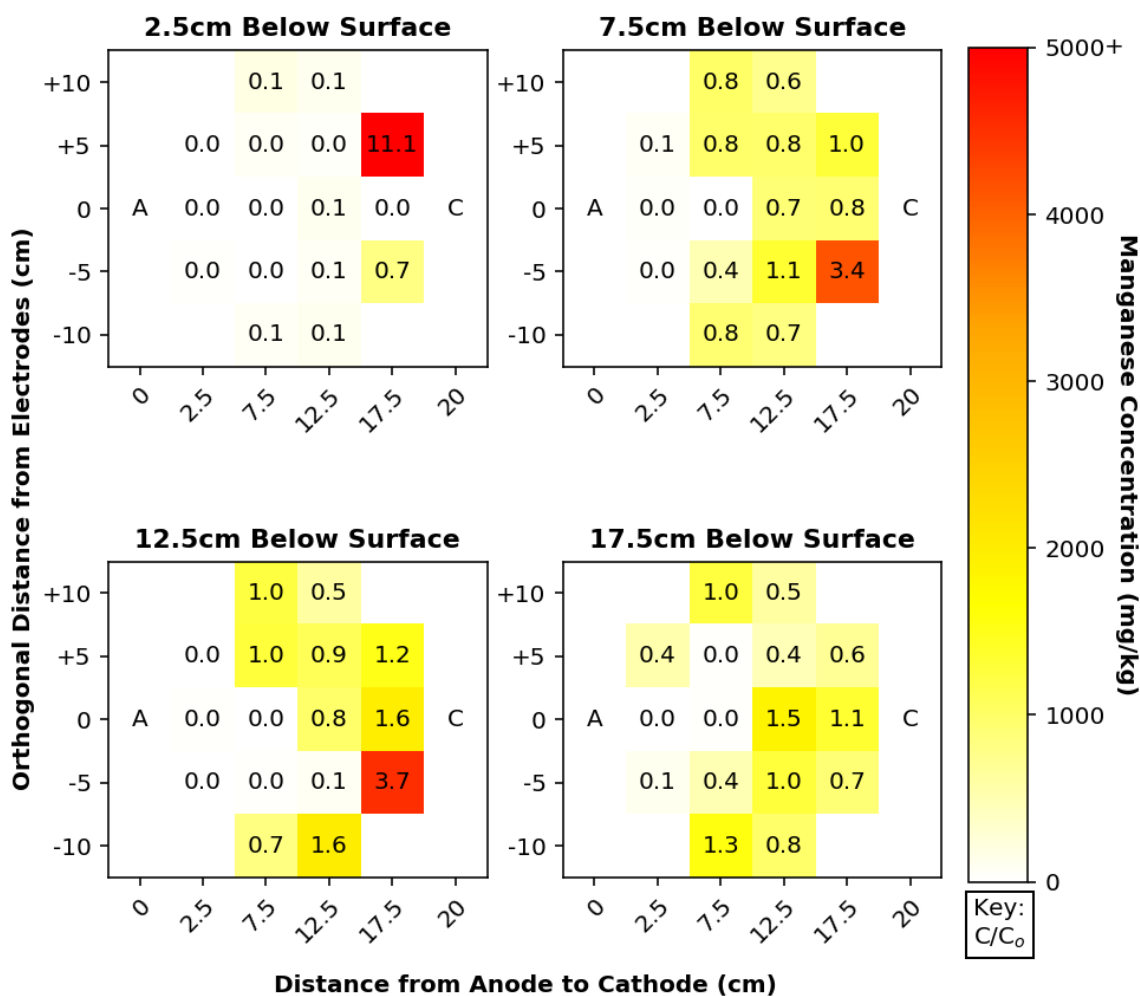


Figure 30. Graph. Final manganese concentration distribution by depth below soil surface (experiment 5). The color-bar scale excludes outlier 17.5, +5, 2.5 (X,Y,Z: cm). The numbers shown for each sample point indicate the treated concentration normalized by the initial concentration (C/C₀).

The third week of treatment substituted citrate buffer for SCPS as an electrolyte system. The SCPS was used in an attempt to elevate the post-treatment pH to near neutral and fortify the structural integrity of the soil via calcium replacement. As indicated by results of the post-treatment UCS testing (Table 17) and the pH (Figure 32), the SCPS amendment was unsuccessful. This lack of success may be attributed to the problems with the electro-osmotic flow, which otherwise would have aided in SCPS distribution.

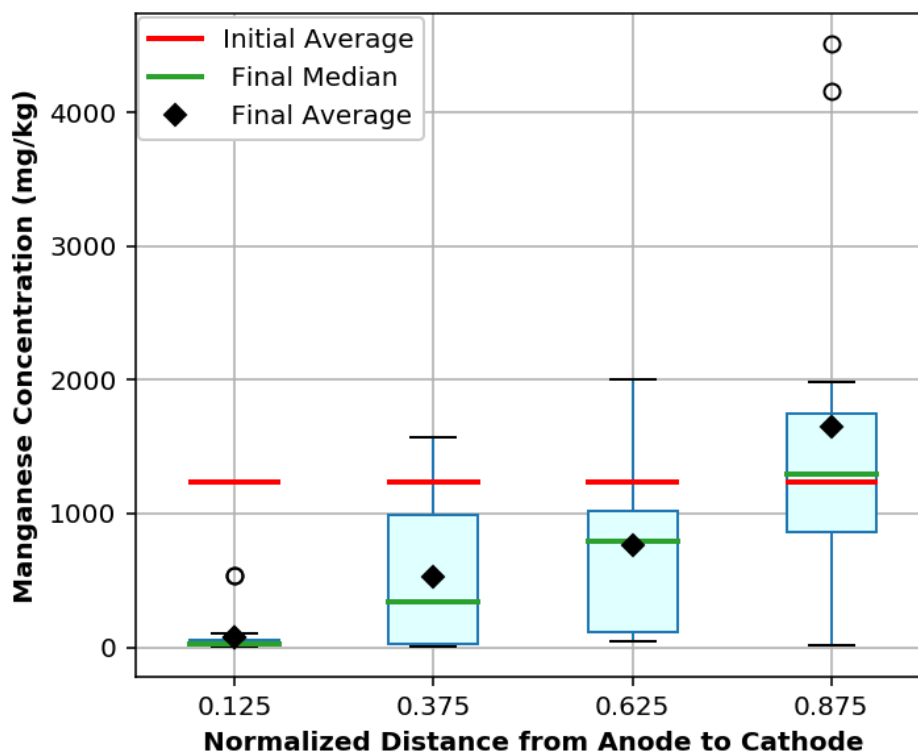


Figure 31. Graph. Final manganese concentration distribution by normalized distance (distance/total distance) from anode to cathode. Outlier 17.5, +5, 2.5 (X,Y,Z: cm) was excluded (experiment 5). The lower horizontal lines (inside of box) represent the final median values and the upper horizontal lines represent the initial averages for each box and whisker column.

The addition of manganese reversed the direction of flow relative to other experiments, resulting in moisture accumulation near the anode (Figure 33). This observation is significant because the electromigrative flux flowed counter to the electro-osmotic flow and retarded the rate of fluid transfer. This retardation is highly apparent from the total electro-osmotic flow rate of only 5,500 mL over 21 days, as compared to the lowest flow of 9,990 mL over 14 days from experiments 1–4. These results indicate a need to optimize the chemical regime for the support of electro-osmotic flow such that it can augment the electromigrative extraction as opposed to countering it. Similarly, the electro-osmotic flow is necessary to distribute H_2O_2 , and electromigration is not an effective means of removing organic contaminants, meaning the chemicals must be further optimized for successful remediation of soils co-contaminated with HMW-PAHs and metals despite promising manganese removal.

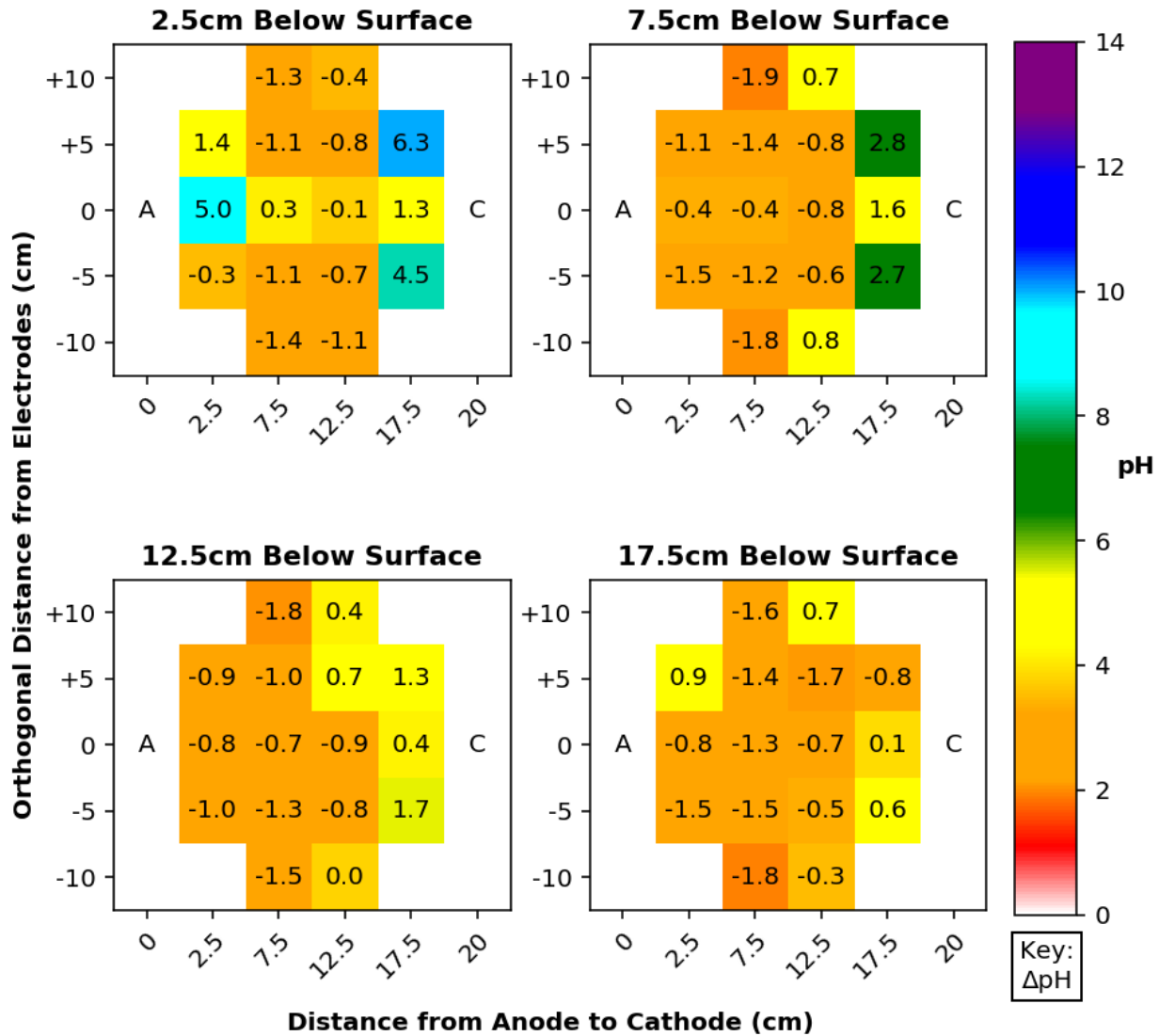


Figure 32. Graph. Final pH distribution by depth below soil surface (experiment 5). The numbers shown for each sample point indicate the change in pH from the initial conditions (Δ pH).

Table 17. Summary of Unconfined Compressive Strength Testing Results (Experiment 5)

Sample	UCS (kPa)	Percent Reduction
Pretreatment	2066	—
Anode-side: 2.5 cm BGS	784.6	62.0%
Anode-side: 7.5 cm BGS	931.5	54.9%
Anode-side: 12.5 cm BGS	1162	39.9%
Anode-side: 17.5 cm BGS	1251	39.4%
Cathode-side: 2.5 cm BGS	1751	15.3%
Cathode-side: 7.5 cm BGS	1241	39.9%
Cathode-side: 12.5 cm BGS	1116	46.0%
Cathode-side: 17.5 cm BGS	1096	46.9%

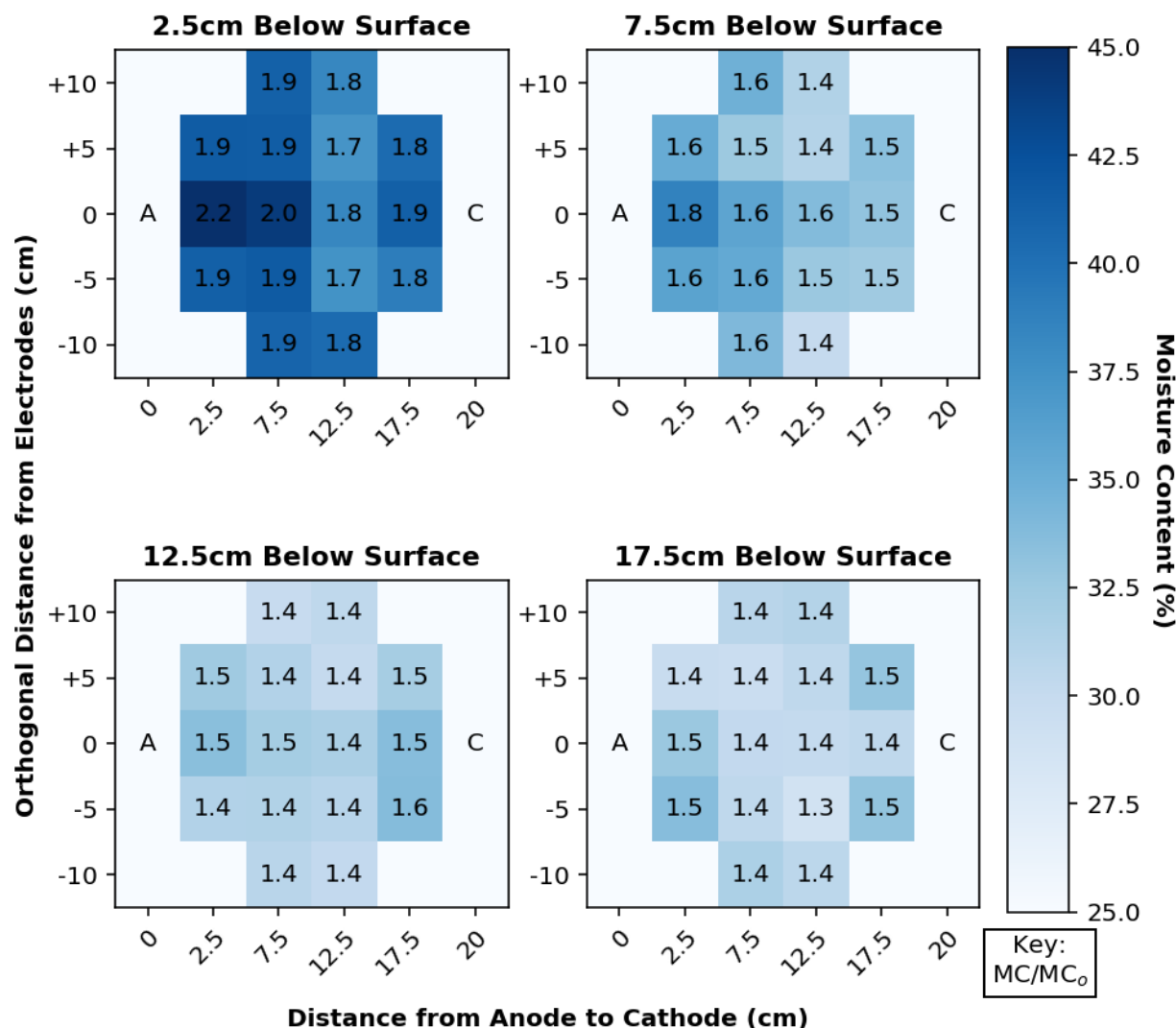


Figure 33. Graph. Final moisture content distribution by depth below soil surface (experiment 5). The numbers shown for each sample point indicate the final MC normalized by the initial MC (MC/MC₀).

EXPERIMENT 6: PYRENE AND CHROMIUM TREATMENT WITH A SURCHARGE, H₂O₂, CITRATE BUFFER, AND EXPLORATORY ELECTRODE-WELL pH AMENDMENTS

The extraction-based treatment of 163 mg/kg chromium and destruction-based treatment of 300 mg/kg pyrene were concurrently evaluated over 28 days. Electrokinetics were augmented with electro-osmotically supplied H₂O₂ and a surcharge load. An electrostatic potential gradient of 1.5 V/cm was used to supply an electrolytic treatment solution of 10% H₂O₂ with 0.1 M citrate buffer. Various anode-well and cathode-well pH amendments were applied throughout the treatment process until an effective chemical regime was found that augmented the electro-osmotic flow. Days 18–23 and 25–28 utilized the most efficient chemical regime with respect to electro-osmotic flow. The pH amendments entailed the following: 1) citric acid supplied to the cathode well once daily to lower the pH to 3.7 ± 0.6 and 2) 5:1 calcium hydroxide/potassium hydroxide supplied to the anode well once daily to raise the pH to 9.2 ± 0.7 .

Chromium accumulated at a normalized distance (distance/total distance) of 0.625 from anode to cathode (Figures 34 and 35). With an average chromium removal of only 4.5%, over 57.4% of the remaining chromium was present at this distance. This finding is consistent with Gent (2004), who attributed a low percent of complete extraction to the formation of a chromium band, caused by precipitation where the acidic and basic fronts met near the cathode. The progression of a basic front as shown by the positive ΔpH (Figure 36) throughout the 12.5 cm and 17.5 cm sample locations supports this precipitation theory. The accumulation of chromium near the cathode is thought to have benefited overall pyrene removal efficiency by catalyzing CHP reactions most effectively at a greater distance downgradient.

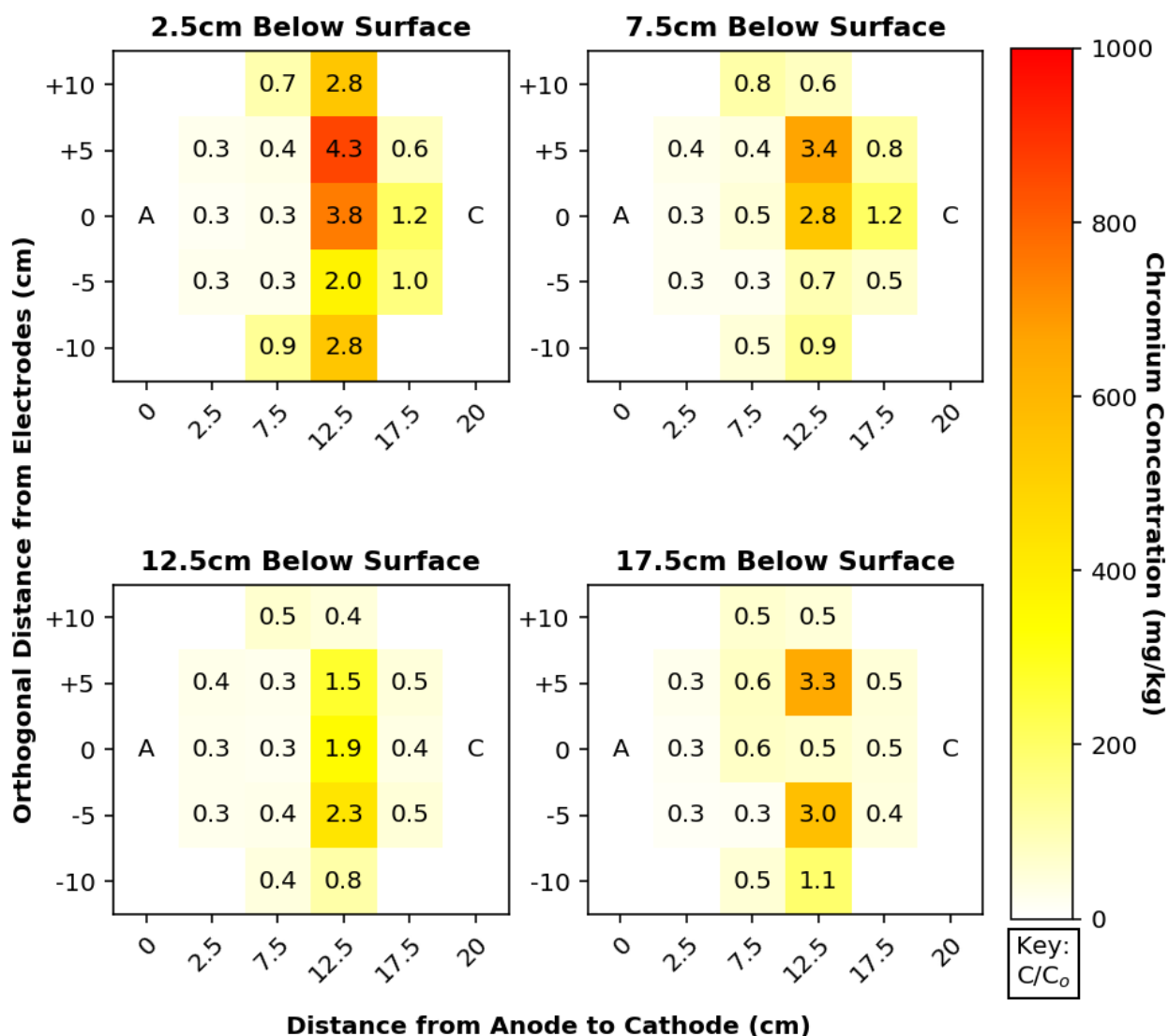


Figure 34. Graph. Final chromium concentration distribution by depth below soil surface (experiment 6). The numbers shown for each sample point indicate the treated concentration normalized by the initial concentration (C/C_0).

Despite the low average removal of chromium, pyrene removal was successful. Approximately 100% of the pyrene was destroyed homogenously throughout the soil, with no detectable degradation products, likely explained by chromium as an added CHP catalyst. The lowest electro-osmotic flow of all experiments (3,249 mL) was achieved in this experiment, and in the direction of cathode to anode (Figure 37), opposite of what was desired. Additionally, only 6.7 L of electrolytic treatment solution were utilized, the lowest volume consumed across all experiments, which suggests highly efficient use of the minimally distributed H_2O_2 by Cr-CHP.

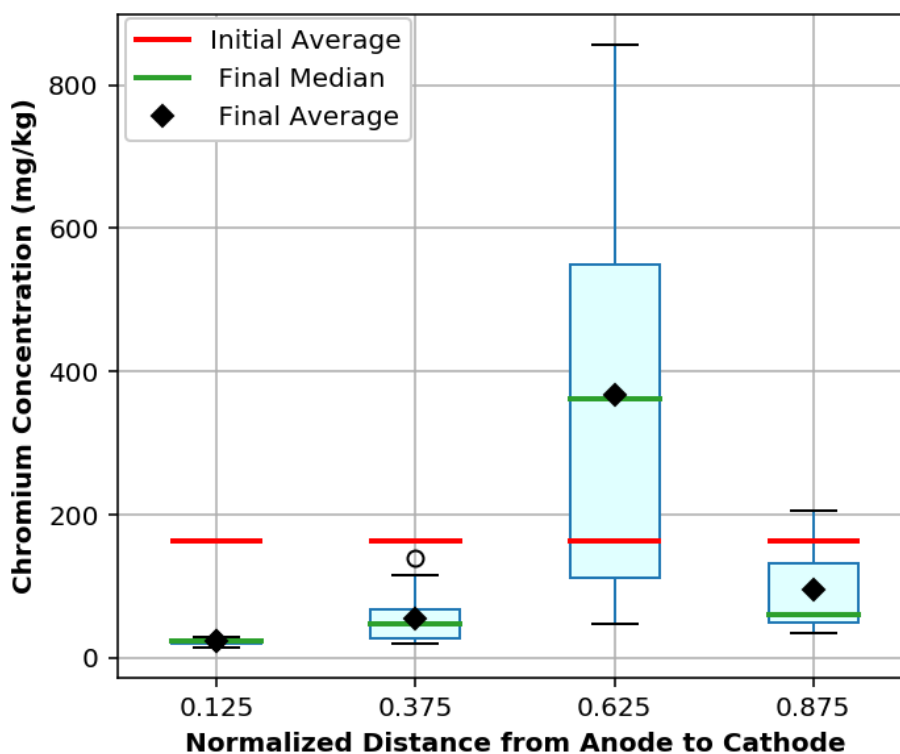


Figure 35. Graph. Final chromium concentration distribution by normalized distance (distance/total distance) from anode to cathode (experiment 6). The lower horizontal lines (inside of box) represent the final median values and the upper horizontal lines represent the initial averages for each box and whisker column.

Another explanation for the high degree of pyrene removal was the extended length of treatment employed. Experiments 1–4 only allowed 14 days for pyrene destruction to occur. As desorption is the rate limiting step for HMW-PAH treatment, the additional 14 days of treatment in this experiment were highly beneficial. An additional two weeks of treatment during which the majority of pyrene is present in the aqueous phase would promote ample contaminant-oxidant contact unattainable in previous experiments. The effective pyrene removal suggests electrochemical treatment as an appreciable approach to addressing clayey soils co-contaminated with HMW-PAHs and metals.

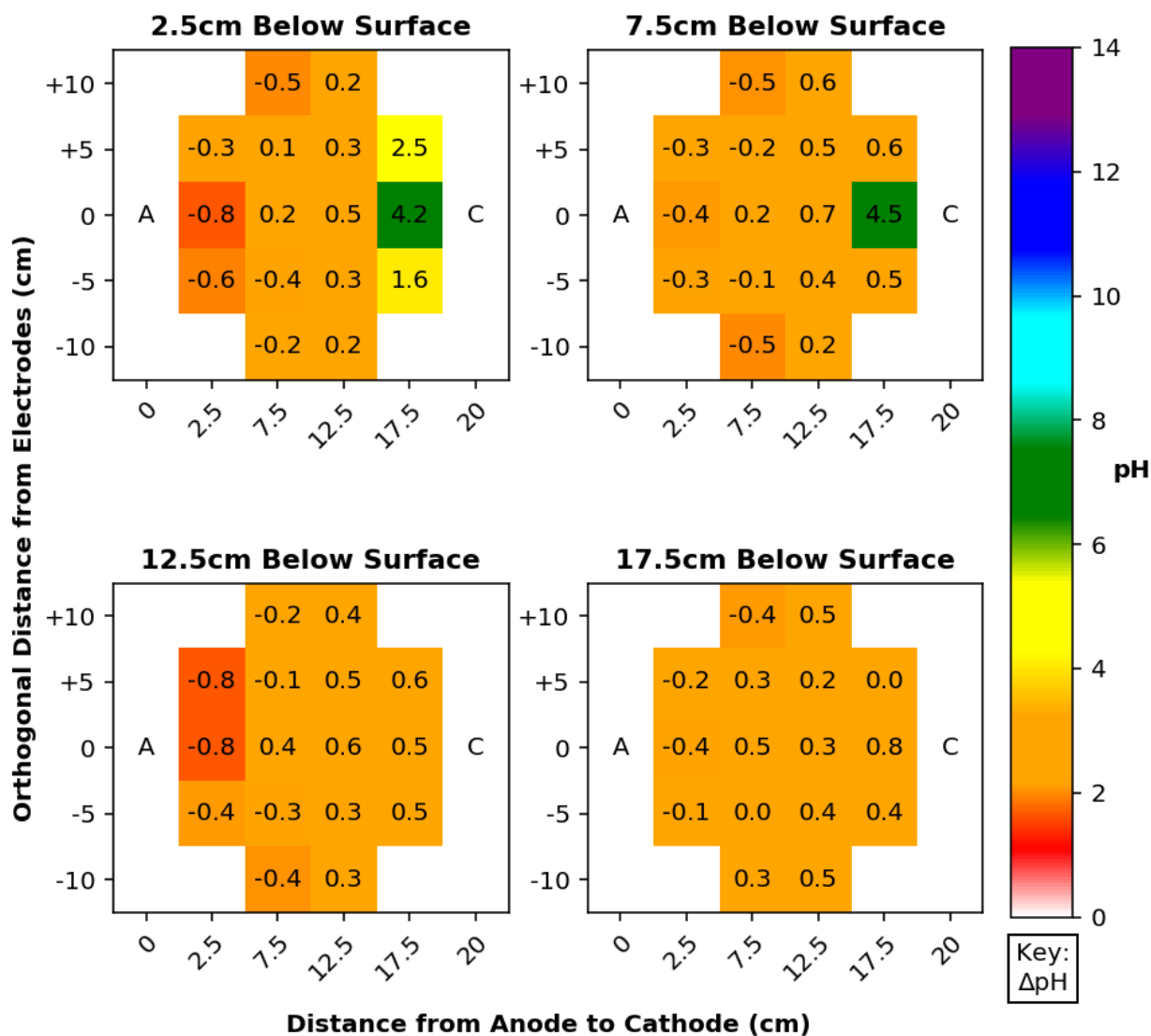


Figure 36. Graph. Final pH distribution by depth below soil surface (experiment 6). The numbers shown for each sample point indicate the change in pH from the initial conditions (ΔpH).

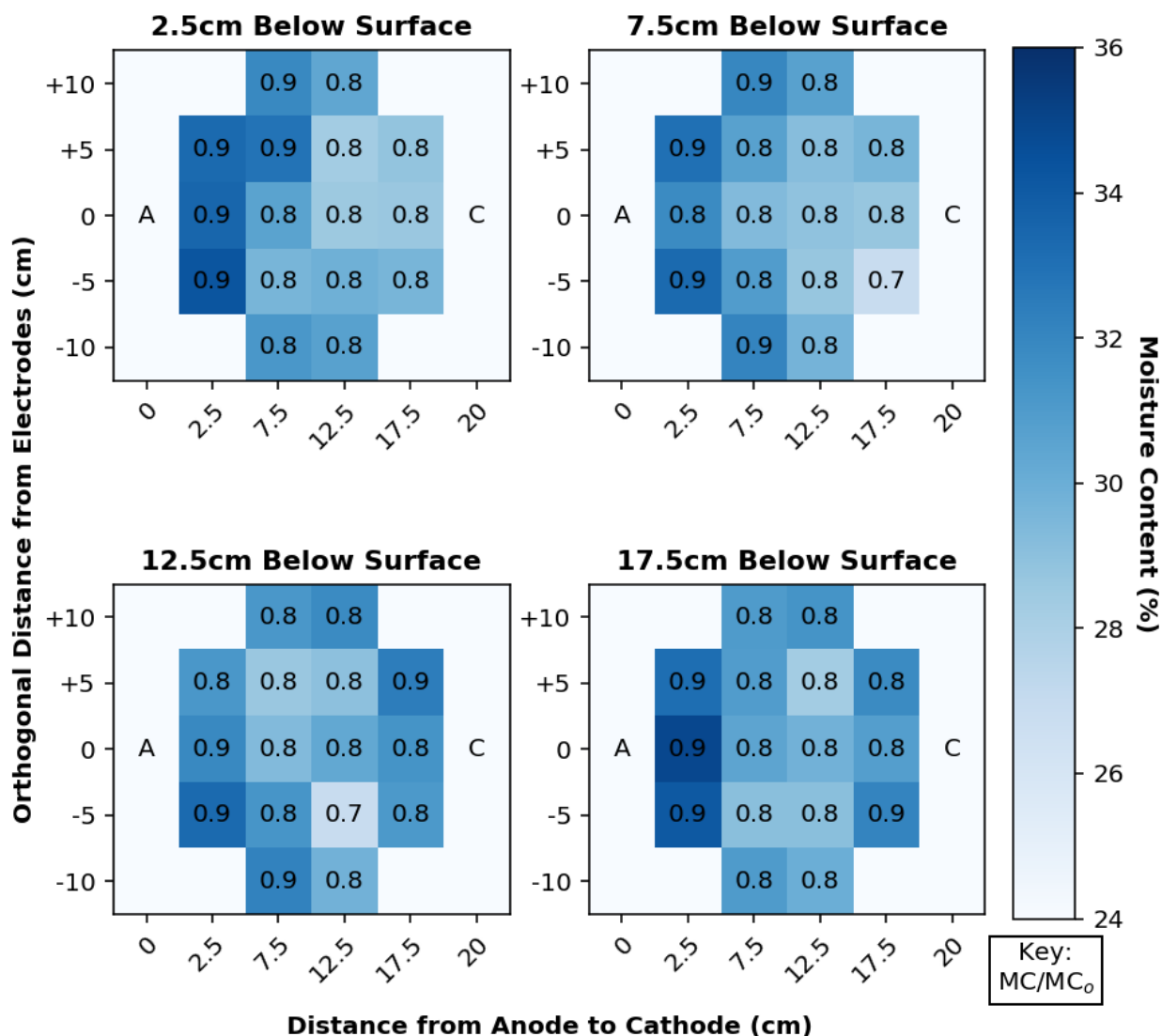


Figure 37. Graph. Final moisture content distribution by depth below soil surface (experiment 6). The numbers shown for each sample point indicate the final MC normalized by the initial MC (MC/MC_0).

COMPARISON OF EXPERIMENTS

Table 18 summarizes the results from each experiment. The highest pyrene removal (100%) occurred in experiment 6. This experiment utilized parameters highly influenced from the prior experimentation. The chemical regime from experiment 1 was utilized because it achieved the second highest pyrene removal (58.0%). A surcharge plate was utilized because experiments 4 and 5 demonstrated its ability to homogenize the treatment with respect to depth and prevent soil swelling. However, the surcharge plate used in experiment 6 was constructed of a semiporous reaction-bonded alumina as opposed to the HDPE-lined concrete plate used in experiments 4 and 5. This modification was made to allow for the escape of gas generated from CHP reactions. As hypothesized after experiment 4, the porous surcharge plate was able to both prevent swelling and negate the negative impacts of gas generation from CHP reactions. Interestingly, experiment 6

exhibited the lowest electro-osmotic flow volume over the longest treatment duration, whereas the chemical regime utilized in experiment 2 yielded the highest electro-osmotic flow rate over the shortest treatment duration. This conflict suggests that the successive addition of a nonionic surfactant and H₂O₂ could be beneficial toward increasing the efficacy of reagent distribution for pH amendment and complete extraction of the chromium. Overall, this work demonstrates the ability for electrochemical treatment to address both HMW-PAH and metal contaminants in clayey soil and proves further investigation into the optimization of these systems to be highly worthwhile.

Table 18. Summary of Post-Treatment Results by Experiment

Experiment	Electro-osmotic Flow (mL)			Contaminant Removal (%)				Avg. pH	Avg. Moisture Content (%)
	Daily Avg.	Total		Min.	Max.	Avg.	S.D.		
1	976	13,670	Pyr:	-48.2	99.4	58.0	38.6	2.1	32.1
2	1,159	16,220	Pyr:	-37.8	93.8	56.8	28.4	2.5	38.9
3	714	9,990	Pyr:	-42.9	94.8	23.8	26.5	2.6	34.7
4	1,108	15,512	Pyr:	-23.0	99.7	52.6	33.1	2.3	31.3
5	291	5,500	Mn:	-265.4	99.6	42.3	70.6	3.6	34.3
6	116	3,249	Pyr:	99.9	100.0	100.0	0.0	2.8	30.7
			Cr:	-334.9	71.8	4.5	99.1		

*Negative contaminant removal indicates transport/accumulation as opposed to destruction. S.D. = Standard Deviation.

CHAPTER 5: SUMMARY OF FINDINGS, FUTURE WORK, AND CONSIDERATIONS

SUMMARY AND CONCLUSIONS

The objective of this work was to develop an accelerated in situ treatment approach adaptable for use at the typical Illinois construction site to remove HMW-PAHs and metals from clayey soil in a time frame comparable to excavation and disposal. For this reason, the electrochemical treatment of clayey soils contaminated with HMW-PAHs and metals commonly encountered in Illinois was evaluated at the bench scale. Results from six electrochemical soil treatment experiments demonstrated several phenomena important for the optimization of a field-scale electrochemical treatment implementation. The first four experiments evaluated pyrene removal over 14 days. Relatively symmetrical pyrene destruction across the horizontal extents in experiments 1–4 uncovered the need for a gridded electrode configuration from which H_2O_2 is introduced at multiple anode wells. The highest pyrene removal obtained over 14 days was 58.0%, on average, using 10% H_2O_2 with a 0.1 M citrate buffer (pH = 4.5) that was initially supplied to both electrode wells and replenished at the anode. This work found that the addition of the nonionic surfactant Brij™35 can result in anode disintegration and soil pore clogging and is ultimately ineffective for the removal of pyrene, despite successes in literature for higher molecular weight PAHs such as benzo(a)pyrene (BaP) (Alcántara et al., 2008a; Gómez et al., 2009; Madadian et al., 2014). Conversely, the successive addition of Brij™35 followed by 10% H_2O_2 resulted in the highest electro-osmotic flow rate while preventing cathodic electrodeposition. A similar successive surfactant/oxidant approach may prove beneficial to the complete extraction of metal co-contaminants.

The fifth experiment successfully removed manganese from clayey soil in 21 days. Using an unoptimized electrochemical regime, the quantities of manganese removed and concentrated at the cathode rivaled that of electrochemical approaches used by others (Genc et al., 2009; Maini et al., 2000; Nogueira et al., 2007; Ricart et al., 1999; Shu et al., 2015). Overall, 42.3% of the manganese was fully extracted and 66% of the remaining manganese was spatially concentrated at a 0.875 normal distance from anode to cathode. The observation that 94% of the manganese at a 0.125 normal distance from anode to cathode was removed suggests the treatment is capable of complete extraction given longer time to operate. Electrochemical extraction of manganese was highly effective when augmented with citric acid and hydrogen peroxide systems. Despite similar successes in literature where manganese was electrokinetically removed using only water or citric acid (Genc et al., 2009; Ricart et al., 1999; Shu et al., 2015), the addition of H_2O_2 served to concurrently destroy organic contaminants. The final experiment evaluated the treatment of pyrene and chromium co-contaminated soil. Chromium contamination was demonstrated as a highly effective CHP catalyst. Using electrochemical treatment, pyrene was 100% homogenously destroyed over 28 days, while most of the chromium was spatially concentrated as a stable precipitant. Only 4.5% of the chromium was extracted, yet of the remaining chromium 57.4% was spatially concentrated at a 0.625 normal distance from anode to cathode. This experiment exhibited the lowest electro-osmotic flow rate. Combined interpretation of experiments 1–6 prove that single daily pH amendments are ineffective for controlling the soil pH, and typically ineffective for controlling the electrode-well pH for 24 hours.

More effective pH control is necessary to optimize electro-osmotic flow for reagent distribution in clayey soil contaminated with metals such that complete extraction can be achieved.

FUTURE WORK AND CONSIDERATIONS

The experiments carried out in this work are intended to inform an investigation aimed at field-scale implementation of electrochemical treatment to address a co-contaminated clayey soil. As such, further bench-scale optimization is necessary prior to recommending an electrochemical regime for pilot-scale investigation. With successful demonstration of both HMW-PAH and metal removal from a control kaolinite clay by electrochemical systems, the next step is to optimize the system for a co-contaminated field-collected soil.

Recommended Reactor Modifications

Several changes to the bench-scale reactor should be made prior to experimentation with field soils. First, the electrode wells need to include a circulation to electrolyte conditioning tanks such that powders are not directly added to the electrode wells. This type of amendment addition was found to interfere with operation of the float switch, and frequently clogged the overflow port. Previous attempts at using peristaltic pumps in continuous operation for a similar purpose failed because of ruptured tubing. For this reason, an innovative solution should provide circulation while maintaining chemical resistance, nonconductivity, and physical integrity. This modification should consider replenishing the anode well from the top rather than the side, which would allow for overflow from the anode well in the case of flow reversal. For the reactor used in experiments 1–6, flow reversal was observed in the metal-contaminated experiments, yet disallowance of overflow from the anode well prevented accurate measurement of the flow volume. Another reactor modification worth investigating would be to replenish the anode well from the bottom port to encourage more circulation. Currently, the electrode wells are prone to settling issues, which formed undesirable concentration and conductivity gradients. As evident from the pH adjustments tested in experiment 6 (Table 41), pH adjustment induced diffusion via electrochemical gradients and altered the soil zeta potential, and thus electro-osmotic flow direction can greatly influence the system flow rate.

Finally, neither the HDPE-lined concrete nor the alumina surcharge plate were ideal for application of a surcharge load. A geosynthetic liner similar to what would be implemented in field-scale treatment efforts would be highly practical if a method to apply it inside the reactor in a watertight fashion was developed.

Recommended Next Steps

Following reactor modification, the electrochemical regime should be optimized for co-contaminated field soils. Table 19 shows the contaminants present in a field soil collected from Illinois. It is recommended that the experimental evaluation of the field soil utilize the electrochemical regime optimized in experiment 6 for chromium and pyrene. Arsenic is an anionic metallic that behaves similarly to chromium, and benzo(a)pyrene is an HMW-PAH that behaves similarly to pyrene. A 28-day treatment period that leverages pH control by electrolyte conditioning at each electrode well is recommended, and the results from this work suggest promising treatment efficiency.

Table 19. Summary of Initial Field Soil Properties for Future Experiments

Soil	Contaminants	Concentration (mg/kg)	
		Dry	Wet
Field Soil (0–5 ft); Maintenance Yard; Silty Sand, Clay, Silty Clay; Rock Falls, Illinois	Arsenic		7.9
	Benzo(a)pyrene	–	0.13
	Manganese		726

The findings from this research can be used to influence pilot-scale electrochemical treatment at a contaminated Illinois construction site. The electrochemical regime optimized during the future field soil-treatment experiment will be implemented through a gridded array of electrode wells with graphite electrodes as determined necessary by this work. Successful pilot-scale demonstration will prove this treatment approach as a practical and robust statewide solution to contaminated Illinois soils. Broader implications of this work will include progress toward commercialization of the technology and the potential for implementation in less-regulated countries where contamination is widespread.

REFERENCES

- AATDF. (1997). *Technology practices manual for surfactants and cosolvents*. Retrieved from <https://clu-in.org/PRODUCTS/AATDF/Toc.htm>
- Acar, Y. B., & Alshawabkeh, A. N. (1993). Principles of electrokinetic remediation. *Environmental Science & Technology*, 27(13), 2638–2647. <https://doi.org/10.1021/es00049a002>
- Acar, Y. B., & Hamed, J. (1991). Electrokinetic soil processing in waste remediation and treatment: Synthesis of available data. *Transportation Research Record*, 1312, 9.
- Adewunmi, W. (2019). Drummer Illinois State Soil. Retrieved from <https://www.soils4teachers.org/files/s4t/k12outreach/il-state-soil-booklet.pdf>
- Akin, I., & Likos, W. (2017a). Tensile strength of compacted clay between residual saturation and air entry. *Geotechnical Frontiers 2017*, 72–81. <https://doi.org/10.1061/9780784480472.008>
- Akin, I., & Likos, W. (2017b). Brazilian tensile strength testing of compacted clay. *Geotechnical Testing Journal*, 40(4), 20160180. <https://doi.org/10.1520/GTJ20160180>
- Alcántara, M. T., Gómez, J., Pazos, M., & Sanromán, M. A. (2008a). Combined treatment of PAHs contaminated soils using the sequence extraction with surfactant–electrochemical degradation. *Chemosphere*, 70(8), 1438–1444. <https://doi.org/10.1016/j.chemosphere.2007.08.070>
- Alcántara, M. T., Pazos, M., Gouveia, S., Cameselle, C., & Sanromán, M. A. (2008b). Remediation of phenanthrene from contaminated kaolinite by electroremediation-Fenton technology. *Journal of Environmental Science and Health, Part A*, 43(8), 901–906. <https://doi.org/10.1080/10934520801974418>
- Alexander, M. (2000). Aging, bioavailability, and overestimation of risk from environmental pollutants. *Environmental Science & Technology*, 34(20), 7.
- Bard, A. J., & Faulkner, L. R. (2000). *Electrochemical methods: Fundamentals and applications* (2nd ed.). Wiley.
- Bokare, A. D., & Choi, W. (2010). Chromate-induced activation of hydrogen peroxide for oxidative degradation of aqueous organic pollutants. *Environmental Science & Technology*, 44(19), 7232–7237. <https://doi.org/10.1021/es903930h>
- Bokare, A. D., & Choi, W. (2011). Advanced oxidation process based on the Cr(III)/Cr(VI) redox cycle. *Environmental Science & Technology*, 45(21), 9332–9338. <https://doi.org/10.1021/es2021704>
- Brown, D. G., Knightes, C. D., & Peters, C. A. (1999). Risk assessment for polycyclic aromatic hydrocarbon NAPLs using component fractions. *Environmental Science & Technology*, 33(24), 4357–4363. <https://doi.org/10.1021/es9902423>
- Cahill, R. A. (2017). *Inorganic chemical composition of Illinois soils* (Circular no. 590). Illinois State Geological Survey, Prairie Research Institute, University of Illinois at Urbana-Champaign. <http://hdl.handle.net/2142/98958>
- Cameselle, C., & Pena, A. (2016). Enhanced electromigration and electro-osmosis for the remediation of an agricultural soil contaminated with multiple heavy metals. *Process Safety and Environmental*

- Protection*, 104, 209–217. <https://doi.org/10.1016/j.psep.2016.09.002>
- Chu, K. T. (2005). *Asymptotic analysis of extreme electrochemical transport*. PhD diss., Department of Mathematics, Massachusetts Institute of Technology.
- Corbin, J. F., Teel, A. L., Allen-King, R. M., & Watts, R. J. (2007). Reactive oxygen species responsible for the enhanced desorption of dodecane in modified Fenton's systems. *Water Environment Research*, 79(1), 37–42. <https://doi.org/10.2175/106143006X136793>
- Diamond, M. L., & Hodge, E. (2007). Urban contaminant dynamics: From source to effect. *Environmental Science & Technology*, 41(11), 3796–3800. <https://doi.org/10.1021/es072542n>
- Duan, L., Naidu, R., Thavamani, P., Meaklim, J., & Megharaj, M. (2015). Managing long-term polycyclic aromatic hydrocarbon contaminated soils: A risk-based approach. *Environmental Science and Pollution Research*, 22(12), 8927–8941. <https://doi.org/10.1007/s11356-013-2270-0>
- ELI. (2013). *State constraints: State-imposed limitations on the authority of agencies to regulate waters beyond the scope of the federal Clean Water Act* (No. 0931-01). Environmental Law Institute.
- Françoise, R. C., & Bourg, A. C. M. (1991). Aqueous geochemistry of chromium: A review. *Water Research*, 25(7), 807–816.
- FRTR. (2007a). *Home page: Remediation technologies screening matrix and reference guide, Version 4.0*. Retrieved March 4, 2018, from, https://frtr.gov/matrix2/top_page.html
- FRTR. (2007b). *4.28 Excavation, retrieval, and off-site: Remediation technologies screening matrix and reference guide, Version 4.0*. Retrieved March 4, 2018, from, <https://frtr.gov/matrix2/section4/4-29.html>
- FRTR. (2007c). *Table 3.2: Treatment technologies screening matrix*. Retrieved March 4, 2018, from, https://frtr.gov/matrix2/section3/table3_2.pdf
- Furman, O., Laine, D., Blumenfeld, A., Teel, A., Shimzu, K., Cheng, F., & Watts, R. (2009). Enhanced reactivity of superoxide in water–solid matrices. *Environmental Science & Technology*, 43(5), 1528–1533.
- Garrido-Ramírez, E. G., Theng, B. K. G., & Mora, M. L. (2010). Clays and oxide minerals as catalysts and nanocatalysts in Fenton-like reactions—A review. *Applied Clay Science*, 47(3–4), 182–192. <https://doi.org/10.1016/j.clay.2009.11.044>
- Genaro-Mattos, T., Lopes, A., Alonso, A., Hermes-Lima, M., & Freitas Lopes, T. (2009). Chromium mediated hydroxyl radical formation: The longest-lasting Fenton-type reaction reported so far. *Free Radical Biology and Medicine*, 47(S188).
- Genc, A., Chase, G., & Foos, A. (2009). Electrokinetic removal of manganese from river sediment. *Water, Air, and Soil Pollution*, 197(1–4), 131–141. <https://doi.org/10.1007/s11270-008-9796-7>
- Gent, D. (2004). Bench- and field-scale evaluation of chromium and cadmium extraction by electrokinetics. *Journal of Hazardous Materials*, 110(1–3), 53–62. <https://doi.org/10.1016/j.jhazmat.2004.02.036>

- Gómez, J., Alcántara, M. T., Pazos, M., & Sanromán, M. A. (2009). A two-stage process using electrokinetic remediation and electrochemical degradation for treating benzo[a]pyrene spiked kaolin. *Chemosphere*, 74(11), 1516–1521. <https://doi.org/10.1016/j.chemosphere.2008.11.019>
- Haag, W. R., & Yao, C. C. D. (1992). Rate constants for reaction of hydroxyl radicals with several drinking water contaminants. *Environmental Science & Technology*, 26(5), 1005–1013. <https://doi.org/10.1021/es00029a021>
- Haber, F., & Weiss, J. (1934). The catalytic decomposition of hydrogen peroxide by iron salts. *Proceedings of the Royal Society of London. Series A—Mathematical and Physical Sciences*, 147(861), 332–351. <https://doi.org/10.1098/rspa.1934.0221>
- Haight, G. P. Jr., Huang, T. J., & Shakhasiri, B. Z. (1970). Reactions of chromium(IV). *Journal of Inorganic and Nuclear Chemistry*, 33(7), 2169–2175.
- Hatzinger, P. B., & Alexander, M. (1995). Effect of aging of chemicals in soil on their biodegradability and extractability. *Environmental Science & Technology*, 29(2), 537–545. <https://doi.org/10.1021/es00002a033>
- Hoytink, G. J. (1968). Electrochemiluminescence of aromatic hydrocarbons. *Discussions of the Faraday Society*, 45, 14. <https://doi.org/10.1039/df9684500014>
- Huling, S. G., & Pivetz, B. E. (2006). *In-situ chemical oxidation* (No. EPA/600/R-06/072). US EPA Archive Document.
- Hunter, R. J., & James, M. (1992). Charge reversal of kaolinite by hydrolyzable metal ions: An electroacoustic study. *Clays and Clay Minerals*, 40(6), 644–649. <https://doi.org/10.1346/CCMN.1992.0400603>
- ICT. (2017, September 1). *Request for Proposal (RFP) #17-01: Evaluation of On-site and In-situ Treatment Alternatives for Contaminated Soils*. Illinois Center for Transportation.
- Illinois Administrative Code, 35 IAC §1100 §§F (2012). AUTHORITY: Implementing Sections 5, 3.160, 22.51, and 22.51a and authorized by Sections 3.160, 22.51, 22.51a, and 27 of the Environmental Protection Act [415 ILCS 5/5, 22.51, 22.51a, and 27]. SOURCE: Adopted in R06-19 at 30 Ill. Reg.14534, effective August 24, 2006; amended in R12-9 at 36 Ill. Reg. 13892, effective August 27, 2012. <http://www.ilga.gov/commission/jcar/admincode/035/03501100sections.html>.
- Jacobsen, F., Holcman, J., & Sehested, K. (1998). Oxidation of manganese(II) by ozone and reduction of manganese(III) by hydrogen peroxide in acidic solution. *International Journal of Chemical Kinetics*, 30(3), 207–214. [https://doi.org/10.1002/\(SICI\)1097-4601\(1998\)30:3<207::AID-KIN6>3.0.CO;2-W](https://doi.org/10.1002/(SICI)1097-4601(1998)30:3<207::AID-KIN6>3.0.CO;2-W)
- James, B. R. (1996). Peer reviewed: The challenge of remediating chromium-contaminated soil. *Environmental Science & Technology*, 30(6), 248A–251A. <https://doi.org/10.1021/es962269h>
- Jardine, P. M., Stewart, M. A., Barnett, M. O., Basta, N. T., Brooks, S. C., Fendorf, S., & Mehlhorn, T. L. (2013). Influence of soil geochemical and physical properties on chromium(VI) sorption and bioaccessibility. *Environmental Science & Technology*, 47(19), 11241–11248. <https://doi.org/10.1021/es401611h>

- Khan, L. I. (1991). *Study of electroosmosis in soil: A modified theory and its applications in soil decontamination*. PhD diss., Department of Civil and Environmental Engineering, Lehigh University.
- Kim, E.-J., Oh, D., Lee, C.-S., Gong, J., Kim, J., & Chang, Y.-S. (2017). Manganese oxide nanorods as a robust Fenton-like catalyst at neutral pH: Crystal phase-dependent behavior. *Catalysis Today*, 282, 71–76. <https://doi.org/10.1016/j.cattod.2016.03.034>
- Ko, S., Crimi, M., Marvin, B. K., Holmes, V., & Huling, S. G. (2012). Comparative study on oxidative treatments of NAPL containing chlorinated ethanes and ethenes using hydrogen peroxide and persulfate in soils. *Journal of Environmental Management*, 108, 42–48. <https://doi.org/10.1016/j.jenvman.2012.04.034>
- Kuppusamy, S., Thavamani, P., Venkateswarlu, K., Lee, Y. B., Naidu, R., & Megharaj, M. (2017). Remediation approaches for polycyclic aromatic hydrocarbons (PAHs) contaminated soils: Technological constraints, emerging trends and future directions. *Chemosphere*, 168, 944–968. <https://doi.org/10.1016/j.chemosphere.2016.10.115>
- Kwan, W. P., & Voelker, B. M. (2003). Rates of hydroxyl radical generation and organic compound oxidation in mineral-catalyzed Fenton-like systems. *Environmental Science & Technology*, 37(6), 1150–1158. <https://doi.org/10.1021/es020874g>
- Lee, L. S., Zhai, X., & Lee, J. (2007). *INDOT guidance document for in-situ soil flushing* (No. FHWA/IN/JTRP-2006/28-2). Retrieved from Joint Transportation Research Program, Indiana Department of Transportation and Purdue University. <https://doi.org/10.5703/1288284314230>
- Liang, X., Zhu, L., & Zhuang, S. (2016). Sorption of polycyclic aromatic hydrocarbons to soils enhanced by heavy metals: Perspective of molecular interactions. *Journal of Soils and Sediments*, 16(5), 1509–1518. <https://doi.org/10.1007/s11368-015-1341-x>
- Luthy, R. G., Aiken, G. R., Brusseau, M. L., Cunningham, S. D., Gschwend, P. M., Pignatello, J. J., ... Westall, J. C. (1997). Sequestration of hydrophobic organic contaminants by geosorbents. *Environmental Science & Technology*, 31(12), 3341–3347. <https://doi.org/10.1021/es970512m>
- Madadian, E., Gitipour, S., Amiri, L., Alimohammadi, M., & Saatloo, J. (2014). The application of soil washing for treatment of polycyclic aromatic hydrocarbons contaminated soil: A case study in a petrochemical complex. *Environmental Progress & Sustainable Energy*, 33(1), 107–113. <https://doi.org/10.1002/ep.11759>
- Maini, G., Sharman, A. K., Knowles, C. J., Sunderland, G., & Jackman, S. A. (2000). Electrokinetic remediation of metals and organics from historically contaminated soil. *Journal of Chemical Technology & Biotechnology*, 75(8), 657–664. [https://doi.org/10.1002/1097-4660\(200008\)75:8<657::AID-JCTB263>3.0.CO;2-5](https://doi.org/10.1002/1097-4660(200008)75:8<657::AID-JCTB263>3.0.CO;2-5)
- Menzie, C. A., Potocki, B. B., & Santodonato, J. (1992). Exposure to carcinogenic PAHs in the environment. *Environmental Science & Technology*, 26(7), 1278–1284. <https://doi.org/10.1021/es00031a002>
- Merdoud, O., Cameselle, C., Boulakradeche, M. O., & Akretche, D. E. (2016). Removal of heavy metals from contaminated soil by electrodialytic remediation enhanced with organic acids. *Environmental Science: Processes & Impacts*, 18(11), 1440–1448. <https://doi.org/10.1039/C6EM00380J>

- Minghua, Z., Oturan, M. A., & Sirés, I, eds. (2018). *Electro-Fenton process: New trends and scale-up*. Springer. <https://doi.org/10.1007/978-981-10-6406-7>
- Monahan, M. J., Teel, A. L., & Watts, R. J. (2005). Displacement of five metals sorbed on kaolinite during treatment with modified Fenton's reagent. *Water Research*, 39(13), 2955–2963. <https://doi.org/10.1016/j.watres.2005.04.064>
- Newman, J., & Thomas-Alyea, K. E. (2004). *Electrochemical systems* (3rd ed.). Wiley-Interscience.
- Nogueira, M. G., Pazos, M., Sanromán, M. A., & Cameselle, C. (2007). Improving on electrokinetic remediation in spiked Mn kaolinite by addition of complexing agents. *Electrochimica Acta*, 52(10), 3349–3354. <https://doi.org/10.1016/j.electacta.2006.03.115>
- Page, M. M., & Page, C. L. (2002). Electroremediation of contaminated soils. *Journal of Environmental Engineering*, 128(3), 208–219. [https://doi.org/10.1061/\(ASCE\)0733-9372\(2002\)128:3\(208\)](https://doi.org/10.1061/(ASCE)0733-9372(2002)128:3(208))
- Pamukcu, S. (2009). Electrochemical transport and transformations. In K. R. Reddy & C. Cameselle (Eds.), *Electrochemical remediation technologies for polluted soils, sediments and groundwater* (pp. 29–64). Wiley.
- Patnaik, P. (2007). *A comprehensive guide to the hazardous properties of chemical substances* (3rd ed). John Wiley.
- Pelletier, A.J. (2019). Electrochemical remediation of co-contaminated clayey soil. Master's thesis, Washington State University.
- Purdue Engineering. (2019). Hydrologic Soil Groups. Retrieved August 25, 2019, from, <https://engineering.purdue.edu/mapserve/LTHIA7/documentation/hsg.html>
- Quan, H. N., Teel, A. L., & Watts, R. J. (2003). Effect of contaminant hydrophobicity on hydrogen peroxide dosage requirements in the Fenton-like treatment of soils. *Journal of Hazardous Materials*, 102(2–3), 277–289. [https://doi.org/10.1016/S0304-3894\(03\)00214-0](https://doi.org/10.1016/S0304-3894(03)00214-0)
- Reddy, K. R., & Al-Hamdan, A. Z. (2013). Enhanced sequential flushing process for removal of mixed contaminants from soils. *Water, Air, & Soil Pollution*, 224(12). <https://doi.org/10.1007/s11270-013-1709-8>
- Reddy, K. R., Al-Hamdan, A. Z., & Ala, P. (2011). Enhanced soil flushing for simultaneous removal of PAHs and heavy metals from industrial contaminated soil. *Journal of Hazardous, Toxic, and Radioactive Waste*, 15(3), 166–174. [https://doi.org/10.1061/\(ASCE\)HZ.1944-8376.0000076](https://doi.org/10.1061/(ASCE)HZ.1944-8376.0000076)
- Reddy, K. R., & Cameselle, C. (2009). *Electrochemical remediation technologies for polluted soils, sediments, and groundwater*. University of Illinois at Chicago, University of Vigo, Hoboken, New Jersey and Canada: John Wiley & Sons, INC.
- Reddy, K. R., & Karri, M. R. (2008). Effect of oxidant dosage on integrated electrochemical remediation of contaminant mixtures in soils. *Journal of Environmental Science and Health, Part A*, 43(8), 881–893. <https://doi.org/10.1080/10934520801974392>
- Ricart, M. T., Cameselle, C., Lucas, T., & Lema, J. M. (1999). Manganese removal from spiked kaolinitic soil and sludge by electromigration. *Separation Science and Technology*, 34(16), 3227–3241. <https://doi.org/10.1081/SS-100100832>

- Rock, M. L., James, B. R., & Helz, G. R. (2001). Hydrogen peroxide effects on chromium oxidation state and solubility in four diverse, chromium-enriched soils. *Environmental Science & Technology*, 35(20), 4054–4059. <https://doi.org/10.1021/es010597y>
- Romanias, M. N., Andrade-Eiroa, A., Shahla, R., Bedjanian, Y., Zogka, A. G., Philippidis, A., & Dagaut, P. (2014). Photodegradation of pyrene on Al_2O_3 Surfaces: A detailed kinetic and product study. *The Journal of Physical Chemistry A*, 118(34), 7007–7016. <https://doi.org/10.1021/jp504725z>
- Rueffer, M., Bejan, D., & Bunce, N. J. (2011). Graphite: An active or an inactive anode? *Electrochimica Acta*, 56(5), 2246–2253. <https://doi.org/10.1016/j.electacta.2010.11.071>
- Saichek, R. E., & Reddy, K. R. (2005). Surfactant-enhanced electrokinetic remediation of polycyclic aromatic hydrocarbons in heterogeneous subsurface environments. *Journal of Environmental Engineering and Science*, 4(5), 327–339. <https://doi.org/10.1139/s04-064>
- Schumb, W. (1957). Stabilization of concentrated solutions of hydrogen peroxide. *Industrial & Engineering Chemistry*, 49(10), 1759–1762. <https://doi.org/10.1021/ie50574a044>
- Semple, K. T., Morriss, A. W. J., & Paton, G. I. (2003). Bioavailability of hydrophobic organic contaminants in soils: Fundamental concepts and techniques for analysis. *European Journal of Soil Science*, 54(4), 809–818. <https://doi.org/10.1046/j.1351-0754.2003.0564.x>
- Shang, J. Q., Inculet, I. I., & Lo, K. Y. (1994). Low frequency dielectrophoresis in clay-water-electrolyte systems. *Journal of Electrostatics*, 33(2), 229–244.
- Shi, X., & Dalal, N. (1990). ESR spin trapping detection of hydroxyl radicals in the reactions of Cr(V) complexes with hydrogen peroxide. *Free Radical Research Communications*, 10(1–2), 17–26.
- Shi, X., Dalal, N., & Kasprzak, K. S. (1993). Generation of free radicals from hydrogen peroxide and lipid hydroperoxides in the presence of Cr(III). *Archives of Biochemistry and Biophysics*, 1, 294–299.
- Shi, X., Leonard, S. S., Liu, K. J., Zang, L., Gannett, P. M., Rojanasakul, Y., ... Vallyathan, V. (1998). Cr(III)-mediated hydroxyl radical generation via Haber-Weiss cycle. *Journal of Inorganic Biochemistry*, 69(4), 263–268. [https://doi.org/10.1016/S0162-0134\(97\)10037-X](https://doi.org/10.1016/S0162-0134(97)10037-X)
- Shi, X., Mao, Y., Knapton, A. D., Ding, M., Rojanasakul, Y., Gannett, P. M., ... Liu, K. (1994). Reaction of Cr(VI) with ascorbate and hydrogen peroxide generates hydroxyl radicals and causes DNA damage role of a Cr(IV)-mediated Fenton-like reaction. *Carcinogenesis*, 15(11), 2475–2478.
- Shu, J., Liu, R., Liu, Z., Du, J., & Tao, C. (2015). Electrokinetic remediation of manganese and ammonia nitrogen from electrolytic manganese residue. *Environmental Science and Pollution Research*, 22(20), 16004–16013. <https://doi.org/10.1007/s11356-015-4817-8>
- Siegrist, R. L., Crimi, M., & Simpkin, T. J. (2011). *In situ chemical oxidation for groundwater remediation*. Springer Science & Business Media.
- Smith, B. A., Teel, A. L., & Watts, R. J. (2004). Identification of the reactive oxygen species responsible for carbon tetrachloride degradation in modified Fenton's systems. *Environmental Science & Technology*, 38(20), 5465–5469. <https://doi.org/10.1021/es0352754>
- Smith, B. A., Teel, A. L., & Watts, R. J. (2006). Mechanism for the destruction of carbon tetrachloride and chloroform DNAPLs by modified Fenton's reagent. *Journal of Contaminant Hydrology*, 85(3–

- 4), 229–246. <https://doi.org/10.1016/j.jconhyd.2006.02.002>
- Smith, B. A., Teel, A. L., & Watts, R. J. (2009). Destruction of trichloroethylene and perchloroethylene DNAPLs by catalyzed H₂ O₂ propagations. *Journal of Environmental Engineering*, 135(7), 535–543. [https://doi.org/10.1061/\(ASCE\)0733-9372\(2009\)135:7\(535\)](https://doi.org/10.1061/(ASCE)0733-9372(2009)135:7(535))
- Soil Survey Staff, NRCS, USDA. (2017). Web Soil Survey. Retrieved September 5, 2019, from <https://websoilsurvey.sc.egov.usda.gov/>
- Sposito, G. (2016). *The Chemistry of Soils* (3rd ed.). Oxford University Press.
- State of California. (2019). *List of authorized injection material amendments—chemical oxidant activators, chelating agents: Sodium citrate, sodium phytate, sodium Malonate*. Retrieved from https://www.waterboards.ca.gov/losangeles/board_decisions/adopted_orders/WDR_Update/
- Teel, A., Teel, A., Cutler, L., & Watts, R. (2009). Effect of sorption on contaminant oxidation in activated persulfate systems. *Journal of Environmental Science and Health, Part A: Toxic/Hazardous Substances & Environmental Engineering*, 44(11), 1098–1103. <https://doi.org/10.1080/10934520903005095>
- Tsou, T.-C., & Yang, J.-L. (1996). Formation of reactive oxygen species and DNA strand breakage during interaction of chromium(III) and hydrogen peroxide in vitro: Evidence for a chromium(III)-mediated Fenton-like reaction. *Chemico-Biological Interactions*, 102(3):133–53. [https://doi.org/10.1016/s0009-2797\(96\)03740-4](https://doi.org/10.1016/s0009-2797(96)03740-4)
- USDA. (2010). *Illinois understanding soil*. Retrieved November 13, 2018, from <http://www.illinoissoils.org/files/85070546.pdf>
- USDA. (2015). Drummer Series. Website for Official Soil Series Descriptions and Series Classification Retrieved December 24, 2020, from https://soilseries.sc.egov.usda.gov/OSD_Docs/D/DRUMMER.html
- USDA. (2019). *Drummer—Illinois state soil*. Retrieved January 10, 2019, from, https://extension.illinois.edu/soil/st_soils/il_soil.htm
- USDA, NRCS. (1986). *Urban hydrology for small watersheds* (No. TR-55). United States Department of Agriculture, Natural Resources Conservation Service.
- USEPA. (2004). *Cleaning up the nation's waste sites: Markets and technology trends* (pp. 3–9). Office of Solid Waste and Emergency Response.
- USEPA. (2021a). Method 9045D Soil and Waste pH. United States Environmental Protection Agency. Retrieved May 19, 2021 from, <https://www.epa.gov/sites/production/files/2015-12/documents/9045d.pdf>
- USEPA. (2021b). Method 3050B Acid Digestion of Sediments, Sludges, and Soils. United States Environmental Protection Agency. Retrieved May 19, 2021 from, <https://www.epa.gov/sites/production/files/2015-06/documents/epa-3050b.pdf>
- USEPA. (2021c). Method 6020B Inductively Coupled Plasma-Mass Spectrometry. United States Environmental Protection Agency. Retrieved May 19, 2021 from, <https://www.epa.gov/sites/production/files/2015-12/documents/6020b.pdf>

- Vasil'ev, R. F. (1970). Chemiluminescence excitation mechanisms. *Russian Chemical Reviews*, 39(6), 529–544. <https://doi.org/10.1070/RC1970v039n06ABEH002004>
- Wang, W. H., Hoag, G. E., Collins, J. B., & Naidu, R. (2013). Evaluation of surfactant-enhanced in situ chemical oxidation (S-ISCO) in contaminated soil. *Water, Air, & Soil Pollution*, 224(12). <https://doi.org/10.1007/s11270-013-1713-z>
- Watts, R. J., Bottenberg, B. C., Hess, T. F., Jensen, M. D., & Teel, A. L. (1999). Role of reductants in the enhanced desorption and transformation of chloroaliphatic compounds by modified Fenton's reactions. *Environmental Science & Technology*, 33(19), 3432–3437. <https://doi.org/10.1021/es990054c>
- Watts, R. J., Finn, D. D., Cutler, L. M., Schmidt, J. T., & Teel, A. L. (2007). Enhanced stability of hydrogen peroxide in the presence of subsurface solids. *Journal of Contaminant Hydrology*, 91(3–4), 312–326. <https://doi.org/10.1016/j.jconhyd.2006.11.004>
- Watts, R. J., Haeri-McCarroll, T. M., & Teel, A. L. (2008). Effect of contaminant hydrophobicity in the treatment of contaminated soils by catalyzed H₂O₂ propagations (modified Fenton's reagent). *Journal of Advanced Oxidation Technologies*, 11(2). <https://doi.org/10.1515/jaots-2008-0221>
- Watts, R. J., Sarasa, J., Loge, F. J., & Teel, A. L. (2005). Oxidative and reductive pathways in manganese-catalyzed Fenton's reactions. *Journal of Environmental Engineering*, 131(1), 158–164. [https://doi.org/10.1061/\(ASCE\)0733-9372\(2005\)131:1\(158\)](https://doi.org/10.1061/(ASCE)0733-9372(2005)131:1(158))
- Watts, R. J., & Teel, A. L. (2005). Chemistry of modified Fenton's reagent (catalyzed H₂O₂ propagations–CHP) for in situ soil and groundwater remediation. *Journal of Environmental Engineering*, 131(4), 612–622. [https://doi.org/10.1061/\(ASCE\)0733-9372\(2005\)131:4\(612\)](https://doi.org/10.1061/(ASCE)0733-9372(2005)131:4(612))
- Watts, R., Udell, M., Kong, S., & Leung, S. (1999). Fenton-like soil remediation catalyzed by naturally occurring iron minerals. *Environ. Eng. Sci.*, 16(1), 93–103. <https://doi.org/10.1089/ees.1999.16.93>
- Wick, L. Y. (2009). Coupling electrokinetics to the bioremediation of organic contaminants: Principles and fundamental interactions. In Reddy K. R. and Cameselle C. (Ed.), *Electrochemical Remediation Technologies for Polluted Soils, Sediments and Groundwater* (pp.367–387). John Wiley & Sons, Inc.
- Williamson, J., & Isgor, O. B. (2016). The effect of simulated concrete pore solution composition and chlorides on the electronic properties of passive films on carbon steel rebar. *Corrosion Science*, 106, 82–95. <https://doi.org/10.1016/j.corsci.2016.01.027>
- Yang, S., Li, J., & Song, Y. (2017). Application of surfactant Tween 80 to enhance Fenton oxidation of polycyclic aromatic hydrocarbons (PAHs) in soil pre-treated with Fenton reagents. *Geology, Ecology, and Landscapes*, 1(3), 197–204. <https://doi.org/10.1080/24749508.2017.1361152>
- Yeung, A. T. (2009). Geochemical processes affecting electrochemical remediation. In Reddy K. R. and Cameselle C. (Ed.), *Electrochemical Remediation Technologies for Polluted Soils, Sediments and Groundwater* (pp. 65–94). John Wiley & Sons, Inc.

APPENDICES

APPENDIX A: CHAPTER 1 SUPPLEMENTARY INFORMATION

Table 20. Summary of Actual and Lowest MAC Exceedances from the Preliminary Dataset

Site Name: District #	Site Description	Sample Date	Sample Depth (m)	Exceedance Concentration (mg/kg)	Samples in Exceedance
Aluminum					
“Actual Mac Exceedances”					
036 Orland Park: 1	Commercial	2008	0–2.4	9,500–16,000	25
003 Rohlwing Road: 1	Commercial	2010	0–2.4	9,500–15,000	34
022 Grayslake: 1	Commercial	2011	0–1.5	11,000–17,000	7
063 US Rt. 45 LaGrange Road: 1	Commercial	2012	0–4.6	9,500–22,000	186
Additional “Lowest Mac Exceedances”					
036 Orland Park: 1	Commercial	2008	0–2.4	9,300	1
003 Rohlwing Road: 1	Commercial	2010	0–2.4	9,400	1
063 US Rt. 45 LaGrange Road: 1	Commercial	2012	0–4.6	9,400	1
Arsenic					
“Actual Mac Exceedances”					
WO 044 Dan Ryan II: 1	Transportation	2004	0–2.1	14–17	2
036 Orland Park: 1	Commercial	2008	1–1.8	13–14	5
003 Rohlwing Road: 1	Commercial	2010	0–1.8	13–16	4
063 US Rt. 45 LaGrange Road: 1	Commercial	2012	0–4.6	13–30	13
035 Channahon: 1	Commercial	2015	0–1.5	13.7	1
046 Barrington: 1	Commercial	2016	0–3.0	13.8–25.2	4
Additional “Lowest Mac Exceedances”					
003 Rohlwing Road: 1	Commercial	2010	0–1.8	12–13	2
063 US Rt. 45 LaGrange Road: 1	Commercial	2012	0–4.6	12–13	3
035 Channahon: 1	Commercial	2015	0–1.5	12–13.7	2
046 Barrington: 1	Commercial	2016	0–3.0	11.8–13.8	3
Benzo(a)anthracene					
“Actual Mac Exceedances”					
003 Rohlwing Road: 1	Commercial	2010	0–0.6	1.8–5.9	3
022 Grayslake: 1	Commercial	2011	0–1.5	3.6–4.2	2
063 US Rt. 45 LaGrange Road: 1	Commercial	2012	0–1.8	3.3–4.1	3
046 Barrington: 1	Commercial	2016	0–1.2	9.1	1
Additional “Lowest Mac Exceedances”					
WO 055 LaSalle: 3	Residential	2005	1.2	1.2	1
036 Orland Park: 1	Commercial	2008	0.15–0.8	1.1–1.2	2
003 Rohlwing Road: 1	Commercial	2010	0–0.6	0.93–1.8	5
022 Grayslake: 1	Commercial	2011	0–1.5	1.4	1
063 US Rt. 45 LaGrange Road: 1	Commercial	2012	0–1.8	1.3	1
035 Channahon: 1	Commercial	2015	0–1.2	1.02	1

Table 20. Summary of Actual and Lowest MAC Exceedances from the Preliminary Dataset

Site Name: District #	Site Description	Sample Date	Sample Depth (m)	Exceedance Concentration (mg/kg)	Samples in Exceedance
Benzo(a)pyrene					
“Actual Mac Exceedances”					
003 Rohlwing Road: 1	Commercial	2010	0–0.6	2.1–5.8	2
022 Grayslake: 1	Commercial	2011	0–1.5	6.5	2
063 US Rt. 45 LaGrange Road: 1	Commercial	2012	0–1.8	3.8–7.3	3
046 Barrington: 1	Commercial	2016	0–1.2	8.5	1
Additional “Lowest Mac Exceedances”					
WO 044 Dan Ryan II: 1	Transportation	2004	0–2.1	0.15–0.67	6
WO 055 LaSalle: 3	Residential	2005	0.06–2.7	0.15–1.1	5
036 Orland Park: 1	Commercial	2008	0–1.5	0.099–1.4	9
003 Rohlwing Road: 1	Commercial	2010	0–3.0	0.091–5.8	52
022 Grayslake: 1	Commercial	2011	0–1.5	0.093–6.5	9
063 US Rt. 45 LaGrange Road: 1	Commercial	2012	0–2.4	0.096–7.3	35
035 Channahon: 1	Commercial	2015	0–4.6	0.0987–0.838	30
046 Barrington: 1	Commercial	2016	0–1.5	0.2–8.5	4
015 Jonesville: 3	Commercial	2017	0–0.3	0.099–0.13	4
Benzo(b)fluoranthene					
“Actual Mac Exceedances”					
003 Rohlwing Road: 1	Commercial	2010	0–0.6	2.6–7.1	3
022 Grayslake: 1	Commercial	2011	0–1.5	2.3–7.6	3
063 US Rt. 45 LaGrange Road: 1	Commercial	2012	0–2.1	4.7–5.2	3
046 Barrington: 1	Commercial	2016	0–1.2	12	1
Additional “Lowest Mac Exceedances”					
WO 044 Dan Ryan II: 1	Transportation	2004	0–1.8	0.95	1
036 Orland Park: 1	Commercial	2008	0.15–0.8	1.6–1.7	2
003 Rohlwing Road: 1	Commercial	2010	0–0.6	1.1–7.1	11
022 Grayslake: 1	Commercial	2011	0–1.5	1.6–7.6	4
063 US Rt. 45 LaGrange Road: 1	Commercial	2012	0–2.1	1–5.2	7
046 Barrington: 1	Commercial	2016	0–1.2	12	1
Chromium					
“Actual Mac Exceedances”					
036 Orland Park: 1	Commercial	2008	0.6–1.2	22	1
003 Rohlwing Road: 1	Commercial	2010	0–2.4	22–37	6
063 US Rt. 45 LaGrange Road: 1	Commercial	2012	0–4.6	22–42	44
035 Channahon: 1	Commercial	2015	0–3.0	21.1–395	10
046 Barrington: 1	Commercial	2016	0–3.0	21.1–39.9	34
015 Jonesville: 3	Recreational	2017	0–0.3	25	1
“Lowest Mac Exceedances” – Same as Actual					

Table 20. Summary of Actual and Lowest MAC Exceedances from the Preliminary Dataset

Site Name: District #	Site Description	Sample Date	Sample Depth (m)	Exceedance Concentration (mg/kg)	Samples in Exceedance
Dibenzo(a,h)anthracene					
“Actual Mac Exceedances”					
003 Rohlwing Road: 1	Commercial	2010	0–0.6	0.43–1.3	3
022 Grayslake: 1	Commercial	2011	0–1.5	0.46–2.4	4
063 US Rt. 45 LaGrange Road: 1	Commercial	2012	0–1.8	0.81–1.1	3
046 Barrington: 1	Commercial	2016	0–1.2	1.6	1
Additional “Lowest Mac Exceedances”					
WO 044 Dan Ryan II: 1	Transportation	2004	0–1.8	0.12	1
WO 055 LaSalle: 3	Residential	2005	0.06–1.2	0.1–0.18	5
036 Orland Park: 1	Commercial	2008	0–0.5	0.1–3.4	2
003 Rohlwing Road: 1	Commercial	2010	0–0.6	0.12–1.3	15
022 Grayslake: 1	Commercial	2011	0–1.5	0.097–2.4	6
063 US Rt. 45 LaGrange Road: 1	Commercial	2012	0–2.1	0.096–1.1	12
046 Barrington: 1	Commercial	2016	0–1.2	1.6	1
Indeno(1,2,3-cd)pyrene					
“Actual Mac Exceedances”					
003 Rohlwing Road: 1	Commercial	2010	0–0.6	4.2	1
022 Grayslake: 1	Commercial	2011	0–1.5	4.3–5	2
063 US Rt. 45 LaGrange Road: 1	Commercial	2012	0–1.8	2.3–5.1	3
046 Barrington: 1	Commercial	2016	0–1.2	5.5	1
Additional “Lowest Mac Exceedances”					
003 Rohlwing Road: 1	Commercial	2010	0–0.6	0.95–4.2	5
022 Grayslake: 1	Commercial	2011	0–1.5	1.2–5	4
063 US Rt. 45 LaGrange Road: 1	Commercial	2012	0–2.1	0.97–5.1	4
046 Barrington: 1	Commercial	2016	0–1.2	5.5	1
Lead					
“Actual Mac Exceedances”					
WO 044 Dan Ryan II: 1	Transportation	2004	0–2.1	140	1
003 Rohlwing Road: 1	Commercial	2010	0–0.6	150	1
063 US Rt. 45 LaGrange Road: 1	Commercial	2012	0–0.8	180	1
035 Channahon: 1	Commercial	2015	0–2.1	227–234	2
015 Jonesville: 3	Recreational	2017	0–0.3	330–480	3
“Lowest Mac Exceedances” – Same as Actual					

Table 20. Summary of Actual and Lowest MAC Exceedances from the Preliminary Dataset

Site Name: District #	Site Description	Sample Date	Sample Depth (m)	Exceedance Concentration (mg/kg)	Samples in Exceedance
Manganese					
“Actual Mac Exceedances”					
036 Orland Park: 1	Commercial	2008	0.3–2.4	870–1,300	3
003 Rohlwing Road: 1	Commercial	2010	0–2.4	640–1,200	9
063 US Rt. 45 LaGrange Road: 1	Commercial	2012	0–4.6	660–2,100	13
035 Channahon: 1	Commercial	2015	0–4.3	637–1,150	16
046 Barrington: 1	Commercial	2016	0–2.4	726–1,300	2
015 Jonesville: 3	Recreational	2017	0–0.3	640–870	14
Additional “Lowest Mac Exceedances”					
036 Orland Park: 1	Commercial	2008	0.3–2.4	870–1,300	3
003 Rohlwing Road: 1	Commercial	2010	0–2.4	640–1,200	9
063 US Rt. 45 LaGrange Road: 1	Commercial	2012	0–4.6	660–2,100	13
035 Channahon: 1	Commercial	2015	0–4.3	635–1,150	17
046 Barrington: 1	Commercial	2016	0–2.4	726–1,300	2
015 Jonesville: 3	Recreational	2017	0–0.3	640–870	14

Table 21. Approximate Soil Properties for Sites with MAC Exceedances from the Preliminary Dataset

Site with MAC Exceedance	Web Soil Survey Map Unit, Slopes, and Unit Composition	Typical Profile	Depth to Water Table (cm)	Maximum Carbonate Content (%)	Hydrologic Soil Group
044 Dan Ryan II District 1 Chicago	392A—nearly level Urban land: 70% Orthents/loamy and similar soils: 20% Minor components: 10%	H1—0–20.3 cm.: loam H2—20.3–152.4 cm.: clay loam	~107–152	20	C
WO 055 LaSalle District 3	317A—0%–2% slopes Millsdale and similar soils: 94% Minor components: 6%	H1—0–45.7 cm.: silty clay loam H2—45.7–91.4 cm.: silty clay loam R3—91.4–152.4 cm.: bedrock	~0–30.5	15	C/D
036 Orland Park District 1	531C2—4%–6% slopes Markham and similar soils: 96% Minor components: 4%	H1—0–20.3 cm.: silt loam H2—20.3–50.8 cm.: silty clay loam H3—50.8–73.7 cm.: silty clay loam H4—73.7–152.4 cm.: silty clay loam	~70–107	30	C
003 Rohlwing Road District 1	146A—0%–2% slopes Elliott and similar soils: 94% Minor components: 6%	Ap—0–15.2 cm.: silt loam A—15.2–27.9 cm.: silty clay loam Bt1—27.9–40.6 cm.: silty clay 2Bt2—40.6–104.1 cm.: silty clay loam 2Cd—104.1–152.4 cm.: silty clay loam	~30.5–70.0	35	C/D
022 Grayslake District 1	146B—2%–4% slopes Elliott and similar soils: 94% Minor components: 6%	Ap—0–22.9 cm.: silt loam A—22.9–33.0 cm.: silty clay loam 2Bt1—33.0–43.2 cm.: silty clay 2Bt2—43.2–88.9 cm.: silty clay loam 2Cd—35–152.4 cm.: silty clay loam	~30.5–70.0	35	C/D

*Continued on next page. (Soil Survey Staff, NRCS, USDA, 2017)

Table 21. Approximate soil properties for sites with MAC exceedances from the preliminary dataset

Site with MAC Exceedance	Web Soil Survey Map Unit, Slopes, and Unit Composition	Typical Profile	Depth to Water Table (cm)	Maximum Carbonate Content (%)	Hydrologic Soil Group
063 US Rt. 45 LaGrange Road District 1	228B—2%–4% slopes Nappanee and similar soils: 92% Minor components: 8%	H1—0–10.2 cm.: silt loam H2—4–22.9 cm.: silt loam H3—22.9–58.4 cm.: silty clay H4—58.4–116.8 cm.: silty clay H5—116.8–152.4 cm.: silty clay loam	~15.2–70.0	35	D
035 Channahon District 1	329A—0%–2% slopes Will and similar soils: 94% Minor components: 6%	H1—0–40.6 cm.: silty clay loam H2—40.6–70.0 cm.: loam H3—70.0–152.4 cm.: stratified gravelly loamy sand to gravelly coarse sand	~0–30.5	35	B/D
046 Barrington District 1	531B—2%–4% slopes Markham and similar soils: 92% Minor components: 8%	H1—0–20.3 cm.: silt loam H2—20.3–53.3 cm.: silty clay loam H3—53.3–81.3 cm.: silty clay loam H4—81.3–152.4 cm.: silty clay loam	~70.0–107	30	C
015 Jonesville District 3	152A—0%–2% slopes Drummer and similar soils: 94% Minor components: 6%	Ap—0–35.6 cm.: silty clay loam Btg—35.6–104.1 cm.: silty clay loam 2Btg—104.1–119.4 cm.: loam 2Cg—47–152.4 cm.: stratified sandy loam to clay loam	~0–30.5	30	B/D
Average Soil	2% slopes	0–152.4 cm.: silty clay loam	52.6	29.4	C

B “is silt loam or loam. It has a moderate infiltration rate when thoroughly wetted and consists chiefly or moderately deep to deep, moderately well to well drained soils with moderately fine to moderately coarse textures” (Purdue Engineering, 2019; USDA, 1986).

C “are sandy clay loam. They have low infiltration rates when thoroughly wetted and consist chiefly of soils with a layer that impedes downward movement of water and soils with moderately fine to fine structure” (Purdue Engineering, 2019; USDA, 1986).

D “soils are clay loam, silty clay loam, sandy clay, silty clay or clay. This HSG has the highest runoff potential. They have very low infiltration rates when thoroughly wetted and consist chiefly of clay soils with a high swelling potential, soils with a permanent high water table, soils with a claypan or clay layer at or near the surface and shallow soils over nearly impervious material” (Purdue Engineering, 2019; USDA, 1986).

Table 22. MACs for the 10 Most Frequently Encountered Contaminants Resulting in Exceedance

Chemical Name	MACs (mg/kg)
<u>Aluminum</u>	
within an MSA county	Total: 9,500
within a non-MSA county	Total: 9,200
<u>Arsenic</u>	
within an MSA county	Total: 13
within a non-MSA county	Total: 11.3
Benzo(a)anthracene	
within Chicago corporate limits	1.1
within a populated area in a MSA excluding Chicago	1.8
within a populated area in a non-MSA county	0.9
outside a populated area	0.9
<u>Benzo(a)pyrene</u>	
within Chicago corporate limits	1.3
within a populated area in a MSA excluding Chicago	2.1
within a populated area in a non-MSA county	0.98
outside a populated area	0.09
<u>Benzo(b)fluoranthene</u>	
within Chicago corporate limits	1.5
within a populated area in a MSA excluding Chicago	2.1
within a populated area in a non-MSA county	0.9
outside a populated area	0.9
<u>Chromium</u>	Total: 21
<u>Dibenzo(a,h)anthracene</u>	
within Chicago corporate limits	0.20
within a populated area in a MSA excluding Chicago	0.42
within a populated area in a non-MSA county	0.15
outside a populated area	0.09
<u>Indeno(1,2,3-cd)pyrene</u>	
within Chicago corporate limits	0.9
within a populated area in a MSA excluding Chicago	1.6
within a populated area in a non-MSA county	0.9
outside a populated area	0.9
<u>Lead</u>	Total: 107
<u>Manganese</u>	
within an MSA county	Total: 636
within a non-MSA county	Total: 630

(35 IAC §1100 §5F, 2012)

APPENDIX B: CHAPTER 3 SUPPLEMENTARY INFORMATION

Proper understanding of field-scale electrokinetics requires that the electrical field strength be broken down into its underlying components, including interphase layer conductivity, to account for localized fluctuations in electrostatic potential. To do this, the electrical field must be considered as a function of both electrical double layer conductance and ionic conductance in series (Pamukcu, 2009). First, the total current, i , through the soil may be set equal to the combined current carried by ions along clay particle surfaces, i_s , and by ions suspended in the bulk solution, i_b (Eq. B.1). Secondly, E_x is the electrostatic potential across the field length, L , and Ohm's law (Eq. B.2) allows one to represent E_x as either a function of surface resistance, R_s , or the bulk resistance, R_b , over L (Eq. B.3). Further, by considering the tortuous path current may travel throughout clay microcapillaries in which electrical double layers are connected, the effective flow area A_{flow} and effective field length L' may be considered functions of porosity, n , and tortuosity, τ , respectively. In doing so, the relations $A_{flow} = nA$ and $L' = L\tau$ may be used to develop an equation for R_s as a function of surface conductivity, σ_s (Eq. B.4). Because electro-osmosis is majorly a function of electrical conductance along the stern layer (Eq. B.5), these assumptions allow for an expression, K , for volumetric electro-osmotic flow rate per electrical charge dependent upon localized soil intrinsic properties (Eq. B.6) (Khan, 1991).

Table 23. Equations B1–B6

Equation	Equation #
$i = i_s + i_b$	(B.1)
$i = \frac{V}{R}$	(B.2)
$E_x = \frac{R_s i_s}{L} = \frac{R_b i_b}{L}$	(B.3)
$R_s = \frac{L'}{\sigma_s A_{flow}}$	(B.4)
$i_s = \left(\frac{R_b}{R_s + R_b} \right) i$	(B.5)
$v_{eo} = k_{eo} \frac{R_s i_s}{L} = \left[\frac{k_{eo} \tau}{\sigma_s n} \right] \cdot \frac{i_s}{A} \rightarrow v_{eo} A = Q_{eo} = K i_s$	(B.6)

APPENDIX C: CHAPTER 4 SUPPLEMENTARY INFORMATION

Table 24. Post-treatment Soil Parameters (experiment 1)

X	Y	Z	pH	M.C. (%)	Pyr (C/C ₀)	Pyr (mg/kg)	X	Y	Z	pH	M.C. (%)	Pyr (C/C ₀)	Pyr (mg/kg)
2.5	0	2.5	2.06	27.0	1.040	324.1	12.5	0	2.5	2.5	2.38	28.9	0.574
2.5	0	7.5	1.86	28.7	0.167	52.0	12.5	0	7.5	7.5	2.27	36.5	0.064
2.5	0	12.5	1.94	26.7	0.084	26.1	12.5	0	12.5	12.5	2.25	37.4	0.021
2.5	0	17.5	2.03	24.5	0.022	6.7	12.5	0	17.5	17.5	2.24	26.3	0.032
2.5	5	2.5	1.83	28.0	1.122	349.7	12.5	5	2.5	2.5	2.38	33.3	0.519
2.5	5	7.5	1.78	28.7	0.504	157.1	12.5	5	7.5	7.5	2.31	35.1	0.326
2.5	5	12.5	1.79	25.1	0.334	104.1	12.5	5	12.5	12.5	2.29	36.0	0.068
2.5	5	17.5	1.79	26.0	0.146	45.5	12.5	5	17.5	17.5	2.24	26.5	0.171
2.5	-5	2.5	1.63	29.4	1.122	349.6	12.5	-5	2.5	2.5	2.01	32.4	0.523
2.5	-5	7.5	1.83	27.1	0.305	95.1	12.5	-5	7.5	7.5	2.07	32.0	0.230
2.5	-5	12.5	1.59	25.9	0.217	67.7	12.5	-5	12.5	12.5	2.29	41.7	0.068
2.5	-5	17.5	1.94	25.8	0.016	5.1	12.5	-5	17.5	17.5	2.18	26.6	0.153
7.5	0	2.5	1.93	29.1	1.234	384.7	12.5	10	2.5	2.5	2.18	32.8	0.721
7.5	0	7.5	2.17	28.5	0.158	49.3	12.5	10	7.5	7.5	2.21	31.0	0.559
7.5	0	12.5	2.12	24.6	0.018	5.8	12.5	10	12.5	12.5	2.29	35.3	0.896
7.5	0	17.5	2.22	22.5	0.008	2.5	12.5	10	17.5	17.5	2.32	28.2	0.381
7.5	5	2.5	1.79	29.5	1.140	355.3	12.5	-10	2.5	2.5	2.14	33.1	0.932
7.5	5	7.5	2.17	32.6	0.268	83.5	12.5	-10	7.5	7.5	2.43	38.2	0.390
7.5	5	12.5	1.99	26.4	0.302	94.0	12.5	-10	12.5	12.5	2.21	36.6	0.644
7.5	5	17.5	2.14	24.7	0.006	2.0	12.5	-10	17.5	17.5	2.38	26.6	0.468
7.5	-5	2.5	1.80	27.9	0.645	201.0	17.5	0	2.5	2.5	nan	nan	nan
7.5	-5	7.5	nan	nan	nan	nan	17.5	0	7.5	7.5	2.46	45.0	0.211
7.5	-5	12.5	2.26	27.3	0.147	45.9	17.5	0	12.5	12.5	2.29	50.8	0.295
7.5	-5	17.5	2.26	24.0	0.013	4.0	17.5	0	17.5	17.5	2.14	45.8	0.185
7.5	10	2.5	1.98	28.5	1.482	461.8	17.5	5	2.5	2.5	nan	nan	nan
7.5	10	7.5	2.12	30.5	1.212	377.7	17.5	5	7.5	7.5	2.50	47.7	0.219
7.5	10	12.5	2.15	28.5	0.060	18.6	17.5	5	12.5	12.5	2.35	48.9	0.403
7.5	10	17.5	2.27	23.6	0.018	5.6	17.5	5	17.5	17.5	2.26	43.5	0.627
7.5	-10	2.5	2.25	28.9	0.747	232.8	17.5	-5	2.5	2.5	nan	nan	nan
7.5	-10	7.5	2.17	32.4	0.824	256.8	17.5	-5	7.5	7.5	2.25	47.1	0.215
7.5	-10	12.5	2.27	28.4	1.037	323.3	17.5	-5	12.5	12.5	2.34	56.3	0.157
7.5	-10	17.5	2.26	24.3	0.016	4.9	17.5	-5	17.5	17.5	2.16	43.9	0.724

*7.5,-5,7.5: Sample location missed during sampling.

*17.5,0,2.5: No soil was available to sample at this location due to soil swelling induced shifting.

*17.5,5,2.5: No soil was available to sample at this location due to soil swelling induced shifting.

*17.5,-5,2.5: No soil was available to sample at this location due to soil swelling induced shifting.

*nan = not a number.

Table 25. Summary of Statistics for Post-treatment Samples (experiment 1)

Coordinates (cm)	Pyrene Concentration (mg/kg)				Pyrene Concentration (C/C ₀)			
Depth Below Surface	Min	Max	Avg.	S.D.	Min	Max	Avg.	S.D.
2.5	161.8	461.8	282.9	92.3	0.519	1.482	0.908	0.296
7.5	20.0	377.7	117.4	90.2	0.064	1.212	0.377	0.289
12.5	5.8	323.3	92.6	93.8	0.018	1.037	0.297	0.301
17.5	2.0	225.6	58.2	71.2	0.006	0.724	0.187	0.228
Distance from Anode to Cathode	Min	Max	Avg.	S.D.	Min	Max	Avg.	S.D.
2.5	5.1	349.7	131.9	127.6	0.016	1.122	0.423	0.410
7.5	2.0	461.8	153.1	157.4	0.006	1.482	0.491	0.505
12.5	6.6	290.4	120.6	86.4	0.021	290.4	0.387	0.277
17.5	49.0	225.6	105.1	60.6	0.157	0.724	0.337	0.194
Orthogonal Distance from Electrodes	Min	Max	Avg.	S.D.	Min	Max	Avg.	S.D.
-10	4.9	323.3	197.0	96.7	0.016	1.037	0.632	0.310
-5	4.0	349.6	101.0	95.5	0.013	1.122	0.324	0.307
0	2.5	85.4	384.7	114.9	0.008	1.234	0.274	0.369
+5	2.0	355.3	127.9	101.7	0.006	1.140	0.410	0.326
+10	5.6	461.8	207.5	151.9	0.018	1.482	0.666	0.487
Coordinates (cm)	pH				Moisture Content (%)			
Depth Below Surface	Min	Max	Avg.	S.D.	Min	Max	Avg.	S.D.
2.5	1.6	2.4	2.0	0.2	27.0	33.3	29.9	2.1
7.5	1.8	2.5	2.2	0.2	27.1	47.7	34.7	6.6
12.5	1.6	2.4	2.2	0.2	24.6	56.3	34.7	9.8
17.5	1.8	2.4	2.2	0.1	22.5	45.8	28.9	7.6
Distance from Anode to Cathode	Min	Max	Avg.	S.D.	Min	Max	Avg.	S.D.
2.5	1.6	2.1	1.8	0.1	24.5	29.4	26.9	1.5
7.5	1.8	2.3	2.1	0.1	22.5	32.6	27.5	2.8
12.5	2.0	2.4	2.3	0.1	26.3	41.7	32.7	4.4
17.5	2.1	2.5	2.3	0.1	43.5	56.3	47.7	3.8
Orthogonal Distance from Electrodes	Min	Max	Avg.	S.D.	Min	Max	Avg.	S.D.
-10	2.1	2.4	2.3	0.1	24.3	38.2	31.1	0.1
-5	1.6	2.3	2.0	0.2	24.0	56.3	33.4	9.5
0	1.9	2.5	2.2	0.2	22.5	50.8	32.1	8.5
+5	1.8	2.5	2.1	0.2	24.7	48.9	32.8	7.8
+10	2.0	2.3	2.2	0.1	23.6	35.3	29.8	3.3

Table 26. Summary of Operational Parameters Monitored during Treatment (Experiment 1)

Day	Anode Well				Cathode Well				Overflow						Electrical Properties							
	pH	Temp.	H ₂ O ₂ Conc.	Pyr Conc.	pH	Temp.	H ₂ O ₂ Conc.	Pyr Conc.	pH	Temp.	H ₂ O ₂ Conc.	Pyr Conc.	Flow (mL)		Power Supply		Cathode to Anode		Cathode to Auxiliary		Auxiliary to Anode	
	(°C)	(°C)	(%)	µg/L	(°C)	(°C)	(%)	µg/L	(°C)	(°C)	(%)	µg/L	Daily	Total	Volts	Amps	Volts	Amps	Volts	Amps	Volts	Amps
0	4.4	21.6	10.0	0.0	4.4	21.6	10.0	0.0	0.0	0.0	0.0	0.0	0	0	30.1	0.11	30.0	nan	18.1	nan	11.9	nan
1	2.4	21.2	8.8	33.7	11.8	21.8	0.4	68.9	9.4	22.1	1.4	38.7	1,515	1,515	30.1	0.09	30.0	nan	21.8	nan	8.2	nan
2	2.1	22.1	8.9	28.2	12.2	22.1	0.0	54.0	11.9	21.4	0.1	34.3	470	1,985	30.1	0.18	30.0	nan	20.5	nan	9.5	nan
3	2.5	22.6	8.7	50.7	12.5	24.2	0.1	171.7	11.4	20.3	0.8	40.7	1,150	3,135	30.1	0.17	30.0	nan	18.3	nan	11.6	nan
4	3.0	24.9	8.9	25.1	13.0	25.3	0.1	52.6	11.7	21.9	0.6	45.9	930	4,065	24	0.50	24.0	nan	12.8	nan	11.2	nan
5	1.6	25.1	8.8	23.1	12.8	26.8	0.1	91.8	12.9	21.3	0.1	59.5	1,410	5,475	26.8	0.50	26.7	nan	14.0	nan	12.7	nan
6	0.9	23.7	9.8	17.8	12.8	24.0	0.2	134.0	12.9	21.7	0.2	59.4	1,105	6,580	21.7	0.50	21.6	nan	13.8	nan	7.8	nan
7	1.5	26.0	8.3	115.4	12.4	31.5	0.1	1,114.3	11.4	25.4	0.4	2,678.0	1,975	8,555	30.1	0.79	29.9	nan	18.1	nan	11.8	nan
8	0.9	26.0	8.1	22.8	12.3	30.5	0.0	202.6	12.5	21.0	0.0	434.2	1,380	9,935	30.1	0.83	29.9	nan	20.7	nan	9.2	nan
9	0.7	25.7	7.9	110.7	12.4	30.5	0.0	874.8	12.6	21.7	0.0	581.7	955	10,890	30.1	0.70	30.0	nan	22.9	nan	7.0	nan
10	0.7	24.2	7.9	113.6	12.4	29.3	0.1	747.7	12.6	21.7	0.0	397.2	650	11,540	30.1	0.56	30.0	nan	24.5	nan	5.5	nan
11	0.7	22.6	8.1	118.0	12.1	28.0	0.0	708.6	12.4	20.6	0.0	23.5	500	12,040	30.1	0.46	nan	nan	nan	nan	nan	nan
12	0.9	23.9	8.0	15.6	11.7	31.1	0.0	41.8	12.2	21.0	0.0	19.2	530	12,570	30.1	0.50	nan	nan	nan	nan	nan	nan
13	0.7	23.5	7.8	14.1	11.3	29.5	0.0	193.4	11.6	21.4	0.0	81.6	620	13,190	30.1	0.60	nan	nan	nan	nan	nan	nan
14	0.8	23.9	8.5	18.1	11.2	27.4	0.0	175.0	11.1	21.9	0.0	107.3	480	13,670	30.1	0.58	nan	nan	nan	nan	nan	nan

Current not a number (nan) due to highly unstable measurement.



Figure 38. Photo. Post-treatment soil surface with swelling induced changes in soil structure (experiment 1).

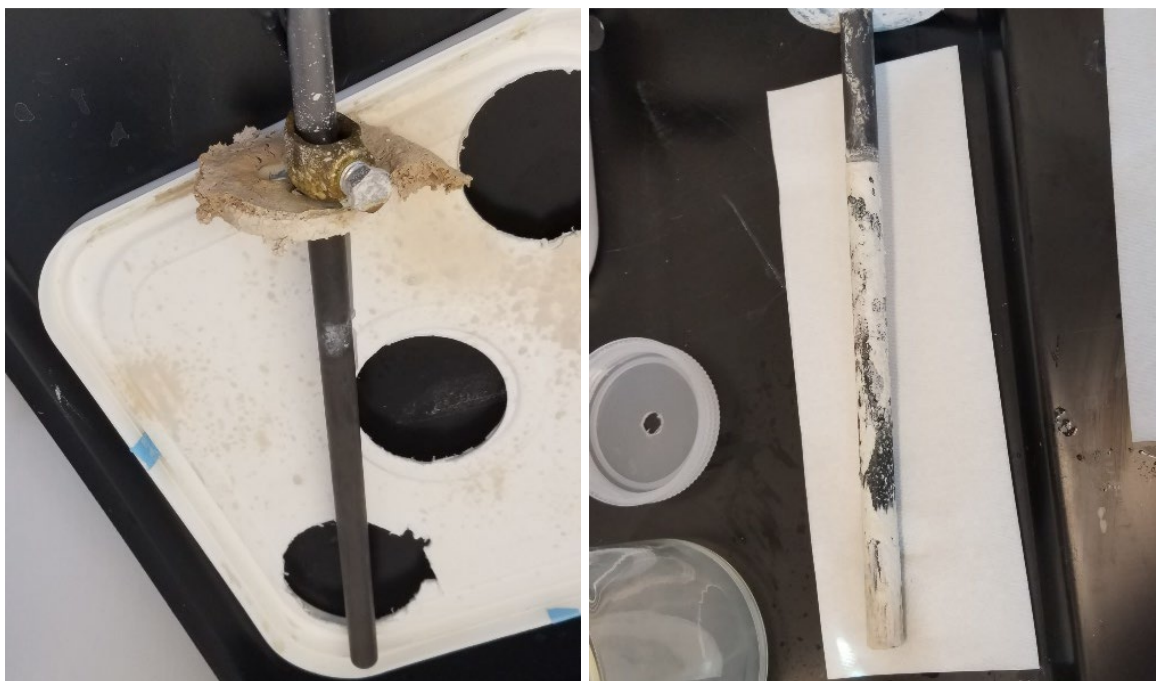


Figure 39. Photos. Post-treatment electrodes. Left = anode. Right = Cathode (experiment 1).

Table 27. Post-treatment Soil Parameters (Experiment 2)

X	Y	Z	pH	M.C. (%)	Pyr (C/C ₀)	Pyr (mg/kg)	X	Y	Z	pH	M.C. (%)	Pyr (C/C ₀)	Pyr (mg/kg)
2.5	0	2.5	2.48	36.2	0.452	148.2	12.5	0	2.5	2.42	43.8	0.417	136.7
2.5	0	7.5	2.49	32.4	0.186	60.9	12.5	0	7.5	2.54	48.2	0.064	20.9
2.5	0	12.5	2.50	32.1	0.093	30.4	12.5	0	12.5	2.51	43.2	0.374	122.5
2.5	0	17.5	2.17	28.6	0.170	55.7	12.5	0	17.5	2.57	34.2	0.330	108.1
2.5	5	2.5	2.46	35.4	0.375	122.8	12.5	5	2.5	2.39	42.6	0.647	212.0
2.5	5	7.5	2.47	31.0	0.197	64.6	12.5	5	7.5	2.48	44.7	0.491	161.0
2.5	5	12.5	2.52	31.2	0.082	26.8	12.5	5	12.5	2.46	40.9	0.339	111.1
2.5	5	17.5	2.38	28.6	0.146	47.8	12.5	5	17.5	2.53	37.4	0.326	106.7
2.5	-5	2.5	2.43	34.9	0.437	143.2	12.5	-5	2.5	2.39	40.3	0.620	203.1
2.5	-5	7.5	2.48	30.7	0.103	33.8	12.5	-5	7.5	2.50	41.5	0.136	44.6
2.5	-5	12.5	2.52	29.9	0.228	74.6	12.5	-5	12.5	2.48	42.1	0.225	73.7
2.5	-5	17.5	2.46	30.2	0.087	28.4	12.5	-5	17.5	2.51	35.0	0.500	163.7
7.5	0	2.5	2.40	39.2	0.326	106.7	12.5	10	2.5	2.47	43.1	0.610	199.8
7.5	0	7.5	2.49	34.2	0.149	48.9	12.5	10	7.5	2.55	44.5	1.199	392.8
7.5	0	12.5	2.53	35.0	0.193	63.3	12.5	10	12.5	2.53	39.5	0.714	234.0
7.5	0	17.5	2.57	28.7	0.290	95.0	12.5	10	17.5	2.49	34.1	0.596	195.4
7.5	5	2.5	2.40	36.5	0.266	87.2	12.5	-10	2.5	2.48	42.3	0.614	201.2
7.5	5	7.5	2.49	35.1	0.106	34.9	12.5	-10	7.5	2.58	45.6	1.409	461.7
7.5	5	12.5	2.52	33.8	0.110	36.1	12.5	-10	12.5	2.54	41.4	0.798	261.3
7.5	5	17.5	2.54	31.4	0.339	111.0	12.5	-10	17.5	2.46	37.3	0.948	310.7
7.5	-5	2.5	2.40	36.4	0.527	172.5	17.5	0	2.5	2.43	56.4	0.156	51.2
7.5	-5	7.5	2.49	34.1	0.095	31.2	17.5	0	7.5	2.48	50.2	0.501	164.0
7.5	-5	12.5	2.51	39.3	0.077	25.2	17.5	0	12.5	2.46	48.4	0.756	247.7
7.5	-5	17.5	2.53	30.3	0.338	110.6	17.5	0	17.5	2.43	42.5	0.177	57.9
7.5	10	2.5	2.41	36.4	0.746	244.3	17.5	5	2.5	2.41	54.5	0.659	215.9
7.5	10	7.5	2.54	38.7	0.653	213.8	17.5	5	7.5	2.45	51.0	0.887	290.6
7.5	10	12.5	2.53	35.3	0.722	236.5	17.5	5	12.5	2.48	44.3	0.519	170.0
7.5	10	17.5	2.57	30.6	0.155	50.7	17.5	5	17.5	2.49	41.1	0.847	277.5
7.5	-10	2.5	2.41	38.1	0.361	118.2	17.5	-5	2.5	2.44	54.6	0.528	173.1
7.5	-10	7.5	2.49	39.9	0.672	220.1	17.5	-5	7.5	2.46	47.9	0.896	293.6
7.5	-10	12.5	2.51	40.0	0.723	236.7	17.5	-5	12.5	2.56	45.6	0.641	209.9
7.5	-10	17.5	2.57	34.1	0.606	198.5	17.5	-5	17.5	2.51	41.2	0.362	118.5

Table 28. Summary of Statistics for Post-treatment Samples (Experiment 2)

Coordinates (cm)	Pyrene Concentration (mg/kg)				Pyrene Concentration (C/C₀)			
Depth Below Surface	Min	Max	Avg.	S.D.	Min	Max	Avg.	S.D.
2.5	51.2	244.3	158.5	51.5	0.156	0.746	0.484	0.157
7.5	20.9	461.7	158.6	136.6	0.064	1.409	0.484	0.417
12.5	25.2	261.3	135.0	87.9	0.077	0.798	0.412	0.268
17.5	28.4	310.7	127.3	79.7	0.087	0.948	0.388	0.243
Distance from Anode to Cathode	Min	Max	Avg.	S.D.	Min	Max	Avg.	S.D.
2.5	26.8	148.2	69.8	42.4	0.082	0.452	0.213	0.129
7.5	25.2	244.3	122.1	76.4	0.077	0.746	0.373	0.233
12.5	20.9	461.7	186.0	107.1	0.064	1.409	0.568	0.327
17.5	51.2	293.6	189.1	79.6	0.156	0.896	0.577	0.243
Orthogonal Distance from Electrodes	Min	Max	Avg.	S.D.	Min	Max	Avg.	S.D.
-10	118.2	461.7	251.0	94.9	0.361	1.409	0.766	0.290
-5	25.2	293.6	118.7	77.4	0.077	0.896	0.362	0.236
0	20.9	247.7	94.9	57.3	0.064	0.756	0.290	0.175
+5	26.8	290.6	129.7	81.7	0.082	0.887	0.396	0.249
+ 10	50.7	392.8	220.9	87.0	0.155	1.199	0.674	0.266
Coordinates (cm)	pH				Moisture Content (%)			
Depth Below Surface	Min	Max	Avg.	S.D.	Min	Max	Avg.	S.D.
2.5	2.4	2.5	2.4	0.0	34.9	56.4	41.9	7.0
7.5	2.5	2.6	2.5	0.0	30.7	51.0	40.6	6.8
12.5	2.5	2.6	2.5	0.0	29.9	48.4	38.9	5.3
17.5	2.2	2.6	2.5	0.1	28.6	42.5	34.1	4.5
Distance from Anode to Cathode	Min	Max	Avg.	S.D.	Min	Max	Avg.	S.D.
2.5	2.2	2.5	2.4	0.1	28.6	36.2	31.8	2.4
7.5	2.4	2.6	2.5	0.1	28.7	40.0	35.4	3.3
12.5	2.4	2.6	2.5	0.1	34.1	48.2	41.1	3.8
17.5	2.4	2.6	2.5	0.0	41.1	56.4	48.1	5.1
Orthogonal Distance from Electrodes	Min	Max	Avg.	S.D.	Min	Max	Avg.	S.D.
-10	2.4	2.6	2.5	0.1	34.1	45.6	39.8	3.3
-5	2.4	2.6	2.5	0.0	29.9	54.6	38.4	6.9
0	2.2	2.6	2.5	0.1	28.6	56.4	39.6	8.0
+5	2.4	2.5	2.5	0.0	28.6	54.5	38.7	7.1
+ 10	2.4	2.6	2.5	0.0	30.6	44.5	37.8	4.3

*S.D. = Standard Deviation

Table 29. Summary of Operational Parameters Monitored during Treatment (Experiment 2)

Day	Anode Well				Cathode Well				Overflow						Electrical Properties							
	pH	Temp.	H ₂ O ₂ Conc.	Pyr Conc.	pH	Temp.	H ₂ O ₂ Conc.	Pyr Conc.	pH	Temp.	H ₂ O ₂ Conc.	Pyr Conc.	Flow (mL)		Power Supply		Cathode to Anode		Cathode to Auxiliary		Auxiliary to Anode	
	(°C)	(%)	µg/L		(°C)	(%)	µg/L		(°C)	(%)	µg/L		Daily	Total	Volts	Amps	Volts	Amps	Volts	Amps	Volts	Amps
0	4.2	20.6	0.0	0.0	4.2	20.6	0.0	0.0	0.0	0.0	0.0	0.0	0	0	30	0.10	nan	0.11	nan	0.15	nan	0.14
1	2.9	22.4	0.0	33.6	12.8	22.3	0.0	2,391.2	12.3	21.0	0.0	314.8	1,545	1,545	30.1	0.25	nan	0.25	nan	0.33	nan	0.47
2	1.7	25.2	0.0	0.0	13.0	24.5	0.0	3,321.7	13.1	20.5	0.0	396.9	1,145	2,690	30.1	0.55	nan	0.55	nan	1.16	nan	0.69
3	1.6	24.8	0.0	18.6	13.1	24.0	0.0	371.8	13.1	20.7	0.0	288.9	785	3,475	30.1	0.55	nan	0.55	nan	1.06	nan	0.65
4	1.7	25.0	0.0	5.3	13.0	23.9	0.0	266.3	13.2	20.7	0.0	63.2	840	4,315	30.1	0.62	nan	0.62	nan	1.19	nan	0.74
5	1.7	25.9	0.0	61.3	13.2	23.0	0.0	1,134.8	13.2	21.0	0.0	77.9	720	5,035	30.1	0.62	nan	0.62	nan	1.17	nan	0.71
6	1.5	25.5	0.0	32.6	13.1	23.7	0.0	112.6	13.0	20.7	0.0	46.2	680	5,715	30.1	0.65	nan	0.65	nan	1.15	nan	0.75
7	1.5	25.4	0.0	33.2	13.1	23.7	0.0	264.9	13.1	20.7	0.0	28.3	690	6,405	30.1	0.64	29.7	0.64	11.3	1.11	18.4	0.76
8	1.7	26.2	7.9	24.7	12.9	24.9	0.0	126.5	13.1	21.1	0.0	97.3	890	7,295	30.1	0.65	29.8	0.65	11.2	1.23	18.6	0.82
9	1.9	25.3	8.2	17.2	12.9	25.3	0.0	133.0	12.9	20.6	0.0	151.5	1,220	8,515	30.1	0.67	29.8	0.66	11.8	1.19	18.0	0.85
10	1.4	26.9	6.3	24.9	12.8	26.6	0.1	115.2	13.0	21.1	0.0	192.3	900	9,415	30.1	0.62	29.8	0.62	14.1	1.02	15.7	0.93
11	1.4	25.8	7.6	52.8	5.0	26.3	0.6	25,648.1	10.3	21.0	0.1	3827.5	1,300	10,715	30.1	0.62	29.9	0.61	14.4	1.02	15.6	0.93
12	1.4	26.5	8.1	0.0	4.0	27.1	1.2	1,509.9	4.6	22.1	0.9	1766.8	1,860	12,575	30.1	0.59	29.9	0.59	15.5	0.95	14.4	0.98
13	1.3	26.1	8.1	0.0	4.0	29.0	1.8	238.0	4.2	21.5	1.5	175.6	1,965	14,540	30.1	0.65	29.8	0.65	17.1	0.95	12.7	1.19
14	1.5	25.8	8.6	0.0	3.7	26.5	1.6	9.7	3.9	22.1	1.6	84.1	1,680	16,220	30.1	0.59	29.9	0.59	15.9	0.91	14.0	0.99

T:0–6 current not a number (nan) due to highly unstable measurement.



Figure 40. Photo. Post-treatment electrodes. Top = Anode. Bottom = Cathode (experiment 2).

Table 30. Post-treatment Soil Parameters (Experiment 3)

X	Y	Z	pH	M.C. (%)	Pyr (C/C ₀)	Pyr (mg/kg)	X	Y	Z	pH	M.C. (%)	Pyr (C/C ₀)	Pyr (mg/kg)
2.5	0	2.5	2.21	37.7	0.225	65.9	12.5	0	2.5	2.59	36.2	0.653	191.6
2.5	0	7.5	2.66	28.6	0.373	109.3	12.5	0	7.5	2.48	35.5	0.880	258.2
2.5	0	12.5	2.29	28.5	1.066	312.8	12.5	0	12.5	2.56	33.2	0.788	231.3
2.5	0	17.5	2.63	26.9	0.944	277.0	12.5	0	17.5	2.75	31.9	0.589	172.7
2.5	5	2.5	2.51	37.6	0.052	15.2	12.5	5	2.5	2.61	35.3	0.612	179.5
2.5	5	7.5	2.68	28.5	0.293	85.9	12.5	5	7.5	2.54	29.2	0.650	190.8
2.5	5	12.5	2.63	27.1	0.735	215.7	12.5	5	12.5	2.57	31.0	0.724	212.5
2.5	5	17.5	2.75	26.2	1.333	391.1	12.5	5	17.5	2.71	31.8	0.609	178.8
2.5	-5	2.5	2.47	39.0	0.252	73.9	12.5	-5	2.5	2.63	34.6	0.551	161.7
2.5	-5	7.5	2.66	32.6	0.675	198.0	12.5	-5	7.5	2.48	31.3	0.509	149.3
2.5	-5	12.5	2.66	29.1	1.129	331.1	12.5	-5	12.5	2.55	31.3	0.641	188.1
2.5	-5	17.5	2.70	35.3	1.104	323.9	12.5	-5	17.5	2.73	30.6	0.843	247.4
7.5	0	2.5	2.45	39.5	0.945	277.1	12.5	10	2.5	2.66	41.5	0.599	175.6
7.5	0	7.5	2.63	29.0	0.801	234.9	12.5	10	7.5	2.61	31.8	0.811	237.8
7.5	0	12.5	2.52	28.2	0.699	205.2	12.5	10	12.5	2.62	32.5	1.429	419.1
7.5	0	17.5	2.55	32.7	0.728	213.4	12.5	10	17.5	2.64	38.7	0.764	224.2
7.5	5	2.5	2.51	39.4	0.986	289.3	12.5	-10	2.5	2.69	41.7	0.541	158.7
7.5	5	7.5	2.61	30.8	0.884	259.2	12.5	-10	7.5	2.66	37.6	1.068	313.1
7.5	5	12.5	2.51	30.7	0.788	231.1	12.5	-10	12.5	2.67	35.2	0.625	183.4
7.5	5	17.5	2.55	27.3	1.125	330.1	12.5	-10	17.5	2.70	32.4	0.730	214.1
7.5	-5	2.5	2.68	36.8	0.847	248.5	17.5	0	2.5	2.70	45.6	0.354	103.9
7.5	-5	7.5	2.59	29.5	0.751	220.2	17.5	0	7.5	2.58	39.8	0.948	278.0
7.5	-5	12.5	2.48	27.4	0.901	264.2	17.5	0	12.5	2.59	37.4	0.644	188.9
7.5	-5	17.5	2.54	28.0	0.823	241.4	17.5	0	17.5	2.41	37.8	0.683	200.4
7.5	10	2.5	2.71	39.3	0.569	167.0	17.5	5	2.5	2.62	50.1	0.475	139.4
7.5	10	7.5	2.69	30.9	1.271	372.9	17.5	5	7.5	2.58	39.7	0.927	271.9
7.5	10	12.5	2.66	28.9	0.970	284.4	17.5	5	12.5	2.69	39.5	0.935	274.4
7.5	10	17.5	2.55	29.0	1.047	307.1	17.5	5	17.5	2.52	40.3	0.724	212.5
7.5	-10	2.5	2.73	41.8	0.577	169.3	17.5	-5	2.5	3.38	51.1	0.340	99.6
7.5	-10	7.5	2.71	33.7	0.897	263.2	17.5	-5	7.5	2.50	43.8	1.123	329.4
7.5	-10	12.5	2.59	32.6	0.796	233.6	17.5	-5	12.5	2.64	40.8	0.976	286.4
7.5	-10	17.5	2.60	38.0	0.823	241.4	17.5	-5	17.5	2.56	38.0	0.633	185.6

Table 31. Summary of Statistics for Post-treatment Samples (Experiment 3)

Coordinates (cm)	Pyrene Concentration (mg/kg)				Pyrene Concentration (C/C ₀)			
Depth Below Surface	Min	Max	Avg.	S.D.	Min	Max	Avg.	S.D.
2.5	15.2	289.3	157.3	72.6	0.052	0.986	0.536	0.248
7.5	85.9	372.9	235.8	74.2	0.293	1.271	0.804	0.253
12.5	183.4	419.1	253.9	61.1	0.625	1.429	0.866	0.208
17.5	172.7	391.1	247.6	60.3	0.589	1.333	0.844	0.206
Distance from Anode to Cathode	Min	Max	Avg.	S.D.	Min	Max	Avg.	S.D.
2.5	15.2	391.1	200.0	121.5	0.052	1.333	0.682	0.414
7.5	167.0	372.9	252.7	48.6	0.569	1.271	0.861	0.166
12.5	149.3	419.1	214.4	60.9	0.509	1.429	0.731	0.208
17.5	99.6	329.4	214.2	71.9	0.340	1.123	0.730	0.245
Orthogonal Distance from Electrodes	Min	Max	Avg.	S.D.	Min	Max	Avg.	S.D.
-10	158.7	313.1	222.1	48.6	0.541	1.068	0.757	0.166
-5	73.9	331.1	221.8	75.2	0.252	1.129	0.756	0.256
0	65.9	312.8	207.5	67.1	0.225	1.066	0.707	0.229
+5	15.2	391.1	217.3	88.1	0.052	1.333	0.741	0.300
+ 10	167.0	419.1	273.5	84.4	0.569	1.429	0.932	0.288
Coordinates (cm)	pH				Moisture Content (%)			
Depth Below Surface	Min	Max	Avg.	S.D.	Min	Max	Avg.	S.D.
2.5	2.2	3.4	2.6	0.2	34.6	51.1	40.4	4.7
7.5	2.5	2.7	2.6	0.1	28.5	43.8	33.3	4.5
12.5	2.3	2.7	2.6	0.1	27.1	40.8	32.1	4.1
17.5	2.4	2.8	2.6	0.1	26.2	40.3	32.8	4.5
Distance from Anode to Cathode	Min	Max	Avg.	S.D.	Min	Max	Avg.	S.D.
2.5	2.2	2.8	2.6	0.2	26.2	39.0	31.4	4.5
7.5	2.5	2.7	2.6	0.1	27.3	41.8	32.7	4.6
12.5	2.5	2.8	2.6	0.1	29.2	41.7	34.2	3.4
17.5	2.4	3.4	2.6	0.2	37.4	51.1	42.0	4.5
Orthogonal Distance from Electrodes	Min	Max	Avg.	S.D.	Min	Max	Avg.	S.D.
-10	2.6	2.7	2.7	0.0	32.4	41.8	36.6	3.5
-5	2.5	3.4	2.6	0.2	27.4	51.1	34.9	6.2
0	2.2	2.8	2.5	0.1	26.9	45.6	34.3	5.1
+5	2.5	2.8	2.6	0.1	26.2	50.1	34.0	6.4
+ 10	2.6	2.7	2.6	0.0	28.9	41.5	34.1	4.7

Table 32. Summary of Operational Parameters Monitored during Treatment (Experiment 3)

Day	Anode Well			Cathode Well			Overflow					Electrical Properties							
	pH	Temp.	Pyr	pH	Temp.	Pyr	pH	Temp.	Pyr	Flow (mL)		Power		Cathode to		Cathode to		Auxiliary	
		(°C)	Conc.		(°C)	Conc.		(°C)	Conc.			Supply		Anode		Auxiliary		to Anode	
			µg/L			µg/L			µg/L	Daily	Total	Volts	Amps	Volts	Amps	Volts	Amps	Volts	Amps
0	4.4	21.4	0.0	4.4	21.4	0.0	0.0	0.0	0.0	0	0	30	0.10	30.1	0.11	17.3	0.14	12.9	0.17
1	2.4	22.3	3.1	12.8	21.5	49.7	5.7	21.4	134.1	650	650	30	0.14	30.0	0.14	21.4	0.16	8.7	0.42
2	1.9	23.1	0.0	12.8	22.9	150.5	12.7	21.1	58.6	870	1,520	30	0.27	30.0	0.27	18.6	0.37	11.3	0.59
3	1.6	28.3	1302.2	12.9	24.4	332.0	12.9	21.6	1,792.3	1,750	3,270	30	0.84	29.9	0.85	11.5	1.63	18.3	1.09
4	1.4	27.6	122.3	13.1	24.7	149.0	13.1	21.7	867.5	1,140	4,410	30	0.77	29.8	0.77	11.5	1.32	18.4	0.92
5	1.4	27.1	30.6	13.1	24.8	116.8	13.2	21.5	584.7	930	5,340	30	0.74	29.8	0.75	12.0	1.17	17.8	0.88
6	1.4	26.1	23.8	13.2	24.0	156.8	13.2	21.2	638.2	790	6,130	30	0.69	29.8	0.70	12.7	1.05	17.1	0.85
7	1.3	27.3	0.0	13.2	24.6	157.0	13.3	21.8	752.2	650	6,780	30	0.67	29.8	0.67	13.5	0.98	16.3	0.86
8	1.3	27.6	24.4	13.1	25.9	160.9	13.2	21.0	948.7	595	7,375	30	0.64	29.8	0.65	14.2	0.93	15.7	0.87
9	1.5	26.6	10.7	13.1	26.1	78.1	13.3	21.0	416.1	560	7,935	30	0.62	29.8	0.63	14.3	0.92	15.5	0.87
10	1.5	27.5	0.0	13.1	25.9	74.4	13.3	21.5	294.9	505	8,440	30	0.66	29.8	0.68	14.4	0.99	15.4	0.93
11	1.5	28.3	0.0	13.1	26.1	182.4	0.0	0.0	0.0	0	8,440	30	0.78	29.7	0.78	12.9	1.26	16.9	1.01
12	1.6	29.4	0.0	13.1	26.6	86.5	13.3	21.5	664.9	535	8,975	30	0.73	29.7	0.74	13.6	1.14	16.1	1.03
13	1.8	24.2	12.2	13.2	23.5	55.5	13.3	21.5	296.3	340	9,315	30	0.36	29.9	0.35	8.8	0.98	21.1	0.43
14	1.7	23.9	4.2	12.8	30.0	73.2	13.2	21.7	225.6	675	9,990	30	0.63	25.2	0.01	29.9	0.63	4.6	0.01



Figure 41. Photos. Surfactant induced saponification during post-treatment sample centrifugation (experiment 3).



Figure 42. Photo. Ponding on day 14 due to surfactant induced soil pore clogging (experiment 3).



Figure 43. Photo. Post-treatment electrodes. Left = anode. Right = Cathode (experiment 3).

Table 33. Post-treatment Soil Parameters (Experiment 4)

X	Y	Z	pH	M.C. (%)	Pyr (C/C ₀)	Pyr (mg/kg)	X	Y	Z	pH	M.C. (%)	Pyr (C/C ₀)	Pyr (mg/kg)
2.5	0	2.5	1.90	38.3	0.759	278.7	12.5	0	2.5	2.37	27.8	0.036	13.2
2.5	0	7.5	1.95	31.1	0.865	317.6	12.5	0	7.5	2.04	28.7	0.003	1.2
2.5	0	12.5	1.75	32.2	0.651	239.1	12.5	0	12.5	2.14	24.4	0.014	5.3
2.5	0	17.5	1.85	43.0	0.495	181.8	12.5	0	17.5	2.37	24.7	0.015	5.7
2.5	5	2.5	1.95	30.1	0.509	186.8	12.5	5	2.5	2.43	32.4	0.187	68.5
2.5	5	7.5	2.01	29.8	1.118	410.6	12.5	5	7.5	2.42	30.4	0.243	89.1
2.5	5	12.5	2.16	27.9	0.297	109.0	12.5	5	12.5	2.09	29.4	0.021	7.9
2.5	5	17.5	2.19	33.1	0.517	189.9	12.5	5	17.5	2.40	27.0	0.032	11.7
2.5	-5	2.5	1.94	27.4	0.429	157.7	12.5	-5	2.5	2.46	38.0	0.295	108.3
2.5	-5	7.5	1.95	27.0	0.588	215.8	12.5	-5	7.5	2.30	29.4	0.005	1.8
2.5	-5	12.5	1.92	29.1	0.819	300.6	12.5	-5	12.5	2.29	27.5	0.323	118.8
2.5	-5	17.5	1.98	25.5	0.389	142.7	12.5	-5	17.5	2.47	26.0	0.371	136.3
7.5	0	2.5	1.98	29.1	0.399	146.6	12.5	10	2.5	2.45	35.8	1.035	380.0
7.5	0	7.5	2.22	27.0	0.063	23.2	12.5	10	7.5	2.40	32.8	0.694	254.7
7.5	0	12.5	1.92	24.9	0.420	154.2	12.5	10	12.5	2.43	30.6	0.956	351.0
7.5	0	17.5	2.18	28.6	0.028	10.2	12.5	10	17.5	2.44	29.7	0.606	222.5
7.5	5	2.5	2.18	27.1	0.011	3.9	12.5	-10	2.5	2.63	37.0	1.230	451.7
7.5	5	7.5	2.25	25.4	0.021	7.8	12.5	-10	7.5	2.50	30.6	0.793	291.3
7.5	5	12.5	2.27	26.3	0.093	34.2	12.5	-10	12.5	2.40	29.8	0.772	283.3
7.5	5	17.5	2.27	26.2	0.080	29.2	12.5	-10	17.5	2.44	29.3	0.467	171.6
7.5	-5	2.5	2.33	26.4	0.251	92.2	17.5	0	2.5	2.49	39.7	0.462	169.6
7.5	-5	7.5	2.20	24.7	0.203	74.7	17.5	0	7.5	2.27	41.9	0.382	140.4
7.5	-5	12.5	2.21	24.9	0.007	2.5	17.5	0	12.5	2.43	39.2	0.277	101.6
7.5	-5	17.5	2.31	25.8	0.236	86.6	17.5	0	17.5	2.47	41.8	0.324	119.0
7.5	10	2.5	2.43	26.5	0.383	140.7	17.5	5	2.5	2.57	46.3	0.921	338.1
7.5	10	7.5	2.38	28.3	0.587	215.4	17.5	5	7.5	2.49	37.8	0.868	318.8
7.5	10	12.5	2.46	27.1	0.764	280.6	17.5	5	12.5	2.58	39.1	0.638	234.3
7.5	10	17.5	2.39	27.2	0.606	222.5	17.5	5	17.5	2.54	40.8	1.042	382.6
7.5	-10	2.5	2.36	30.3	0.852	312.9	17.5	-5	2.5	2.59	48.0	0.974	357.6
7.5	-10	7.5	2.40	26.5	0.810	297.4	17.5	-5	7.5	2.38	45.2	0.723	265.6
7.5	-10	12.5	2.48	26.2	0.864	317.1	17.5	-5	12.5	2.44	30.2	0.385	141.2
7.5	-10	17.5	2.42	25.6	0.629	231.1	17.5	-5	17.5	2.51	41.5	0.482	177.0

*M.C. = Moisture content

Table 34. Summary of Statistics for Post-treatment Samples (Experiment 4)

Coordinates (cm)	Pyrene Concentration (mg/kg)				Pyrene Concentration (C/C ₀)			
Depth Below Surface	Min	Max	Avg.	S.D.	Min	Max	Avg.	S.D.
2.5	3.9	451.7	200.4	131.9	0.011	1.230	0.546	0.359
7.5	1.2	410.6	182.8	130.3	0.003	1.118	0.498	0.355
12.5	2.5	351.0	167.5	116.5	0.007	0.956	0.456	0.317
17.5	5.7	382.6	145.0	98.1	0.015	1.042	0.395	0.267
Distance from Anode to Cathode	Min	Max	Avg.	S.D.	Min	Max	Avg.	S.D.
2.5	109.0	410.6	227.5	82.2	0.297	1.118	0.620	0.224
7.5	2.5	317.1	134.2	110.5	0.007	0.864	0.365	0.301
12.5	1.2	451.7	148.7	140.7	0.003	1.230	0.405	0.383
17.5	101.6	382.6	228.8	96.4	0.277	1.042	0.623	0.263
Orthogonal Distance from Electrodes	Min	Max	Avg.	S.D.	Min	Max	Avg.	S.D.
-10	171.6	451.7	294.5	74.9	0.467	1.230	0.802	0.204
-5	1.8	357.6	148.7	94.9	0.005	0.974	0.405	0.258
0	1.2	317.6	119.2	100.2	0.003	0.865	0.325	0.273
+5	3.9	410.6	151.4	140.7	0.011	1.118	0.412	0.383
+10	140.7	380.0	258.4	72.6	0.383	1.035	0.704	0.198
Coordinates (cm)	pH				Moisture Content (%)			
Depth Below Surface	Min	Max	Avg.	S.D.	Min	Max	Avg.	S.D.
2.5	1.9	2.6	2.3	0.2	26.4	48.0	33.7	6.7
7.5	2.0	2.5	2.3	0.2	24.7	45.2	31.0	5.6
12.5	1.8	2.6	2.2	0.2	24.4	39.2	29.3	4.3
17.5	1.9	2.5	2.3	0.2	24.7	43.0	31.0	6.6
Distance from Anode to Cathode	Min	Max	Avg.	S.D.	Min	Max	Avg.	S.D.
2.5	1.8	2.2	2.0	0.1	25.5	43.0	31.2	4.8
7.5	1.9	2.5	2.3	0.1	24.7	30.3	26.7	1.4
12.5	2.0	2.6	2.4	0.1	24.4	38.0	30.1	3.6
17.5	2.3	2.6	2.5	0.1	30.2	48.0	41.0	4.4
Orthogonal Distance from Electrodes	Min	Max	Avg.	S.D.	Min	Max	Avg.	S.D.
-10	2.4	2.6	2.5	0.1	25.6	37.0	29.4	3.4
-5	1.9	2.6	2.3	0.2	24.7	48.0	31.0	7.4
0	1.8	2.5	2.1	0.2	24.4	43.0	32.7	6.6
+5	2.0	2.6	2.3	0.2	25.4	46.3	31.8	5.9
+10	2.4	2.5	2.4	0.0	26.5	35.8	29.8	3.0

*S.D. = Standard deviation

Table 35. Summary of Operational Parameters Monitored during Treatment (Experiment 4)

Day	Anode Well				Cathode Well				Overflow						Electrical Properties							
	pH	Temp.	H ₂ O ₂ Conc.	Pyr Conc.	pH	Temp.	H ₂ O ₂ Conc.	Pyr Conc.	pH	Temp.	H ₂ O ₂ Conc.	Pyr Conc.	Flow (mL)		Power Supply		Cathode to Anode		Cathode to Auxiliary		Auxiliary to Anode	
	(°C)	(°C)	(%)	mg/L	(°C)	(°C)	(%)	µg/L	(°C)	(°C)	(%)	mg/L	Daily	Total	Volts	Amps	Volts	Amps	Volts	Amps	Volts	Amps
0	4.3	21.0	10.0	0.0	4.3	21.0	10.0	0.0	–	–	–	–	–	–	30.0	0.17	30.0	0.17	16.8	0.30	13.3	0.20
1	2.0	22.6	8.3	0.0	12.6 (3.2)	22.9	0.6	47.0	9.9	21.8	1.6	5.3	1,160	1,160	30.0	0.17	30.0	0.18	22.8	0.60	7.2	0.17
2	1.6	23.7	8.2	0.0	12.9 (3.8)	23.2	0.0	72.0	12.2	21.5	0.1	22.0	1,070	2,230	30.0	0.31	29.9	0.31	19.9	0.73	10.1	0.36
3	1.4	25.2	7.0	0.0	12.8 (4.1)	27.4	0.1	55.7	12.9	21.3	0.8	6.4	1,200	3,430	30.0	0.52	30.0	0.53	19.0	1.01	10.9	0.58
4	1.5	24.7	3.9	0.0	12.1 (4.0)	28.3	0.1	78.7	12.5	21.7	0.0	36.8	1,470	4,900	30.0	0.44	29.9	0.44	21.0	1.00	9.0	0.42
5	1.4	25.1	3.4	488.3	10.3 (3.9)	27.7	0.3	6,938.5	9.5	23.1	0.7	2615.5	530	5,430	30.0	0.53	29.9	0.53	20.7	1.11	9.3	0.49
6	1.4	25.9	3.8	38.0	11.4 (3.9)	29.8	0.1	325.7	8.1	22.1	0.4	1790.2	1,500	6,930	30.0	0.58	29.9	0.58	21.3	1.11	8.6	0.45
7	1.4	26.2	3.9	0.0	9.2 (3.7)	29.9	0.1	147.4	7.2	21.5	0.1	60.4	1,265	8,195	30.0	0.63	29.9	0.63	20.2	1.07	9.6	0.50
8	1.4	26.3	3.8	4.9	6.7 (3.6)	30.1	0.3	134.6	5.3	21.7	0.4	73.8	1,105	9,300	30.0	0.67	29.8	0.67	21.3	1.52	8.5	0.59
9	1.4	27.3	3.2	138.8	6.8 (3.8)	29.7	0.4	188.3	4.7	22.7	0.4	165.8	300	9,600	30.0	0.66	29.8	0.66	19.0	0.85	10.8	0.46
10	1.3	26.5	2.8	0.0	9.6 (3.9)	30.8	0.1	1,514.9	5.5	22.2	0.3	118.1	1,230	10,830	30.0	0.78	29.8	0.76	21.5	1.49	8.3	0.55
11	1.3	27.6	3.3	86.8	8.8 (3.8)	32.3	0.1	437.5	5.5	22.6	0.1	154.7	890	11,720	30.0	0.79	29.8	0.78	20.9	1.29	9.0	0.55
12	1.3	25.9	2.2	0.0	8.8 (3.8)	30.9	0.1	189.1	5.8	22.1	0.1	93.4	1,482	13,202	30.0	0.81	29.8	0.80	21.0	1.36	8.8	0.50
13	1.2	28.8	2.2	0.0	8.6 (3.7)	34.3	0.0	147.5	6.1	22.2	0.0	104.9	1,160	14,362	30.0	0.86	29.8	0.86	21.1	1.44	8.7	0.57
14	1.2	27.4	3.1	0.0	5.5	32.6	0.1	160.3	5.4	22.0	0.1	51.6	1,150	15,512	30.0	0.85	29.8	0.85	21.2	1.54	8.6	0.59

*



Figure 44. Photo. Post-treatment soil surface riddled with sponge-like voids (experiment 4).



**Figure 45. Photo. Post-treatment electrodes. Left photo: Cathode.
Right photo: Left = cathode, Right = anode (experiment 4).**

Table 36. Post-treatment Soil Parameters (Experiment 5)

X	Y	Z	pH	M.C. (%)	Mn (C/C ₀)	Mn (mg/kg)	X	Y	Z	pH	M.C. (%)	Mn (C/C ₀)	Mn (mg/kg)
2.5	0	2.5	8.82	47.5	0.003	4.7	12.5	0	2.5	3.73	38.3	0.073	109.5
2.5	0	7.5	3.39	38.6	0.037	56.1	12.5	0	7.5	3.00	33.8	0.605	907.1
2.5	0	12.5	2.96	33.5	0.017	25.2	12.5	0	12.5	2.91	31.7	0.663	994.8
2.5	0	17.5	3.00	32.6	0.009	14.2	12.5	0	17.5	3.11	30.1	1.242	1,863.7
2.5	5	2.5	5.23	41.6	0.003	4.6	12.5	5	2.5	3.05	37.2	0.027	40.9
2.5	5	7.5	2.75	35.2	0.043	64.4	12.5	5	7.5	3.05	31.1	0.650	975.4
2.5	5	12.5	2.87	32.4	0.005	8.0	12.5	5	12.5	4.49	30.0	0.732	1098.4
2.5	5	17.5	4.65	29.7	0.355	533.2	12.5	5	17.5	2.11	30.4	0.316	473.3
2.5	-5	2.5	3.50	41.3	0.014	21.5	12.5	-5	2.5	3.08	37.4	0.052	78.0
2.5	-5	7.5	2.32	36.0	0.021	31.8	12.5	-5	7.5	3.24	32.6	0.895	1,342.3
2.5	-5	12.5	2.85	31.2	0.011	17.0	12.5	-5	12.5	3.05	30.9	0.062	93.5
2.5	-5	17.5	2.30	33.6	0.071	106.9	12.5	-5	17.5	3.34	28.9	0.849	1,272.9
7.5	0	2.5	4.13	44.1	0.004	6.0	12.5	10	2.5	3.45	38.3	0.066	99.3
7.5	0	7.5	3.37	35.8	0.009	13.9	12.5	10	7.5	4.46	31.3	0.501	751.5
7.5	0	12.5	3.10	32.1	0.007	10.2	12.5	10	12.5	4.21	30.4	0.405	607.6
7.5	0	17.5	2.54	30.2	0.025	37.2	12.5	10	17.5	4.48	31.1	0.415	622.2
7.5	5	2.5	2.69	41.5	0.041	61.4	12.5	-10	2.5	2.75	40.4	0.076	114.2
7.5	5	7.5	2.36	32.5	0.651	976.9	12.5	-10	7.5	4.55	30.0	0.551	826.7
7.5	5	12.5	2.84	31.2	0.859	1,288.2	12.5	-10	12.5	3.78	30.2	1.338	2,007.1
7.5	5	17.5	2.45	29.6	0.018	26.9	12.5	-10	17.5	3.53	30.6	0.663	995.2
7.5	-5	2.5	2.72	41.7	0.012	18.4	17.5	0	2.5	5.13	41.3	0.012	17.5
7.5	-5	7.5	2.62	35.4	0.328	492.6	17.5	0	7.5	5.37	33.1	0.617	925.9
7.5	-5	12.5	2.47	31.3	0.020	30.5	17.5	0	12.5	4.21	33.6	1.320	1,980.2
7.5	-5	17.5	2.35	30.4	0.338	507.2	17.5	0	17.5	3.91	30.4	0.886	1,328.4
7.5	10	2.5	2.50	41.2	0.122	182.6	17.5	5	2.5	10.05	40.4	9.124	13,686.1
7.5	10	7.5	1.95	34.8	0.674	1,011.4	17.5	5	7.5	6.56	33.4	0.863	1,294.5
7.5	10	12.5	2.05	29.9	0.830	1,245.5	17.5	5	12.5	5.13	32.0	1.012	1,517.6
7.5	10	17.5	2.22	30.8	0.841	1,261.9	17.5	5	17.5	3.01	32.9	0.463	694.6
7.5	-10	2.5	2.41	41.0	0.049	72.9	17.5	-5	2.5	8.31	39.0	0.544	815.5
7.5	-10	7.5	2.05	34.0	0.622	933.3	17.5	-5	7.5	6.48	32.4	2.769	4,153.5
7.5	-10	12.5	2.32	30.8	0.555	832.9	17.5	-5	12.5	5.50	33.7	3.008	4,512.6
7.5	-10	17.5	1.96	31.6	1.046	1,569.7	17.5	-5	17.5	4.39	33.0	0.603	904.0

*X,Y,Z: (17.5,5,2.5) 13,686.1 mg/kg excluded from colormap plot scales as an outlier to preserve graphical scale.

Table 37. Summary of Statistics for Post-treatment Samples (Experiment 5)

Coordinates (cm)	Manganese Concentration (mg/kg)				Manganese Concentration (C/C₀)			
Depth Below Surface	Min	Max	Avg.	S.D.	Min	Max	Avg.	S.D.
2.5	4.6	13,686.1	958.3	3,291.7	0.004	11.082	0.776	2.665
7.5	13.9	4,153.5	922.3	938.6	0.011	3.363	0.747	0.760
12.5	8.0	4,512.6	1,016.8	1,133.4	0.006	3.654	0.823	0.918
17.5	14.2	1,863.7	763.2	561.9	0.012	1.509	0.618	0.455
Distance from Anode to Cathode	Min	Max	Avg.	S.D.	Min	Max	Avg.	S.D.
2.5	4.6	533.2	74.0	141.5	0.004	0.432	0.060	0.115
7.5	6.0	1,569.7	529.0	536.6	0.005	1.271	0.428	0.434
12.5	40.9	2,007.1	763.7	570.1	0.033	1.625	0.618	0.462
17.5	17.5	13,686.1	2,652.5	3,570.5	0.014	11.082	2.148	2.891
Orthogonal Distance from Electrodes	Min	Max	Avg.	S.D.	Min	Max	Avg.	S.D.
-10	72.9	2,007.1	919.0	611.6	0.059	1.625	0.713	0.468
-5	17.0	4,512.6	899.9	1,371.4	0.014	3.654	0.729	1.110
0	4.7	1,980.2	518.4	686.8	0.004	1.603	0.420	0.556
+5	4.6	13,686.1	1,421.5	3,208.7	0.004	11.082	1.151	2.598
+10	99.3	1,261.9	722.8	411.1	0.080	1.022	0.585	0.333
Coordinates (cm)	pH				Moisture Content (%)			
Depth Below Surface	Min	Max	Avg.	S.D.	Min	Max	Avg.	S.D.
2.5	2.4	10.1	4.5	2.4	37.2	47.5	40.8	2.5
7.5	2.0	6.6	3.6	1.4	30.0	38.6	33.7	2.1
12.5	2.1	5.5	3.4	1.0	29.9	33.7	31.6	1.2
17.5	2.0	4.7	3.1	0.9	28.9	33.6	31.0	1.3
Distance from Anode to Cathode	Min	Max	Avg.	S.D.	Min	Max	Avg.	S.D.
2.5	2.3	8.8	3.7	1.8	29.7	47.5	36.1	5.0
7.5	2.0	4.1	2.6	0.5	29.6	44.1	34.5	4.6
12.5	2.1	4.6	3.5	0.7	28.9	40.4	32.7	3.4
17.5	3.0	10.1	5.7	1.9	30.4	41.3	34.6	3.4
Orthogonal Distance from Electrodes	Min	Max	Avg.	S.D.	Min	Max	Avg.	S.D.
-10	2.0	4.6	2.9	0.9	30.0	41.0	33.6	4.3
-5	2.3	8.3	3.7	1.7	28.9	41.7	34.3	3.7
0	2.5	8.8	3.9	1.5	30.1	47.5	35.4	5.0
+5	2.1	6.6	4.0	2.0	29.6	41.6	33.8	4.0
+10	2.0	4.5	3.2	1.0	29.9	41.2	33.5	3.9

Table 38. Summary of Operational Parameters Monitored during Treatment (Experiment 5)

Day	Anode Well				Cathode Well				Overflow						Electrical Properties							
	pH	Temp.	H ₂ O ₂	Mn	pH	Temp.	H ₂ O ₂	Mn	pH	Temp.	H ₂ O ₂	Mn	Flow (mL)		Power Supply		Cathode to Anode		Cathode to Auxiliary		Auxiliary to Anode	
	(°C)	(°C)	(%)	mg/L	(°C)	(°C)	(%)	mg/L	(°C)	(°C)	(%)	mg/L	Daily	Total	Volts	Amps	Volts	Amps	Volts	Amps	Volts	Amps
0	3.5	21.5	0.0	-	3.5	21.5	0.0	-	-	-	-	-	-	-	30	0.88	29.7	0.89	20.0	1.81	9.7	1.10
1	0.7	22.3	6.6	-	13.1 (4.4)	24.4	0.1	-	12.9	21.2	0.0	-	340	340	30	0.24	30.0	0.24	27.4	1.92	2.7	0.14
2	1.5	22.4	8.6	-	13.0 (4.0)	23.2	0.0	-	12.1	21.5	0.0	-	150	490	30	0.19	30.0	0.20	28.3	1.90	1.7	0.11
3	0.7	22.5	8.5	-	12.9 (4.0)	22.9	0.0	-	10.6	21.2	0.0	-	190	680	30	0.14	30.0	0.15	28.1	1.60	1.9	0.07
4	0.8	22.4	8.3	-	12.8 (4.5)	22.7	0.0	-	9.4	21.5	0.0	-	105	785	30	0.13	30.0	0.14	28.6	1.83	1.4	0.07
5	0.7	22.3	8.1	-	12.8 (3.9)	22.5	0.0	-	10.4	21.5	0.0	-	110	895	30	0.13	30.0	0.13	28.9	2.50	1.2	0.07
6	0.5	22.1	8.6	-	12.5 (3.7)	23.2	0.0	-	7.0	21.9	0.1	-	125	1020	30	0.13	30.1	0.14	28.8	3.00	1.2	0.11
7	0.7	22.2	8.6	-	12.7 (3.8)	22.6	0.0	-	9.1	21.5	0.0	-	150	1170	30	0.14	30.0	0.15	28.7	3.06	1.3	0.14
8	0.7	23.0	8.3	-	12.7 (3.8)	23.8	0.0	-	10.0	21.6	0.0	-	165	1335	30	0.15	30.0	0.15	28.7	3.17	1.3	0.13
9	2.2	22.1	6.7	-	12.5 (4.2)	26.0	0.1	-	4.5	22.6	0.3	-	1415	2750	30	0.34	30.0	0.34	25.7	2.19	4.3	0.29
10	1.0	23.0	6.2	-	12.8 (5.0)	26.4	0.0	-	12.6	21.3	0.0	-	390	3140	30	0.44	29.9	0.47	25.6	2.87	3.7	0.31
11	1.2	22.5	4.4	-	12.9 (4.5)	23.9	0.0	-	12.8	21.2	0.0	-	290	3430	30	0.17	30.0	0.18	28.9	3.73	1.1	0.16
12	0.9	22.7	5.7	-	12.9 (4.0)	23.6	0.0	-	12.1	21.3	0.0	-	200	3630	30	0.16	30.0	0.16	30.0	0.16	1.0	0.17
13	0.8	22.0	6.3	-	12.9 (4.5)	22.1	0.3	-	11.7	20.3	0.0	-	200	3830	30	0.17	30.0	0.18	28.9	3.71	1.0	0.17
14	0.8	23.0	6.3	-	12.8 (13.5)	23.2	0.0	-	10.7	21.4	0.0	-	250	4080	30	0.18	30.0	0.19	28.9	3.75	1.1	0.18
15	1.6	22.4	0.0	-	13.2	22.7	0.0	-	13.2	20.9	0.0	-	180	4260	30	0.16	30.0	0.17	27.8	2.42	2.1	0.21
16	1.6	22.8	0.0	-	13.1	23.6	0.0	-	12.9	22.1	0.0	-	60	4320	30	0.20	30.0	0.21	27.4	2.28	2.6	0.23
17	1.3	22.5	0.0	-	13.0	23.8	0.0	-	13.0	21.1	0.0	-	255	4575	30	0.20	30.0	0.20	27.8	2.50	2.2	0.20
18	1.4	22.2	0.0	-	13.0	23.1	0.0	-	12.9	21.3	0.0	-	215	4790	30	0.16	29.9	0.17	28.1	2.50	1.9	0.21
19	1.2	22.7	0.0	-	13.1	24.4	0.0	-	13.0	21.7	0.0	-	195	4985	30	0.20	29.9	0.20	27.8	2.21	2.2	0.22
20	1.2	22.4	0.0	-	13.2	23.6	0.0	-	13.2	20.8	0.0	-	165	5150	30	0.22	29.5	0.24	27.3	2.64	2.3	0.26
21	12.6	23.8	0.0	-	13.5	25.8	0.0	-	13.1	21.4	0.0	-	350	5500	30	0.57	29.8	0.58	24.4	2.29	5.4	0.49

*Post-adjustment cathode well pH for days 1–14 is shown in parenthesis.



Figure 46. Photos. Post-treatment cathode shown in both photos (experiment 5).



Figure 47. Photo. Post-treatment cathode well caked with manganese concretions (experiment 5).

Table 39. Post-treatment Soil Parameters (Experiment 6)

X	Y	Z	pH	M.C. (%)	Pyr (C/C ₀)	Pyr (mg/kg)	Cr (C/C ₀)	Cr (mg/kg)
2.5	0	2.5	1.67	33.5	0.000	0.0	0.305	19.1
2.5	0	7.5	2.10	31.8	0.000	0.0	0.321	22.5
2.5	0	12.5	1.68	31.9	0.000	0.0	0.337	25.8
2.5	0	17.5	2.15	34.9	0.000	0.0	0.293	16.7
2.5	5	2.5	2.16	33.3	0.000	0.0	0.335	25.3
2.5	5	7.5	2.21	33.0	0.000	0.1	0.355	29.5
2.5	5	12.5	1.66	31.2	0.000	0.0	0.351	28.5
2.5	5	17.5	2.31	33.1	0.000	0.0	0.337	25.7
2.5	-5	2.5	1.92	34.3	0.000	0.0	0.330	24.2
2.5	-5	7.5	2.18	33.3	0.000	0.0	0.310	20.2
2.5	-5	12.5	2.09	33.3	0.000	0.0	0.332	24.8
2.5	-5	17.5	2.39	34.1	0.000	0.0	0.282	14.3
7.5	0	2.5	2.73	30.6	0.000	0.0	0.342	26.8
7.5	0	7.5	2.67	29.3	0.000	0.0	0.460	51.3
7.5	0	12.5	2.91	29.3	0.000	0.0	0.321	22.4
7.5	0	17.5	2.99	30.5	0.000	0.0	0.587	77.4
7.5	5	2.5	2.62	32.9	0.000	0.0	0.370	32.6
7.5	5	7.5	2.30	30.7	0.000	0.0	0.417	42.2
7.5	5	12.5	2.36	28.6	0.000	0.0	0.329	24.0
7.5	5	17.5	2.84	30.9	0.000	0.0	0.592	78.5
7.5	-5	2.5	2.15	29.6	0.000	0.0	0.340	26.4
7.5	-5	7.5	2.40	30.9	0.000	0.0	0.310	20.1
7.5	-5	12.5	2.17	31.3	0.000	0.0	0.352	28.8
7.5	-5	17.5	2.55	29.1	0.000	0.1	0.306	19.3
7.5	10	2.5	2.01	31.9	0.000	0.1	0.726	106.3
7.5	10	7.5	2.04	32.0	0.000	0.0	0.768	114.9
7.5	10	12.5	2.34	31.2	0.001	0.2	0.529	65.4
7.5	10	17.5	2.08	31.0	0.000	0.0	0.522	64.0
7.5	-10	2.5	2.26	31.2	0.000	0.1	0.890	140.3
7.5	-10	7.5	1.97	32.1	0.000	0.0	0.473	53.8
7.5	-10	12.5	2.07	32.2	0.000	0.1	0.432	45.3
7.5	-10	17.5	2.77	31.0	0.000	0.1	0.487	56.9

X	Y	Z	pH	M.C. (%)	Pyr (C/C ₀)	Pyr (mg/kg)	Cr (C/C ₀)	Cr (mg/kg)
12.5	0	2.5	2.97	28.5	0.000	0.1	3.818	746.5
12.5	0	7.5	3.23	28.9	0.000	0.0	2.809	537.6
12.5	0	12.5	3.05	30.3	0.000	0.0	1.887	346.7
12.5	0	17.5	2.76	29.8	0.000	0.0	0.535	66.7
12.5	5	2.5	2.80	28.3	0.000	0.1	4.349	856.4
12.5	5	7.5	2.95	29.2	0.000	0.1	3.423	664.7
12.5	5	12.5	2.99	29.0	0.000	0.0	1.548	276.5
12.5	5	17.5	2.65	28.3	0.000	0.0	3.330	645.5
12.5	-5	2.5	2.75	29.9	0.000	0.0	2.031	376.5
12.5	-5	7.5	2.87	28.7	0.000	0.0	0.691	99.0
12.5	-5	12.5	2.83	26.9	0.000	0.0	2.283	428.6
12.5	-5	17.5	2.89	29.1	0.000	0.0	2.952	567.1
12.5	10	2.5	2.69	30.4	0.000	0.1	2.832	542.3
12.5	10	7.5	3.09	30.7	0.000	0.0	0.626	85.5
12.5	10	12.5	2.89	31.8	0.000	0.1	0.443	47.7
12.5	10	17.5	2.99	31.4	0.000	0.1	0.471	53.5
12.5	-10	2.5	2.65	30.7	0.000	0.0	2.830	541.9
12.5	-10	7.5	2.69	29.7	0.000	0.0	0.901	142.6
12.5	-10	12.5	2.81	29.8	0.000	0.1	0.772	115.7
12.5	-10	17.5	3.01	30.0	0.000	0.1	1.142	192.4
17.5	0	2.5	6.74	28.6	0.000	0.1	1.204	205.3
17.5	0	7.5	6.97	28.7	0.000	0.0	1.210	206.5
17.5	0	12.5	3.03	31.4	0.000	0.0	0.384	35.4
17.5	0	17.5	3.27	30.8	0.000	0.0	0.452	49.5
17.5	5	2.5	4.96	28.8	0.000	0.0	0.616	83.5
17.5	5	7.5	3.13	29.6	0.000	0.1	0.787	119.0
17.5	5	12.5	3.06	32.4	0.000	0.1	0.456	50.4
17.5	5	17.5	2.53	31.8	0.000	0.1	0.459	51.0
17.5	-5	2.5	4.06	29.6	0.000	0.1	1.033	169.8
17.5	-5	7.5	3.02	26.9	0.000	0.1	0.538	67.4
17.5	-5	12.5	2.96	31.1	0.000	0.1	0.473	53.8
17.5	-5	17.5	2.93	32.1	0.000	0.1	0.422	43.3

Table 40. Summary of Statistics for Post-treatment Samples (Experiment 6)

Coordinates (cm)	Pyrene Concentration (mg/kg)				Pyrene Concentration (C/C ₀)			
Depth Below Surface	Min	Max	Avg.	S.D.	Min	Max	Avg.	S.D.
2.5	0.0	0.1	0.1	0.0	0.000	0.000	0.000	0.000
7.5	0.0	0.1	0.0	0.0	0.000	0.000	0.000	0.000
12.5	0.0	0.2	0.0	0.0	0.000	0.001	0.000	0.000
17.5	0.0	0.1	0.0	0.0	0.000	0.000	0.000	0.000
Distance from Anode to Cathode	Min	Max	Avg.	S.D.	Min	Max	Avg.	S.D.
2.5	0.0	0.1	0.0	0.0	0.000	0.000	0.000	0.000
7.5	0.0	0.2	0.0	0.0	0.000	0.001	0.000	0.000
12.5	0.0	0.1	0.0	0.0	0.000	0.000	0.000	0.000
17.5	0.0	0.1	0.1	0.0	0.000	0.000	0.000	0.000
Orthogonal Distance from Electrodes	Min	Max	Avg.	S.D.	Min	Max	Avg.	S.D.
-10	0.0	0.1	0.1	0.0	0.000	0.000	0.000	0.000
-5	0.0	0.1	0.0	0.0	0.000	0.000	0.000	0.000
0	0.0	0.1	0.0	0.0	0.000	0.000	0.000	0.000
+5	0.0	0.1	0.0	0.0	0.000	0.000	0.000	0.000
+ 10	0.0	0.2	0.1	0.0	0.000	0.001	0.000	0.000
Coordinates (cm)	Chromium Concentration (mg/kg)				Chromium Concentration (C/C ₀)			
Depth Below Surface	Min	Max	Avg.	S.D.	Min	Max	Avg.	S.D.
2.5	19.1	856.4	245.2	270.6	0.305	4.349	1.397	1.307
7.5	20.1	664.7	142.3	181.7	0.310	3.423	0.900	0.878
12.5	22.4	428.6	101.2	124.8	0.321	2.283	0.702	0.603
17.5	14.3	645.5	126.4	186.2	0.282	3.330	0.823	0.900
Distance from Anode to Cathode	Min	Max	Avg.	S.D.	Min	Max	Avg.	S.D.
2.5	14.3	29.5	23.0	4.4	0.282	0.355	0.324	0.021
7.5	19.3	140.3	54.8	33.4	0.306	0.890	0.478	0.161
12.5	47.7	856.4	366.7	252.8	0.443	4.349	1.984	1.221
17.5	35.4	206.5	94.6	61.6	0.384	1.210	0.670	0.298
Orthogonal Distance from Electrodes	Min	Max	Avg.	S.D.	Min	Max	Avg.	S.D.
-10	45.3	541.9	161.1	151.9	0.432	2.830	0.991	0.734
-5	14.3	567.1	124.0	168.3	0.282	2.952	0.812	0.813
0	16.7	746.5	153.5	208.3	0.293	3.818	0.954	1.006
+5	24.0	856.4	189.6	266.0	0.329	4.349	1.128	1.285
+ 10	47.7	542.3	135.0	155.6	0.443	2.832	0.865	0.752

Coordinates (cm)	Pyrene Concentration (mg/kg)				Pyrene Concentration (C/C₀)			
Depth Below Surface	Min	Max	Avg.	S.D.	Min	Max	Avg.	S.D.
2.5	1.7	6.7	2.9	1.3	28.3	34.3	30.7	1.9
7.5	2.0	7.0	2.9	1.1	26.9	33.3	30.4	1.7
12.5	1.7	3.1	2.6	0.5	26.9	33.3	30.7	1.6
17.5	2.1	3.3	2.7	0.3	28.3	34.9	31.1	1.7
Distance from Anode to Cathode	Min	Max	Avg.	S.D.	Min	Max	Avg.	S.D.
2.5	1.7	2.4	2.0	0.2	31.2	34.9	33.2	1.0
7.5	2.0	3.0	2.4	0.3	28.6	32.9	30.8	1.1
12.5	2.7	3.2	2.9	0.2	26.9	31.8	29.6	1.1
17.5	2.5	7.0	3.9	1.5	26.9	32.4	30.1	1.6
Orthogonal Distance from Electrodes	Min	Max	Avg.	S.D.	Min	Max	Avg.	S.D.
-10	2.0	3.0	2.5	0.4	29.7	32.2	30.8	0.9
-5	1.9	4.1	2.6	0.5	26.9	34.3	30.6	2.3
0	1.7	7.0	3.2	1.5	28.5	34.9	30.6	1.8
+5	1.7	5.0	2.7	0.7	28.3	33.3	30.7	1.8
+10	2.0	3.1	2.5	0.4	30.4	32.0	31.3	0.5

Table 41. Summary of Operational Parameters Monitored during Treatment (Experiment 6)

Day	Anode Well				Cathode Well				Overflow				Electrical Properties									
	pH	Temp.	H ₂ O ₂	Pyr	pH	Temp.	H ₂ O ₂	Pyr	pH	Temp.	H ₂ O ₂	Pyr	Flow (mL)	Power Supply		Cathode to Anode		Cathode to Auxiliary		Auxiliary to Anode		
			Conc.	Conc.			Conc.	Conc.			Conc.	Conc.										
			(°C)	(%)			µg/L	(°C)			(%)	µg/L										(°C)
0	4.2	10.5	10.0	0.0	4.2	10.5	10.0	0.0	nan	nan	0.0	0.0	0	0	30	2.11	29.5	1.95	15.4	nan	13.9	1.86
1	0.6 (5.1)	21.6 (25.3)	5.8	23.0	12.9	22.4	0.0	32.5	nan	nan	nan	nan	0	0	30	0.05	30.0 3	0.05	29.48	nan	0.54	0.06
2	9.3	36.0	2.0	29.5	nan (0.8)	nan (25.7)	nan (10.0)	nan (25.3)	8.6	22.9	2.0	32.0	0	0	30	0.21	28.4 5	1.97	5.31	nan	23.17	4.37
3	0.4 (2.9)	22.9 (24.6)	2.2	27.1	13.1	27.0	0.0	25.9	nan	nan	nan	nan	0	0	30	0.32	29.8 9	0.32	28.89	4.92	1.01	0.16
4	2.5 (8.8)	21.8 (24.8)	2.2	34.3	13.3	23.1	0.0	24.3	nan	nan	nan	nan	0	0	30	0.11	29.0 5	0.12	29.97	0.12	-0.93	0.12
5	7.5	22.0	1.0	31.1	13.2	21.7	0.0	22.0	8.4	21.0	1.1	29.5	40	40	30	0.08	28.8 8	0.09	29.99	0.08	-1.20	0.05
6	8.3	22.4	2.2	25.2	13.2	22.1	0.0	32.7	10. 9	21.6	0.0	32.0	30	70	30	0.06	29.7 3	0.07	29.73	0.07	-1.16	0.07
7	13.1	21.7	1.0	28.7	2.9 (5.0)	22.1 (22.7)	0.0	21.3	nan	nan	nan	nan	0	70	30	0.04	29.8 8	0.05	29.62	5.01	0.30	0.04
8	0.9	21.9	1.3	30.2	13.0 (3.6)	22.8 (22.7)	0.0	23.0	9.5	21.3	0.1	32.0	40	110	30	0.07	30.0 1	0.08	29.46	5.00	0.55	0.11
9	0.3	22.3	2.4	25.8	13.0 (3.4)	24.2 (23.2)	0.0	23.8	4.2	21.9	0.8	30.2	90	200	30	0.11	30.0 0	0.12	29.40	5.00	0.58	0.14

10	0.4	23.3	2.3	35.0	13.0 25.9 (3.0) (22.9)	0.0	29.1	3.9	22.3	0.5	29.7	70	270	30	0.18	29.9 7	0.18	29.35	5.00	0.61	0.20
11	0.3	21.9	2.6	39.3	13.0 23.5 (2.9) (18.0)	0.0	34.4	3.8	21.2	0.4	31.1	90	360	30	0.15	29.9 8	0.16	29.28	5.01	0.68	0.21
12	0.4	24.8		54.5	12.9 24.8 (1.2) (2.48)	0.0	51.5	3.5	21.3	3.7	41.7	162	522	30	0.16	29.9 8	0.17	29.14	4.95	0.84	0.20
13	0.4	23.2		47.5	13.1 26.4 (1.3) (22.2)	0.0	51.2	3.9	21.4	0.9	47.3	112	634	30	0.24	29.9 2	0.25	28.66	4.93	1.26	0.27
14	0.3	23.4	1.9	50.8	13.0 27.8	0.0	48.6	4.2	22.2	3.7	50.3	180	814	30	0.29	29.8 4	0.30	28.30	4.83	1.59	0.30

*Post-adjustment electrode well pH and temperature shown in parenthesis; T:0-2 cathode-auxiliary current not a number (nan) due to highly unstable measurement.

*Table continued on next page.

Day	Anode Well				Cathode Well				Overflow						Electrical Properties							
	pH	Temp.	H ₂ O ₂ Conc.	Pyr Conc.	pH	Temp	H ₂ O ₂ Conc	Pyr Conc	pH	Temp	H ₂ O ₂ Conc	Pyr Conc.	Flow (mL)		Power Supply		Cathode to Anode		Cathode to Auxiliary		Auxiliary to Anode	
		(°C)	(%)	µg/L		(°C)	(%)	µg/L		(°C)	(%)	µg/L	Daily	Total	Volt s	Amp s	Volts	Amps	Volts	Amps	Volts	Amps
15	0.6	22.1	6.0	50.5	13.1	23.7	0.1	49.3	nan	nan	nan	nan	0	814	30	0.14	28.94	0.15	29.73	5.00	-0.82	0.15
16	0.4 (9.7)	22.6 (35.7)	3.8	49.5	13.2	24.8	0.0	31.1	8.0	21.8	1.0	46.3	174	988	30	0.27	29.86	0.28	28.46	4.91	1.40	0.32
17	3.9	22.3	4.1	44.0	13.1	23.3	0.0	45.7	nan	nan	nan	nan	0	988	30	0.14	29.96	0.15	28.90	4.95	1.07	0.17
18	3.0 (9.8)	22.0 (24.0)	2.9	41.9	13.0 (3.7)	22.8 (23.4)	0.0	43.5	12.8	21.0	0.1	37.9	40	1,028	30	0.10	29.98	0.11	29.02	4.96	0.95	0.19
19	0.5 (9.0)	23.5 (32.4)	6.5	39.6	12.8 (3.6)	28.8 (29.9)	0.1	37.5	5.9	21.6	0.3	38.9	300	1,328	30	0.62	29.46	0.62	26.32	4.18	3.13	0.52
20	2.2 (8.5)	26.3 (32.1)	8.9	21.4	13.0 (4.0)	34.3 (40.0)	0.4	30.9	12.1	22.0	2.0	5.2	330	1,658	30	1.36	29.13	1.35	24.40	4.48	4.75	0.97
21	0.3 (8.7)	24.3 (32.6)	5.9	12.1	12.9 (3.5)	30.3 (32.0)	0.0	12.9	12.5	22.9	0.0	21.6	350	2,008	30	0.55	29.71	0.57	28.18	4.29	1.54	0.30
22	0.5 (4.3)	23.6 (27.9)	3.8	17.9	13.0 (3.4)	28.9 (27.5)	0.0	24.3	5.3	21.5	0.0	31.8	220	2,228	30	0.43	29.23	0.44	28.06	4.80	1.16	0.33
23	0.6 (9.6)	22.6 (34.6)	8.6	31.5	12.9 (3.6)	28.3 (26.9)	0.0	30.8	4.6	21.5	0.6	33.7	186	2,414	30	0.38	29.84	0.39	28.70	4.76	1.13	0.25
24	2.5	22.4	5.2	33.9	12.9	27.8	1.4	29.4	4.3	21.5	1.4	34.4	235	2,649	30	0.41	29.79	0.41	27.78	3.58	1.93	0.32

	(2.6) (21.8)	(12.9 (28.4))																		
25	0.4 27.3 (10.3) (37.9)	13.0 27.3 (5.2) (32.0)	0.8 33.3	nan	nan	nan	nan	0	2,649	30	0.30	29.89	0.31	28.58	3.76	1.31	0.25			
26	3.3 22.6 4.9 38.7	12.8 26.0 (3.6) (27.6)	0.0 33.3	12.6	20.4	0.2	35.3	220	2,869	30	0.32	29.71	0.33	28.12	3.20	1.58	0.25			
27	1.0 22.3 (8.2) (27.0)	12.6 26.2 (2.9) (26.3)	0.0 34.0	5.8	21.4	0.4	35.3	220	3,089	30	0.32	29.70	0.33	28.1	3.20	1.60	0.25			
28	0.9 22.4 6.7 35.6	12.9 25.1 0.0 34.4		4.1	23.3	0.8	31.9	160	3,249	30	0.44	29.70	0.45	28.0	3.70	1.80	0.29			

*Post-adjustment electrode-well pH and temperature shown in parenthesis; T:O-2 Cathode-Auxiliary Current (nan) due to highly unstable measurement.

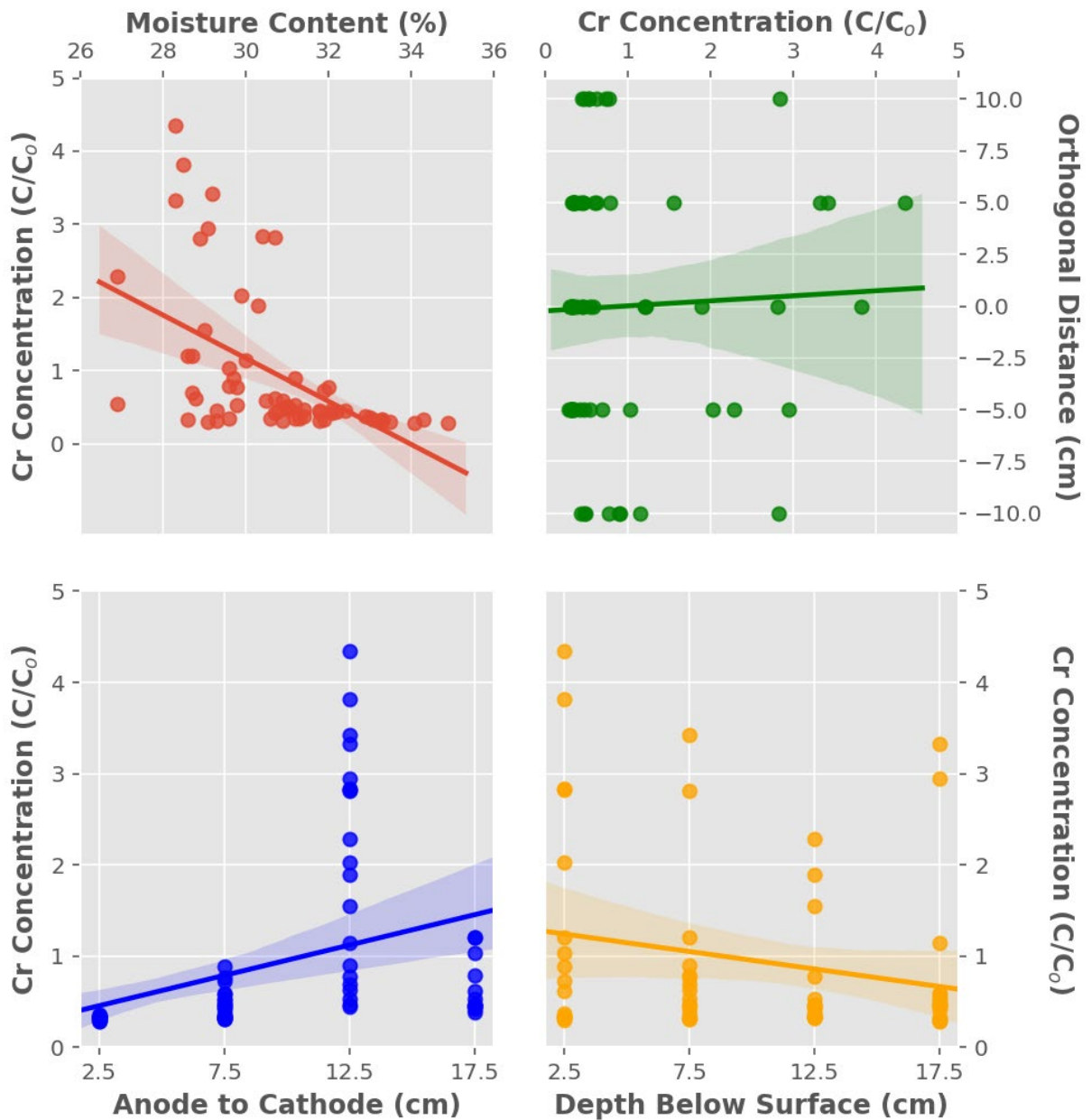


Figure 48. Graph. Chromium concentration as a function of moisture content and each spatial dimension (experiment 6). The shaded regions represent the 95% confidence intervals of the linear regressions.



I ILLINOIS